UNIVERSITY OF OKLAHOMA

GRADUATE COLLEGE

DEVELOPMENT OF BIOMATERIALS FOR CALVARIAL BONE REGENERATION AND APPLICATION TO TRAUMATIC BRAIN INJURY

A DISSERTATION

SUBMITTED TO THE GRADUATE FACULTY

In partial fulfillment of the requirements for the

Degree of

DOCTOR OF PHILOSOPHY

By

JAKOB M. TOWNSEND
Norman, Oklahoma
2017

Downloaded from SHAREOK. Persistent Handle URL: https://hdl.handle.net/11244/52412

DEVELOPMENT OF BIOMATERIALS FOR CALVARIAL BONE REGENERATION AND APPLICATION TO TRAUMATIC BRAIN INJURY

A DISSERTATION APPROVED FOR THE
STEPHENSON SCHOOL OF BIOMEDICAL ENGINEERING

BY

Dr. Michael Detamore, Chair

Dr. Barbara Safiejko-Mroczka

Dr. Vassilios Sikavitsas

Dr. Lei Ding

Dr. Bradley Bohnstedt

© Copyright by JAKOB M. TOWNSEND 2017
All Rights Reserved.

Acknowledgments

What a crazy ride it has been. I never could have imagined the amount of personal and professional growth I would experience during my graduate studies. I am forever indebted to my graduate mentors, friends, and family members that have supported my dream of achieving my doctorate. What was once an unobtainable goal is now within reach, I am truly a lucky person to have fallen in the presence of such amazing individuals. I never could have achieved my current academic accomplishments if it was not for the support of those around me. I would like to thank those people:

I would first like to thank my advisor, Dr. Michael Detamore, for his constant support, guidance, and encouragement during my graduate studies. His advice in both professional and personal matters has helped to shape my life for the better. Michael has pushed me to achieve my goals and I couldn't have asked for a better advisor. I am proud to call him both my mentor and friend.

I would like to thank my committee members, Dr. Barbara Safiejko-Mroczka, Dr. Vassilios Sikavitsas, Dr. Lei Ding, and Dr. Bradley Bohnstedt for their guidance and support in my graduate studies. The individual perspectives of each committee member have helped to build my graduate work immensely. I would also like to thank my past co-advisor at the University of Kansas, Dr. Cory Berkland, for his continuous support during my time at the University of Kansas and after the move to the University of Oklahoma. I would also like to thank the co-authors who have contributed to the body of work presented: Brian Andrews, Connor Dennis, Erik Van Kampen, Jinxi Wang, Jon Whitlow, Randolph Nudo,

Stevin Gehrke, Taylor Zabel, and Yi Feng. I would also like to thank previous and current collaborators who helped process samples: Hong Liu, Di Wu, and Kar-Ming Fung. Research reported in the dissertation was supported by the National Institute of Dental and Craniofacial Research of the National Institutes of Health under Award Number R01 DE022472 and R03 DE025906. The content is solely the responsibility of the author and does not necessarily represent the official views of the National Institutes of Health.

I would like to thank Peggy and Charles Stephenson for their exceptional generosity and support in starting the Stephenson School of Biomedical Engineering. Peggy and Charles generously provided a graduate fellowship which allowed myself to pursue research full-time and I am very grateful to their kindness.

I would like to thank the undergraduate researchers who have helped in completing the research presented in the current dissertation. I would like to personally thank Taylor Zabel for his hard work in mechanically characterizing hydrogels, and Mike Holtz for hard work in helping to produce materials used throughout the PhD. I would also like to thank Nina Cassidy for help in designing the next-generation of biomaterials past the current dissertation. The research was truly elevated by the hard work put forth by these undergraduates and I only see success in their futures.

I would like to thank the current and past members of the Detamore Lab; Lindsey Ott, BanuPriya Sridharan, Vineet Gupta, Cate Wisdom, A.J. Mellott, Stefan Lohfeld, and Salma Mahzoon who have helped guide the beginning of my

scientific career in regenerative medicine. I would like to thank Peggy Keefe for the countless baked goods, support, and advice given throughout my graduate studies. I would like to thank Jeannie Salash and Emi Kiyotake for being amazing both scientifically and as human beings. I would like to thank Emily Beck for being a wonderful lab-mate, mentor, friend, and sushi buddy. I would like to thank the countless friends I have made during my graduate studies for the constant sanity checks and pressure to stop working and come out for a beer.

I would like to thank my friends at the Shenago Lounge; Chris Golden, Shara Thati, Darrell Goebel, and Brad Black for always cheering me up after the hard days, and for providing a part-time job to escape graduate school life. I would like to thank the new friends I have made at the climbing gym, I am so very happy to be surrounded by such supportive people.

I would like to thank my previous mentors at Oregon State University, Christine Kelly and Curtis Lajoie, for their mentorship in undergraduate research. I would never have known of graduate school as an option if it was not for Christine's support, or believed I was smart enough to tackle such a challenge if it was not for Curtis' encouragement. I will never forget the fond memories I have working in the Kelly lab.

I would like to thank members of the TrilliumFiber Fuels team, Joshua Kitner and Steve Potochnik, who mentored me during a year-long internship. I can attribute my basic lab and research skills to the training I received from my time working with these two individuals.

Lastly, I would like to thank my family. To my parents, Tammy and Michael, I would not be the person I am today if it was not for your constant love, support, and advice. Mom, thank you for going the extra mile to teach me basic math, I will never forget how much I loathed those summer math problems as a kid. Dad, thank you for providing the option to pursue any path in life. To my grandparents, thank you for always supporting my fascination for discovery. I do apologize for taking apart your electronics in an attempt to figure out how they worked. To my sister Erika, thank you for always being there when I needed you the most.

Table of Contents

Acknowledgments iv
Table of Contents viii
List of Figures xii
List of Tables xiii
Abstract xiv
Chapter 1: Introduction 1
Chapter 2: Flow Behavior Prior to Crosslinking: The Need for Precursor Rheology for Placement of Hydrogels in Medical Applications[1] 7
Abstract 7
Introduction 8
Biomedical Hydrogel Perspective 12
Our Inspiration 12
Translation of Technology to Surgeons 14
Biomedical Hydrogel Perspective Summary 15
Surgical Context 16
Injectability/Syringeability and Shear Properties 16
Placement and Recovery Time 18
Retention and Yield Stress 19
Rheological Methods 22
Surgical Context Summary 23
Hydrogel Rheology Properties 24
Paste and Putty Nomenclature 24
Paste and Putty Application 26
Herschel-Bulkley Model 26
Summary 28
Hydrogel Precursor Considerations 28
Chemically Crosslinked Hydrogels 28
Physically Crosslinked Hydrogels 31
Combinational Crosslinking Hydrogels 32
Crosslinking Hydrogels Summary 33
Conclusions 33

Chapter 3: Colloidal Gels with Extracellular Matrix Particles and Growth Factors for Bone Regeneration in Critical Size Rat Calvarial Defects[2] 35
Abstract 35
Introduction 36
Materials and Methods 41
Materials 41
Preparation of Decellularized Cartilage (DCC) 41
Preparation of Colloidal Gels 42
Environmental Scanning Electron Microscopy (ESEM) 43
Rheological Testing 43
Animal Model and Surgical Method 44
Micro-computed Tomography (μCT) 44
Histology and Immunohistochemistry 45
Statistical Methods 46
Results 47
Rheological Analysis 47
Microcomputed Tomography (μCT) Analysis 47
Histological Analysis 48
Immunohistochemical (IHC) Analysis 48
Discussion 49
Conclusion 53
Chapter 4: Decellularized Cartilage-Based Hydrogel Encapsulating Osteoconductive Particles for Calvarial Bone Regeneration[3] 55
Abstract 55
Introduction 56
Materials and Methods 60
Preparation of Decellularized Cartilage (DCC) 60
Synthesis of Methacrylated Solubilized Decellularized Cartilage (MeSDCC) 61
Rat Bone Marrow Harvest and Culture 62
Hydrogel Preparation 63
Rheological Testing of Hydrogel Precursor Solution 64
Mechanical Testing of Crosslinked Hydrogel 65

Animal Model and Surgical Method 66
Micro-computed Tomography (μCT) 66
Histology and Immunohistochemistry (IHC) 67
Statistical Methods 69
Results 69
Rheological Analysis of Hydrogel Precursor 69
Mechanical Analysis of Crosslinked Hydrogel 69
Micro-computed Tomography (μCT) Analysis 70
Histological and Immunohistochemistry (IHC) Analysis 70
Discussion 71
Conclusion 76
Chapter 5: Superior Calvarial Bone Regeneration with Pentenoate-Functionalized Hyaluronic Acid Hydrogels with Devitalized Tendon Particles[4] 78
Abstract 78
Introduction 79
Materials and Methods 82
Preparation of Devitalized Tissue 82
Synthesis of Pentenoate Functionalized Hyaluronic Acid (PHA) 83
Hydrogel Preparation 83
Rheological Testing of Hydrogel Precursor 84
Mechanical Testing of Crosslinked Hydrogel 84
Animal Model and Surgical Method 85
Micro-Computed Tomography (μCT) 86
Histology and Immunohistochemistry (IHC) 86
In Vitro Cell Culture and Experimental Design 87
Biochemical Assays 88
Statistical Methods 88
Results 89
Rheological Analysis of Hydrogel Precursor 89
Mechanical Analysis of Crosslinked Hydrogel 90
Micro-computed Tomography (μCT) Analysis 90
Histological Analysis 91
Biochemical Analysis from In Vitro Study 92

Discussion 93
Conclusion 97
Chapter 6: Conclusion 99
References 106
Appendix A: Figures 127
Appendix B: Tables 148

List of Figures

Chapter 1

Figure 1.1: Illustration of Dissertation Aims 128
Figure 1.2: Illustration of Implanted Hydrogel Pliability 129

Chapter 2

Figure 2.1: Liquid, paste, and Putty Precursor Solutions 130
Figure 2.2: Illustration of Real and Induced Defects 131
Figure 2.3. Defect Retention of Liquid Compared to Paste or Putty 132
Figure 2.4: Methods to Determine Yield Stress 133

Chapter 3

Figure 3.1: Surgical Method and Material ESEM Images 134
Figure 3.2: Aim 1 Hydrogel Precursor Yield Stress 135
Figure 3.3: Aim 1 Regenerated Bone Volume and μCT Imaging 136
Figure 3.4: Aim 1 H&E Staining 137
Figure 3.5: Aim 1 Immunohistochemistry 138

Chapter 4

Figure 4.1: Aim 2 Hydrogel Precursor Yield Stress 139
Figure 4.2: Aim 2 Hydrogel Compressive Modulus 140
Figure 4.3: Aim 2 Regenerated Bone Volume and μCT Imaging 141
Figure 4.4: Aim 2 H&E Staining 142
Figure 4.5: Aim 2 Immunohistochemistry 143

Chapter 5

Figure 5.1: Aim 3 Mechanical Characterization 144
Figure 5.2: Aim 3 Regenerated Bone Volume and μCT Imaging 145
Figure 5.3: Aim 3 H&E Staining 146
Figure 5.4: Aim 3 Biochemical Analysis 147

List of Tables

Chapter 1

No Tables

Chapter 2

Table 2.1: Summary of Hydrogel Rheological Properties 149

Chapter 3

No Tables

Chapter 4

No Tables

Chapter 5

No Tables

Chapter 6

No Tables

Abstract

In the treatment of severe traumatic brain injury (TBI), a two-stage surgical intervention is routinely performed. In the first surgery, decompressive craniectomy (DC) is performed to remove a large portion of calvarial bone to allow unimpeded brain swelling. A second surgery termed cranioplasty, usually performed weeks to months later, is then employed to rebuild the cranium. Hydrogels have the potential to revolutionize TBI treatment by permitting a single-stage surgical intervention, capable of exhibiting paste-like handling properties in the pre-crosslinked form for *in situ* placement to fill any size or shape of defect, remaining pliable during brain swelling, and tuned to regenerate bone after swelling has subsided. The motive of the current dissertation was to achieve the first step in designing a single-stage surgical intervention for treatment of TBI following DC, being the design of a hydrogel capable of regenerating bone within a critical size calvarial defect. The current dissertation first evaluated the use of colloidal hydrogels of hyaluronic acid, hydroxyapatite, and extracellular matrix (ECM) materials demonstrating promise for decellularized cartilage as a material for bone regenerative medicine. A next-generation biomaterial was then developed utilizing a methacrylated solubilized decellularized cartilage hydrogel encapsulating osteoconductive particles, the results of which demonstrated diminished bone regeneration that was speculated to be due to cartilage processing (i.e., solubilization). In the final study, pentenoate-functionalized hyaluronic acid (PHA) hydrogels encapsulating devitalized ECM materials were evaluated and I found that PHA hydrogels encapsulating devitalized tendon

(DVT) particles successfully regenerated bone in a critical size calvarial defect. Future studies will be conducted to test the use of the PHA-DVT hydrogel in a rat TBI model to evaluate the use of hydrogels in the treatment of TBI following DC. Ultimately, the current dissertation work successfully developed a hydrogel material that exhibits desirable handling properties in the pre-crosslinked form for surgical placement and adequate bone regeneration after 8 weeks of *in vivo* implantation, with promising future applications to bone regeneration and application to treatment of TBI.

Chapter 1: Introduction

The long-term goal of the dissertation was the creation of a material to aid in the treatment of traumatic brain injury (TBI). TBI is a life-threatening condition diagnosed by internal brain herniation. Severe TBI is commonly treated by a two-stage surgical procedure. In the first surgery, a decompressive craniectomy (DC) procedure is conducted to remove a large portion of calvarial bone to allow un-impeded brain swelling beyond the cranial confines. Weeks to months later, a second surgery termed cranioplasty is performed to restore the cranial vault. The current two-stage surgical intervention has disadvantages as it prolongs neurorehabilitation and recovery, increases medical costs, and is associated with causing the neurological condition termed syndrome of the trephined (SoT). SoT, also known as sinking skin flap syndrome, is a neurological condition associated with symptoms such as mood changes, fatigue, headaches, dizziness, fine motor dexterity issues, and difficulties concentrating. SoT is thought to be caused by changing intracranial pressure or deformation of the brain from the overlying scalp after the DC procedure. TBI treatment would greatly benefit from a single-stage surgery using a material that could be implanted in the initial surgery, remain pliable enough to allow brain swelling, then transition to bone after swelling has subsided.

Hydrogels were identified as an attractive material option for application to a single-stage surgical model for TBI treatment. Hydrogels offer the ability for *in situ* placement to fill irregularly shaped defects, crosslinking for material retention at the injury site, a tunable degree of pliability, and selective material properties

for osteogenic promotion (Fig. 1.2). Additionally, hydrogel precursor solutions that exhibit paste or putty-like handling properties would allow for ease of placement and retention into the defect site. With these design parameters in mind, the following specific aims were designed: (1) assessment of physically crosslinked hydrogels composed of extracellular matrix materials (ECM) and growth factors, (2) evaluation of naturally derived crosslinking hydrogels encapsulating synthetic colloids, and (3) evaluation of synthetic crosslinking hydrogels encapsulating ECM colloidal particles (Fig. 1.1).

Aim 1 attempted to utilize a simple non-crosslinking hydrogel design to evaluate the use of hyaluronic acid (HA), synthetic hydroxyapatite, and natural ECM materials of demineralized bone matrix (DBM) or decellularized cartilage (DCC) with or without growth factors to generate new bone formation. The second aim attempted to address the observed issues of aim 1 regarding material retention issues while expanding on the use of DCC as a material for calvarial bone regeneration. **Aim 2** utilized a solubilized and methacrylated DCC (MeSDCC) hydrogel encapsulating synthetic colloids. The third aim attempted to combine the positive aspects of aim 1 and aim 2, the bone regenerative potential and photocrosslinking, respectively. **Aim 3** utilized a pentanoate-functionalized hyaluronic acid (PHA) hydrogel and devitalized tissue particles of bone, cartilage, meniscus, and tendon for evaluation in calvarial bone regeneration. All work presented in the following chapters was a product of my own effort with the exception of the animal surgeries that were conducted by Dr. Yi Feng and Dr. Jinxi Wang at the University of Kansas Medical Center and the histology

sectioning/staining presented in Aim 3 that was conducted by the Stephenson Cancer Tissue Pathology Core at the University of Oklahoma Health Sciences Center. Individual chapters communicate work that is in preparation, submitted, or published as indicted by the footnote at the bottom of each associated chapter. The following chapters represent the chronological organization of the aforementioned aims:

Chapter 2 is a review that provides informative advice to the hydrogel field on rheology and how better evaluation of hydrogel precursor solutions (i.e., hydrogels solutions before crosslinking) can lead to easier clinical adoption. The final hurdle in translating a new treatment from the lab bench to the clinic is clinician adoption and use. A new and potentially impactful technology can be overlooked if the associated learning curve is too difficult. Here I propose yield stress (i.e., the stress required for a material to begin to flow) ranges for liquid (no yield stress), paste (100-2000 Pa), and putty (2000+ Pa) handling properties. By designing materials with similar handling properties to currently available materials the surgeon technology learning curve can be minimized to ease clinician adoption.

Chapter 3 addresses the first aim, using a non-crosslinking hydrogel comprised of HA, hydroxyapatite nanoparticles (HAp), and ECM materials of DBM or DCC to evaluate bone regeneration in an *in vivo* rat critical-size calvarial defect model. The HA-HAp-ECM hydrogels were evaluated for their yield stress, regenerated bone volume by micro-computed tomography (μCT), histology, and immunohistochemistry to compare osteogenic potential *in vivo*. Encouraging

results illustrating comparable bone regeneration between growth factor and DCC-containing materials prompted further research into using a photocrosslinkable cartilage hydrogel in Aim 2. Aim 1 represents our first attempt at using non-traditional ECM materials (i.e., cartilage) to promote bone formation, the work presented heavily influenced the direction of the research and subsequent aims. The aim 1 study was the first to use naturally derived decellularized cartilage extracellular matrix for calvarial bone regeneration.

Chapter 4 addresses the second aim, using a methacrylated solubilized decellularized cartilage (MeSDCC) hydrogel encapsulating synthetic osteogenic particles of hydroxyapatite nanofibers (HAPnf), bioglass microparticles (BG), or added rat bone marrow-derived mesenchymal stem cells (rMSCs) for bone regeneration in critical-size rat calvarial defects. Particles of HAPnf or BG were added for two specific reasons: 1) delivery of known osteoconductive materials to aid in bone regeneration, and 2) to create hydrogel precursor materials that exhibit paste-like handling properties for physical placement and shaping before crosslinking. Fibrin hydrogels were employed as a control material for the study. Hydrogels used in the study were evaluated for their yield stress before crosslinking, compressive modulus post-crosslinking, regenerated bone volume, histology, and immunohistochemistry to evaluate bone regeneration in a critical-size rat calvarial defect. The use of the MeSDCC hydrogels was inspired by the results of Aim 1 suggesting that DCC particles could promote similar bone regeneration compared to growth factor containing groups. Minimal bone

regeneration using the MeSDCC hydrogels prompted the re-evaluation of crosslinking hydrogels.

Chapter 5 addresses the third aim, using a pentanoate-functionalized hyaluronic acid (PHA) hydrogel encapsulating ECM tissue particles of DBM, devitalized cartilage (DVC), devitalized meniscus (DVM), or devitalized tendon (DVT) for bone regeneration in critical-size rat calvarial defects. After discussions with surgeons, faster material crosslinking times were determined to be of great importance for successful clinical translation. Additionally, hyaluronic acid based colloidal gels used in the first aim demonstrated adequate bone regeneration. For these reasons, pentenoate-functionalized hyaluronic acid (PHA) hydrogels were determined to be an attractive material choice highlighting fast crosslinking times (1-2 minutes). PHA-ECM hydrogels were evaluated for precursor yield stress, post-crosslinking compressive modulus, regenerated bone, and histology to evaluate new bone formation. Leading groups were further refined *in vitro* to determine the minimum ECM particle concentration required to achieve desirable bone formation. Aim 3 was designed in an attempt to combine the positive aspects of both aims 1 and 2 to develop a better material for calvarial bone regeneration. The materials from aim 1 and the crosslinking from aim 2 were combined to create the new crosslinking hydrogels encapsulating different ECM materials.

Chapter 6 serves as the conclusion to the dissertation and provides a summary of the most important findings, comparison between specific aims, and a global perspective of the dissertation work. Recommendations are provided for

future work to design the next generation of materials for calvarial bone regeneration and application to TBI.

Overall, the work presented in the current dissertation provides the first step in the development of materials for application to TBI treatment after DC. The work has focused on developing cost-effective, highly translatable, acellular, pliable, and easy to use hydrogel treatments to achieve a single-stage surgical procedure for the treatment of TBI. Other treatment options such as DBX®, NovaBone Putty®, and custom-made implants generated from μCT scans exist; however, these treatment options cannot be used in a single-stage surgical approach as they do not remain pliable and thus impede brain swelling. A secondary issue with currently available treatment options exists in that the materials themselves do not regenerate adequate bone in the critical size calvarial defect created during DC. Hydrogels are an attractive option as the materials are inherently pliable, and have demonstrated improved bone regeneration. Although the work in the current dissertation did not solve the entire issue associated with developing a treatment for TBI, it did provide the beginning foundation for a hydrogel material with potential for a single-stage surgical approach for the treatment of TBI.

Chapter 2: Flow Behavior Prior to Crosslinking: The Need for Precursor Rheology for Placement of Hydrogels in Medical Applications[1]

Abstract

Hydrogels – water swollen cross-linked networks – have demonstrated considerable promise in tissue engineering and regenerative medicine applications. However, ambiguity over which rheological properties are needed to characterize these gels before crosslinking still exists. Most hydrogel research focuses on the performance of the hydrogel construct after implantation, but for clinical practice, and for related applications such as bioinks for 3D bioprinting, the behavior of the pre-gelled state is also critical. Therefore, the goal of this review is to emphasize the need for more attention paid to the development and characterization of hydrogel precursor formulations with desirable rheological properties. In particular, we consider engineering paste or putty precursor solutions (i.e., suspensions with a yield stress), and distinguish between these differences to ease the path to clinical translation. The connection between rheology and surgical application as well as how the use of paste and putty nomenclature can help to qualitatively identify material properties are explained. Quantitative rheological properties for defining materials as either pastes or putties are proposed to enable easier adoption to current methods. Specifically,

[1]Submitted as: Townsend JM, Beck EC, Gehrke SH, Berkland CJ, Detamore MS. Flow Behavior Prior to Crosslinking: The Need for Precursor Rheology for Placement of Hydrogels in Medical Applications. *Progress in Polymer Science*, 2017.

the three-parameter Herschel-Bulkley model is proposed as a suitable model to correlate experimental data and provide a basis for meaningful comparison between different materials. This model combines a yield stress, the critical parameter distinguishing solutions from pastes (100-2000 Pa) and from putties (>2000 Pa), with power law fluid behavior once the yield stress is exceeded. Overall, successful implementation of paste or putty handling properties to the hydrogel precursor may minimize the surgeon-technology learning time and ultimately ease incorporation into current practice. Furthermore, improved understanding and reporting of rheological properties will lead to better theoretical explanations of how materials affect rheological performances, to better predict and design the next generation of biomaterials.

Introduction

Hydrogels are water-swellable networks held together by physical and/or covalent crosslinks. These networks can be tailored with varying degrees of control of the structural architectures from nano- to microscales and made from a wide variety of materials to suit particular applications.(1) Conventional hydrogel networks can be made from biological polymers (especially proteins and polysaccharides), synthetic polymers (e.g., poly(ethylene glycol)), or chemically modified (semi-synthetic) biopolymers such as cellulose ethers. Less conventional gels can be formed from inorganic colloids or even constructed from harvested tissues.(2-8) The molecular properties (e.g., hydrophilic/hydrophobic balance, net charge or charge distributions) and macroscopic physical properties

(e.g., size) can be tuned based on the desired application.(9) Hydrophilicity and significant water content (typically in the 50-90% range) and a fixed physical geometry once the gel has formed are the defining features that fall under the broadest sense of the term ‘hydrogel’. The versatility of hydrogels has allowed them to be employed in a wide variety of applications, from consumer products such as diapers to various foods to common biomedical devices such as soft contact lenses.(10-18) Hydrogels have contributed to the rapid growth in publications for more complex biomedical engineering applications such as tissue engineering constructs and triggered drug delivery devices over the past 20 years.(19, 20) Most publications characterizing hydrogels focus on the performance of the gel after it has formed, with far less attention being paid to the behavior prior to gelation. For successful translation to surgical applications, the behavior of the pre-gelled solution is critical.

The use of hydrogels in regenerative medicine and biomedical applications has been rapidly increasing over the past 20 years, as the potential of hydrogels to treat complex medical issues has become widely recognized.(21) *In situ* forming hydrogels - those that polymerize or set within the body - can be applied to the treatment of a wide range of complex medical issues such as those requiring filling of defects of various shapes and sizes. Hydrogels can be used to encapsulate and localize both living cells and materials such as hydroxyapatite (HAp) and demineralized bone matrix (DBM). HAp and DBM are commonly used materials in hydrogel formulations for treatment of bone defects.(16, 22) DBX® is a widely used commercially available bone replacement product that combines

DBM and hyaluronic acid, the DBM concentration in these hydrogels modulates material pliability to achieve either paste or putty behavior for *in situ* placement.(16) In fluid mechanics, the yield stress is the stress required for a fluid to begin to flow (as opposed to solid mechanics, where the same 'yield stress' term refers to the point between elastic and plastic deformation), and quantifies where such a fluid lies on the spectrum of paste to putty behavior. Increasing the yield stress allows for different material consistencies as illustrated in Figure 2.1, in which materials with no yield stress exhibit traditional liquid behavior (i.e., flow upon exposure to any stress, no matter how small), while materials with increasing yield stress have paste or putty behavior. DBX® products, for example, vary the yield stress based on the application, employing high yield stress putties for craniofacial applications and lower yield stress pastes for filling mandibular resection defects.(23) The major difference between paste or putty being the route of application, where high yield stress materials can be easily molded and lower yield stress materials can easily flow for injection.

Materials with handling properties that are similar to current products familiar to surgeons would have lower-learning curves associated with them and thus would be easier for them to adopt. To quantitatively assess these properties, we propose the use of rheology instruments to measure precursor solution characteristics such as yield stress, which have direct relevance to clinicians' use of the materials. In practice, the three most relevant rheological parameters are the ease of injection (shear response), time for placement (recovery time), and retention of the hydrogel precursor solution at the defect site (yield stress). A

review of the recent literature revealed 27 studies that have conducted hydrogel precursor rheology for one or more of the three previously mentioned properties of interest to clinicians (Table 2.1). Of these 27 studies, only 10 characterized all three rheologically dependent characteristics. Although research publications commonly state the ability of the hydrogel precursor solution to be injectable or fill any irregularly-shaped defect, few publications reporting new hydrogels actually characterize the precursor solution. Various groups have reported their material to be injectable based only on the ability to pass through a syringe needle. Similarly, investigators have reported gel formation as determined by a simple tube inversion observation.(24, 25) Wang *et al*.(26) demonstrated that a mixture of oppositely charged nanospheres of anionic and cationic gelatins could be injected into a conical tube and inverted while maintaining the position and shape. Although these methods may qualitatively identify yield stress behavior and/or shear thinning properties, they do not provide quantitative or definitive information.

Therefore, the purpose of this review article is to emphasize to biomaterials developers the importance of hydrogel precursor rheological characterization. The connection between rheological properties and surgical application requirements will be explained, and how medical nomenclature can be leveraged as a translational advantage among hydrogel formulation developers. Finally, rheological modeling is proposed as the basis for comparison among hydrogel precursor groups, with additional considerations for physical, chemical, and combinational crosslinking approaches proposed to help move the

community toward material design strategies to create precursor solutions with a target yield stress. In this review, we will show how implementing yield stress in hydrogel precursor solutions has a direct benefit for biomedical applications in terms of clinical translation.

Biomedical Hydrogel Perspective

Our Inspiration

More than 20 years ago, the concept of colloidal gels began to emerge as a potential material for regenerative medicine. At the time, pioneering work by Prof. Jennifer Lewis and others showed novel colloidal inks could be used for printing freestanding 3D structures.(27, 28) Such colloidal inks utilized weak interactions between a multitude of nanoparticles or between nanoparticles and polymers, which could be disrupted to allow the viscous ink to yield and flow before again ‘recovering’ bulk solid properties. We and others recognized these dynamic, viscoelastic colloidal inks offered promise as tissue fillers or as substrates for printing 3D scaffolds for regenerative medicine.(29, 30)

Our team began translating colloidal gels to applications in regenerative medicine based on biodegradable materials suitable for use as tissue fillers while still maintaining the desirable properties of colloidal inks. We rationalized that these dynamic, viscoelastic and biodegradable colloidal gels could facilitate placement of the material, retention at the site of administration, and recovery of elasticity after placement. Our first effort employed combinations of poly(lactic-

co-glycolic acid) (PLGA) nanoparticles with opposite surface charges, which we demonstrated could support viable cells.(31) This work was followed by a study showing zero-order release and *in vivo* suitability for cranial defect repair.(32) Moving in a new direction, we then demonstrated that hyaluronic acid nanoparticles could form a dynamic, viscoelastic material believed to be the result of association of free surface chains, resulting in a colloidal gel viscosupplement that might improve upon the performance of traditional crosslinked or high molecular weight hyaluronic acid.(33) Having demonstrated some fundamental properties of colloidal gels, we then reported efforts to improve material performance by adding colloids such as hydroxyapatite,(34) or creating colloidal gels that could be chemically crosslinked after placement.(35) Today, we continue to explore the performance of colloidal gels *in vivo* as injectable bone or cartilage fillers, and we are refining material properties to create clinician-friendly materials that promote tissue regeneration.(36, 37)

The precursor properties of our materials are of critical importance to clinicians, perhaps even more so than the crosslinked solid mechanics, depending on the application. That is, it is important to have a material that is easy to place in the site and ensure that it will stay there, and that if new hydrogel precursor solutions have behaviors of other moldable materials that surgeons are used to implanting, they may be more likely to adopt the technology.

Translation of Technology to Surgeons

In designing new hydrogel technologies with clinical translation as an end goal, it is important to keep in mind the needs of the clinician and the patient throughout the process. The transition from lab bench to clinic can be an arduous process, and a potentially significant product could be completely ignored if the surgeon must acquire new skills or buy new equipment. Wilson *et al*.(38) proposed that surgeons are attracted to new medical technologies that can be learned by passive observation rather than hands-on training sessions, and thus can be easily adopted into their practice without disruption. The gap between scientific knowledge and clinical application is well known, and with decreasing time available for some clinicians to spend on research, there are less comparative studies being conducted.(39) New methods are being employed to shorten the learning curve associated with new medical technologies and surgical procedures. The use of social media outlets and live streaming has provided the ability for surgeons to collaborate on difficult cases and provide coaching between surgical teams from different continents.(40, 41) Although steps are being taken to ease the translation of new research into the clinic, it is always going to be easier to utilize a surgeon's current skill-set than to require training in a new technique.

Lack of consideration of the method for the physical placement of hydrogels in an intended application directly ignores the needs of the surgeon. In the example of *in situ* hydrogels for cartilage regeneration, some groups have proposed the use of liquid hydrogel precursors with zero yield stress to fill defects

before crosslinking.(42) The issue with this hydrogel precursor design is that it does not account for applications in which the defect may be angled, or in a hard to access area. *In vivo* studies generally employ ideal situations, such as a defect site that is perfectly cylindrical and applied to a single plane.(43) In contrast, real tissue defects are not perfectly cylindrical and uniplanar, as illustrated in Figure 2.2. *In situ* placement using a liquid hydrogel precursor solution with zero yield stress could become difficult as the material may leak after placement. In designing clinically translatable hydrogels, understanding the connection between rheological hydrogel precursor properties and the connection to surgical use is important for successful clinical translation.

Biomedical Hydrogel Perspective Summary

Over the past 10 years, we have evolved from using simple colloidal gels to more complex crosslinkable hydrogels for biomedical applications. A core philosophy of our team has focused on creating biomaterials capable of being translated from the lab to the clinic. A challenge of clinical translation is the poor adoption of new treatments by surgeons if the technique learning curve is too high. For the aforementioned reason, we have identified the handling properties of hydrogels, specifically the hydrogel precursor performance, as a crucial component of hydrogel design to allow future clinical translation.

Surgical Context

Injectability/Syringeability and Shear Properties

“Injectability” is a common buzzword among hydrogel publications to qualitatively communicate the ability of a material to flow through a syringe needle.(34, 44-47) Although prevalent, the use of this term is generally ambiguous with minimal quantitative information provided, as the injection pressure is strongly correlated with injection rate, needle gauge and length (i.e., the Hagen-Poiseuille equation). A similar term that has been used much less frequently in hydrogel publications is syringeability, which has become useful in our own publications to express the ability of the hydrogel precursor solution to flow through a syringe orifice rather than a needle.(2, 48) Both terms, injectability and syringeability, qualitatively express the ability to flow through a certain orifice size. In relation to the medical field, the performance of a material to easily flow from a needle or a syringe can dictate the delivery method and use by the surgeon. An injectable material (i.e., through a needle) could potentially have applications in laparoscopic surgery, whereas a syringeable material (i.e., through a syringe orifice) may require open surgery for placement.

The flow of a material in both situations is governed by the shear response exhibited when a force is applied as a function of flow rate. During extrusion, the material can undergo shear thinning or shear thickening. Shear thinning is where a material will exhibit a decreasing apparent viscosity with increasing rate of applied stress (i.e., shear rate), whereas shear thickening is where the material will exhibit an increasing apparent viscosity with increasing rate of applied stress.

The apparent viscosity can also be time dependent (i.e., thixotropy or rheopecty); however, the instantaneous change when a stress is applied is of more importance for application to biomedical materials as syringing or injection occurs over a short period of time. Hydrogel precursor solutions generally exhibit shear thinning behavior, which makes delivery from a syringe easier because as the shear rate increases in the needle, shear thinning will reduce the apparent viscosity and thus the relative resistance to flow (Table 2.1). Fakhari *et al*.(49) demonstrated shear thinning performance of colloidal gels comprised of hyaluronic acid nanoparticles by showing a decreasing viscosity with increasing shear rate. Similarly, Tsaryk *et al*.(50) indicated shear thinning performance of collagen/hyaluronic acid semi-interpenetrating network loaded with gelatin microspheres by determining the load required to inject the material through a 16-gauge needle, showing a decreasing force required after the material began to flow. We previously fit experimental rheological data to the Herschel-Bulkley equation to determine the shear response, which allowed for a quantitative and comparable method for the degree of shear thinning.(34, 35, 51) The need for shear thinning physical hydrogels was previously identified by Guvendiren *et al.*(52) in biomedical applications; however, the benefit of shear thinning behavior can be extended to all hydrogel precursors. Shear thickening behavior has generally been avoided in biomedical applications due to issues with extruding, although desired in some industry based applications.(53) After injection or syringing, it is important for the material to regain the original properties prior to

being injected or syringed. The time required for transition back to this starting time is referred to as the recovery time.

Placement and Recovery Time

Prior to injection or syringing, the bulk material is static and the microstructure is stable. After disruption, the material properties are in a state of disarray and take time to return to equilibrium. The time required for a material to return to the original equilibrium state is referred to as the recovery time, or the self-healing time.(52) The governing principle associated with the material recovery time is referred to as thixotropy, the reversible and time-dependent manifestation of viscosity-induced structural changes.(54-56) The recovery time of a syringed material is important in terms of initial placement. A material with a relatively slow recovery time could potentially have issues during placement as the material would initially be difficult to retain within the defect site. In terms of clinical usage, a fast recovery time after syringing is necessary for material manipulation or shaping, and especially for placement laparoscopically where it would be difficult to implement precautions for increased material retention. The recommended recovery time, and degree of material recovery for syringed or injected materials has yet to be defined and remains application dependent. We previously proposed the use of colloidal hydrogels comprised of hyaluronic acid, hydroxyapatite, and micronized native extracellular matrix as potential bone defect fillers.(57) The physical hydrogels presented were capable of nearly complete recovery of the storage modulus (G') within 5 minutes after disruption

(Table 2.1). Similarly, in a previous study, we reported hydrogels comprised of UV-crosslinking hyaluronic acid and hyaluronic acid nanoparticles, in which the precursor could recover their original storage modulus within 5 minutes.(35) Even faster recovery times on the magnitude of seconds have been reported.(45, 47, 58) Gaharwar *et al*.(59) demonstrated that an injectable nanocomposite hydrogel of gelatin and synthetic silicate nanoplatelets could be used for the treatment of internal hemorrhaging, as the hydrogel could recover the elastic gel strength in less than 10 seconds after disruption. In general, materials for biomedical applications should aim to have low recovery times to facilitate ease of use. After shearing and material placement, the material must remain in place, this retention is influenced by the yield stress of the material.

Retention and Yield Stress

The stress required for a material to begin to deform under an applied shear stress is referred to as the yield stress, and it plays an important role in material performance. The yield stress is entirely separate from the apparent viscosity, and these two terms must not be confused. The yield stress contributes to both the syringeability/injectability of the material (i.e., initial force required to generate flow) and retention within the defect after placement (i.e., no movement in the absence of applied force). In contrast, the apparent viscosity relates to the force required to continue dispensing from the syringe after flow has commenced. Implementation of yield stress to the hydrogel precursor solution can positively aid in material retention within the defect site after surgical placement. Figure 2.3

illustrates the placement of a hydrogel precursor solution *without* a yield stress compared to a hydrogel precursor solution *with* a yield stress (i.e., exhibiting paste or putty rheological properties). Precursor solutions enabling a yield stress will experience better retention in the defect site, allow for shape-specific fitting, and will be easier for surgeons to handle.(51) Various methods are currently used to determine a material yield stress as depicted in Figure 2.4. The most common methods include 1) empirical model fitting (e.g., Herschel-Bulkley), 2) determining the shear stress at the crossover point of the storage and loss modulus (G'/G"), and 3) determining the shear stress related to a pre-determined deviation of storage modulus from linearity. We previously used a three-parameter fitting technique to the Herschel-Bulkley model to report the yield stress of UV-crosslinking hyaluronic acid hydrogels embedded with hyaluronic acid nanoparticles, and reported yield stress values in the range of ~18 to 160 Pa (Table 2.1).(51) Similarly, in another study, we used the Herschel-Bulkley model to determine the yield stress of hydroxyapatite colloidal gels with either hyaluronic acid or chondroitin sulfate, the resulting yield stress ranged from ~1 to 1400 Pa.(34) Alternatively, Olsen *et al*.(60) demonstrated that hydrogels comprised of self-assembling telechelic proteins had a yield stress of ~1400 Pa using the G'/G" crossover method, and could be injected from a syringe through a 22-gauge needle. Similarly, Liu *et* al.(61), Gao *et al*.(62), and Yu *et al*.(63) used the G'/G" crossover method to determine yield strains of 9.8, 78, and 130%, respectively. Yield strain, similar to yield stress, is the strain at which a fluid begins to flow. We previously used the storage modulus deviation method, choosing a storage

modulus deviation of 10% from linearity, to determine the yield stress range of colloidal hydrogels comprised of hydroxyapatite and glycosaminoglycans from ~1 to 1400 Pa.(57) Gaharwar *et al*.(59) and Glassman *et al*.(46) similarly used the deviation from linearity method in determining the yield stress. As a general rule, yield stress values above 100 Pa are sufficient for material retention prior to secondary crosslinking.(2, 49, 59)

Hydrogel precursor solutions can be created with a yield stress by several different available options. Perhaps the easiest route to employ a yield stress is the addition of micro- or nano-sized particles, the reduction in available space results in a thicker consistency, and we have previously used this method to create a hydrogel precursor solution with a yield stress.(36) Dumas *et al*.(64) developed an injectable self-setting lysine-derived polyurethane scaffold encapsulating allograft bone particles (180 μm) for bone restoration. Allograft bone particles were added to the precursor solution at a concentration of 45% (w/w), providing a modest yield stress of 2.1 Pa. An alternate route to employ a yield stress to a precursor solution is the use of oppositely charged materials, where electrostatic interactions increase precursor consistency. Gaharwar *et al*.(59) used oppositely charged gelatin and silicate nanoplatelets to create injectable self-assembling hydrogels for treatment of internal hemorrhaging. The oppositely-charged gelatin-silicate nanocomposite hydrogels provided a yield stress of 2 to 89 Pa, depending on nanoplatelet concentration. Another potential avenue for achieving a precursor yield stress is the use of fast-acting click chemistry to create materials that self-heal after shearing. For example, Yu *et*

al.(63) proposed the use of a self-healing multi-block copolymer capable of quickly forming covalent bonds between acylhydrazines and aldehyde groups. Rapid covalent bond formation allowed for material healing after injection, creating a dynamic material with many potential applications to regenerative medicine.

Rheological Methods

The assessment of rheological performance can be attained by various rheological testing systems. For in-depth background information regarding the mathematical theories of rheological testing, an introductory polymer rheology textbook by Osswald *et al.(65)* is recommended. Briefly, the two most commonly used testing fixtures, cone-plate and parallel-plate, will be discussed, detailing their individual uses and strengths/weaknesses. The cone-plate fixture allows for a wide variety of rheological tests such as yield stress, creep, recovery time, oscillation, and ramp tests.(65) The wide variety of rheological tests can be attributed to the design of the cone-plate fixture, where an upper cone of a small angle, generally between 1-4°, sandwiches the material being tested between a flat bottom plate. Due to the small angle of the cone, the shear rate and shear stress across the sample is nearly constant, allowing for accurate material measurements. The disadvantage of the cone-plate system is that it is limited to small particle sizes (≤ 10 μm), and thus cannot be used for suspensions of larger particles. Alternatively, the parallel-plate fixture, which sandwiches the material being tested between two flat plates, is not limited by particle size. Due to the

design of the parallel plate fixture, materials with larger particle sizes (≥ 10 μm) can be tested. The disadvantage of the parallel-plate fixture is that the shear rate across the sample increases with radius, so the parameters obtained are average values over the range. while keeping in mind that these differences exist in comparing results between various studies. The cone-plate fixture is the recommended choice when performing a rheological test; however, in cases where the cone-plate fixture may not be used due to particle size, the parallel-plate fixture is recommended. The choice of testing apparatus, and the geometry of the probing fixture can influence the resulting data provided by a rheological test. Testing differences must be noted as sample measurements conducted by two separate studies using the same material and testing conditions, but different testing fixtures, can have varying results. It is necessary to report the choice of testing apparatus (e.g., cone-plate or parallel-plate), fixture geometry (e.g., 20 mm), and testing conditions, while keeping in mind that methodological differences exist in comparing results among various studies. The cone-plate fixture is the recommended choice when performing a rheological test; however, in cases where the cone-plate fixture may not be used due to particle size, the parallel-plate fixture is recommended.

Surgical Context Summary

The connection between rheological terminology and parameters observed in clinical practice is important for any researcher in developing the next generation of hydrogels intended for clinical adoption. In this section, we have

outlined the connection between injectability/syringeability and shear properties, material placement and recovery time, and material retention and yield stress to help bridge the gap between rheology and clinical relevance. Table 2.1 summarizes the rheological properties of published hydrogel precursor solutions. In general, we recommend that the design of *in situ* forming hydrogels for use in biomedical applications includes shear thinning properties that are application dependent for either injection through a needle or syringe orifice, incorporates an adequate recovery time after disruption to minimize any loss of material, and has a suitable yield stress (>100 Pa) to allow for material retention and shape fitting. Additional background information on rheological application has been provided, focusing on choosing the best testing fixture for the material being studied. The cone-plate fixture is recommended overall, but limited to materials with small particle sizes (≤ 10 μm), and the parallel-plate fixture is recommended for materials with larger particle sizes (≥ 10 μm). Implementing desired rheological performance in various hydrogel designs can be challenging, and considerations for implementing these properties are proposed below.

Hydrogel Rheology Properties

Paste and Putty Nomenclature

As previously stated, paste and putty nomenclature has long been used in medical products to distinguish basic rheological properties.(16) Medical professionals and the general public already have a common connection to these words and their distinguishing characteristics. The paste and putty description is

directly related to a material's rheological properties for placement, specifically the material's yield stress. A low yield stress material would exhibit paste-like properties and a high yield stress material would exhibit putty-like properties.(31, 66) Because of the pre-existing connection to paste and putty nomenclature, the biomedical hydrogel community would be wise to adopt these words in describing rheological characteristics.

The distinction between paste and putty performance, although related to yield stress, remains qualitative and has yet to be successfully defined. In part, this review aims to propose relative ranges of yield stresses for both paste and putty solutions for improvement of material reporting. In determining the yield stress range for a paste-like material compared to a putty-like material, we can utilize known materials to help in creating the distinction between the two designations. Samaniuk *et al.*(67) previously published yield stress values for common household items that qualitatively exhibit either paste or putty behavior for reporting the design of a novel rheometer, specifically the yield stress values for mayonnaise and Play-Doh. The yield stress of mayonnaise and Play-Doh, approximately 200 and 3000 Pa, respectively, can be used to help define the ranges for paste and putty distinctions. Using the yield stress of known household items and previous publications from our own group, we have proposed the range of 100 to 2000 Pa for paste-like materials and materials above 2000 Pa to exhibit putty-like properties. By reporting material yield stress in these parameters, it is possible to better connect the hydrogel community to clinicians using a common set of nomenclature.

Paste and Putty Application

The choice between paste and putty behavior for hydrogel precursors remains application dependent, and no “one size fits all” approach exists. Examples of low yield stress, paste-like hydrogel precursors, and high yield stress, putty-like hydrogel precursors will be explored and how they can be beneficial to different applications. Nucleus pulposus regeneration and ophthalmetry are two areas in which hydrogel use has been proposed.(68-71) The aforementioned applications generally propose precursor solutions to exhibit low to no yield stress for injection through a high-gauge needle; however, low yield stress, paste-like hydrogel precursor solutions may be ideal for such applications as they allow for injection through higher gauge needles while providing benefits tailored to the application desired.(72-74) High yield stress, putty-like hydrogel solutions are generally useful in applications where shape fitting is required, such as craniofacial bone regeneration.(75, 76) The higher yield stress precursor solutions and physical gels allow for better material shaping and directed tissue regeneration.

Herschel-Bulkley Model

Although paste and putty nomenclature qualitatively depicts low and high yield stress, the nomenclature alone does not provide enough information for an in-depth comparison. It is important for the hydrogel community to choose a standardized testing method that allows for a deeper look into the relationships

between material properties and rheological performance. When reporting rheological properties of new materials, it is beneficial to fit experimental data to common, pre-existing rheological models for comparison. The Herschel-Bulkley (HB) model is an ideal candidate to fill this need for the hydrogel community. The HB model was first introduced by Winslow Herschel and Ronald Bulkley in 1926 and provides a simple and general model to explain the behavior of a non-Newtonian fluid.(77) The HB model equation shown in Equation 1 relates the fluids shear stress (τ), to the yield stress (τ_0), consistency index (k), shear rate $(\dot{\gamma})$, and flow index (n).

$$\tau = \tau_0 + k\dot{\gamma}^n \qquad \text{(Equation 1)}$$

The fluid exhibits solid properties when $\tau < \tau_0$, and for $\tau > \tau_0$, exhibits shear thinning when $n < 1$ and shear thickening when $n > 1$. The HB model is an attractive option for the hydrogel community because it provides a general model that includes variables for both yield stress and shear response. Previous groups that have characterized hydrogel precursor solutions have reported that experimental results respect the HB model.(78-80) For reporting hydrogel precursor properties, quantification of yield stress and shear response adequately provides information for comparison of materials within the hydrogel community.

Summary

Understanding the nomenclature between clinicians and scientists is important for bridging the gap between the two fields. By incorporating the nomenclature, and defining the parameters, it is possible to better connect the two sides and eliminate the possibility of failed medical translation due to issues of poor surgeon adoption. In this section, we have defined the yield stress attributing to paste and putty nomenclature as the range of 100 to 2000 Pa, and materials above 2000 Pa, respectively. The application dependency of paste and putty precursors were explored, and the Herschel-Bulkley model was proposed as a simple model for reporting rheological parameters such as yield stress. The recommended range for paste and putty materials, and use of the Herschel-Bulkley model, will hopefully increase the reporting of rheological parameters for clinical translatability.

Hydrogel Precursor Considerations

Chemically Crosslinked Hydrogels

Chemically crosslinked hydrogels are distinguished by the creation of covalent bonds between polymers to form an interconnected network.(21) A number of varying methods have been proposed to achieve the crosslinked network, the most common being photo-initiation, and enzymatic/reaction based technologies.(81-83) Various groups have proposed new and insightful ways for the development and application of chemical hydrogels for regenerative medicine; however, the delivery method of the pre-crosslinked form is often

unclear and under-characterized.(83, 84) Choi *et al*.(85) developed a novel visible light crosslinking chitosan hydrogel encapsulating collagen II and TGF-β3 for *in situ* cartilage regeneration. The technology developed has shown promise for the reported application; however, the intended delivery mechanism and subsequent material mechanical characterization were not clearly identified. In designing chemically crosslinked hydrogels for regenerative medicine, it is important to establish a delivery method suitable for the intended user that facilitates the ease of placement, and characterize these rheological properties.(86) Although some groups have proposed circumventing the need for *in situ* placement by crosslinking the hydrogels in Teflon molds, the pre-crosslinking method arguably diminishes the potential of this technology.(87) Although the end result of photo-initiated and reaction-based *in situ* hydrogels are similar in many ways, the considerations for designing their placement are distinct.

Photo-initiated hydrogels combine the positives of user-defined crosslinking initiation with the ability to form tunable covalent bonds to modulate crosslinking density.(81, 88) The downside of this method involves the need for an outside light source for initiation, generally requiring an open surgical site. The necessity of the open surgical site limits the available applications of photo-initiated hydrogels; however, an open surgical site offers many potential benefits for precursor solution placement. Photo-initiation allows for complete control over the precursor placement, enabling possible shaping and defect-fitting if the precursor exhibits the correct rheological properties. Earlier, we proposed the

idea of a photo-initiated hydrogel that could allow for easier surgical placement in cartilage defects if the precursor solution exhibited a sufficient yield stress, enabling a surgeon to form-fit the material to the defect site before crosslinking.(2, 35, 48, 89) A potential limitation of photoinitiated hydrogels is the requirement for light penetration, thus opaque materials may encounter crosslinking issues due to limited light penetration. Reaction-based hydrogels, which are not limited to opacity issues like photoinitiated hydrogels, are generally initiated by the mixing of two solutions to initiate crosslinking and subsequent hydrogel formation.(24) Due to the need for achieving a well-mixed solution, many studies utilized low viscosity, zero yield stress precursor solutions.(90, 91) Although these hydrogels have shown great promise in promoting cell viability and proliferation, the these hydrogels may encounter limitations in the intended surgical application. Employing a yield stress to the mixed precursor solution can greatly increase the available applications for reaction-based hydrogels.(44, 92) Special considerations need to be made for reaction-based hydrogels that employ a precursor yield stress. Issues arise in achieving a well-mixed solution, and an external mixing system such as a dual-syringe and mixing tip may be required. For both photo-initiated and enzymatic/reaction hydrogel precursor solutions, it is strongly recommended to characterize and report the yield stress, recovery time, shear response, and gelation time at physiological conditions.

Physically Crosslinked Hydrogels

Physical hydrogels are classified as hydrogels held together by polymer entanglements and/or secondary forces, and unlike chemical hydrogels, no formation of covalent binding occurs.(21) Some common methods for forming physical hydrogels are based on charge, colloidal flocculation, peptide interactions, and physical thermogelation.(25, 47, 93-97) Compared to chemically crosslinked hydrogels, physical hydrogels require specific rheological considerations as chemical binding does not occur post-placement. Physical hydrogels that exhibit a moderate yield stress, shear thinning behavior, and quick recovery time are ideal for biomedical applications.(34) Many research groups proposing the use of physical hydrogels for biomedical applications have characterized a wide variety of rheological properties.(49, 59) Lu *et al*.(47) is a prime example of a physical hydrogel mechanical characterization study using rheology, providing information on shear response, gel recovery time, and yield stress/strain.

Physical hydrogels based on charge, colloidal flocculation, and peptide interactions require the same rheological considerations. In designing physical hydrogels for biomedical applications, certain key rheological properties must be characterized and reported. Evaluation of yield stress, recovery-time, and shear response are strongly recommended when reporting new physical hydrogels to the community. Additionally, physical hydrogels for biomedical applications must be tested at body temperature as a proof of concept. Physical hydrogels utilizing thermogelation require the same considerations as the charge, colloidal, and

peptide hydrogels; however, additional tests must be taken into consideration. Viscoelastic properties of thermally activated hydrogels should be mapped at varying temperature, and the time required for gelation at body temperature should be characterized.

Combinational Crosslinking Hydrogels

Combinational hydrogels are developed with the intention of utilizing both physical and chemical crosslinking principles in mind. Hydrogels have historically been separated as either chemically or physically crosslinked; however, there are potentially great benefits for hydrogel designs incorporating both physical and chemical crosslinking principles.(98) Lu *et al.*(4) proposed the use of a combinational crosslinking hydrogel utilizing both self-assembling peptides and secondary UV-crosslinkable hyaluronic acid to form covalent bonds. Other groups have proposed the use of combinational hydrogels, such as polymer entanglements combined with UV-crosslinking, and thermogelation combined with reaction based crosslinking.(98, 99) The rheological considerations for the combinational hydrogel precursors should incorporate the necessary experimental tests for both physically and chemically crosslinked hydrogels, as previously mentioned.

Crosslinking Hydrogels Summary

In this section, considerations for hydrogels incorporating chemical, physical, and combinational crosslinking mechanisms have been summarized. A general outline of rheological considerations and characteristics to report have been provided for each of the mentioned cases. The implementation of yield stress to precursor solutions can positively impact all hydrogel types and allow for an easier translation from the lab to clinic, while minimizing surgeon learning curve.

Conclusions

In the current review, we have summarized the need for hydrogel precursor rheological characterization and the advantage of implementing precursor solutions exhibiting yield stress for surgical placement. This review has explored the gap in translation between hydrogel technology and clinical application, and identified the rheology of the hydrogel precursor solution as an often overlooked, yet crucial, design consideration. Basic rheological principles and their connection to the medical world have been explored, providing examples of recent research in application-dependent hydrogel design. Common pre-existing nomenclature of paste and putty behaviors were introduced for explaining low and high yield stress precursor properties, and the Herschel-Bulkley equation was proposed as the model to be used by the hydrogel community in reporting rheological properties for comparison. Considerations for hydrogels utilizing chemical, physical, and combinational crosslinking

mechanisms were explored to better inform the community in designing new hydrogel materials for ease of implantation and surgeon adoption.

Hydrogels proposed for tissue engineering and regenerative medicine applications ultimately aspire to translate from the lab bench to the clinic. The design and intended placement of hydrogels may be tailored specifically with the surgeon in mind, minimizing the surgeon learning curve to ultimately improve translation. An emphasis within the hydrogel community on reporting rheological properties of hydrogel precursor solutions is the first step for meeting the clinical need. By utilizing the Herschel-Bulkley equation, the hydrogel community can easily compare rheological properties in a general and simplified manner that minimizes the need for an in-depth understanding of rheology. By better characterizing and reporting rheological performance of hydrogel precursor solutions, the community can begin to work toward theoretical explanations rather than relying on empirical correlations. By quantifying relationships rooted in fundamentals, future research will allow for better prediction and rational design of precursor solutions. Furthermore, research into precursor rheology will directly benefit other areas of research such as 3D bioprinting applications, which rely on achieving a specific yield stress for extrusion, a hot area in bioink research today.(100-102) We suggest a dialogue bringing together experts in both non-Newtonian fluids and hydrogels, to facilitate an understanding of how to characterize and design better biomaterials. This dialogue will help to bridge the gap in knowledge regarding non-Newtonian rheology and establish new collaborations across different fields.

Chapter 3: Colloidal Gels with Extracellular Matrix Particles and Growth Factors for Bone Regeneration in Critical Size Rat Calvarial Defects[2]

Abstract

Colloidal gels encapsulating natural materials and exhibiting paste-like properties for placement are promising for filling complex geometries in craniofacial bone regeneration applications. Colloidal materials have demonstrated modest clinical outcomes as bone substitutes in orthopedic applications, but limited success in craniofacial applications. As such, development of a novel colloidal gel will fill a void in commercially available products for use in craniofacial reconstruction. One likely application for this technology is cranial reconstruction. Currently, traumatic brain injury (TBI) is often treated with a hemi-craniectomy, a procedure in which half the cranium is removed to allow the injured brain to swell and herniate beyond the enclosed cranial vault. The use of colloidal gels would allow for the design of a pliable material capable of expansion during brain swelling, and facilitate cranial bone regeneration alleviating the need for a second surgery to replace the previously removed hemi-cranium. In the current study, colloidal nanoparticles of hydroxyapatite (Hap), demineralized bone matrix (DBM), and decellularized cartilage (DCC) were combined with hyaluronic acid (HA) to form

[2]Published as: Townsend JM, Dennis SC, Whitlow J, Feng Y, Wang J, Andrews B, Nudo RJ, Detamore MS, Berkland CJ. Colloidal Gels with Extracellular Matrix Particles and Growth Factors for Bone Regeneration in Critical Size Rat Calvarial Defects. *The AAPS Journal*. 2017;19(3):703-11. doi: 10.1208/s12248-017-0045-0

colloidal gels with desirable rheological properties ($\tau_y \geq 100$ Pa). BMP-2 and VEGF growth factors were included to assess extracellular matrix (ECM) contribution of DBM and DCC. The HA-Hap (BMP-2) and HA-Hap-DCC group had 89 and 82% higher bone regeneration compared to the sham group, respectively ($p < 0.01$). Material retention issues observed may be alleviated by implementing chemical crosslinking. Overall, DCC may be a promising material for bone regeneration in general, and colloidal gels may hold significant potential in craniofacial applications.

Introduction

Colloidal gels represent a promising class of injectable materials for use in tissue engineering and regenerative medicine applications because of their high water content, self-assembly, tunable mechanical properties, and implementation of physical crosslinking for minimally invasive delivery.(35) The use of physical crosslinking principles in the development of colloidal hydrogels has resulted in the creation of highly tunable rheological properties capable of exhibiting yield stress for surgical placement and material recovery after injection.(47, 49, 52) In our previous studies utilizing colloidal gel technologies, these properties have been mapped using polymers and colloidal particles to achieve “paste-like” properties ideal for surgical placement.(34, 35) One clinical specialty that will greatly benefit from colloidal gel technology used for bone regeneration is craniofacial surgery.(103) Previous studies have demonstrated that similar colloidal gels have shown promise in bone tissue engineering

applications, highlighting the use of biodegradable natural materials as an attractive alternative to current commercially available options.(31, 66)

Current commercial products have demonstrated a long track record of clinical success in orthopedic long bone regeneration; however, many craniofacial applications are limited by current product designs and physical properties.(16) In particular cranial reconstruction has been problematic due to the large contoured surface area, the constant repetitive pulsation of the underlying dura/brain, limited soft tissue coverage options, and sensitivity of the underlying brain tissue to exothermic biomaterial processes. Commercially available products such as DBX (MTF/Synthes), Dynagraft II (Integra Orthobiologics), Grafton® Gel (Osteotech), and Puros® DBM (Zimmer) have had limited success in calvarial reconstruction due to the low availability of propriogenic stem cells in the cranial diploic space as compared to that of long bones and the inability of all biomaterials to overcome a critical cranial defect size. These limitations of current commercial bone products have led to the need for new materials; and as such, new and innovative approaches should be considered for future cranial bone regenerative biomaterials.

Current bone products focus heavily on the use of micron sized demineralized bone matrix (DBM) colloids as a tissue matrix/scaffold for the promotion of cranial bone formation. Since these materials require bone ingrowth from the surrounding peripheral cranial margins, critical cranial defect size limits the ability to reconstruct large skull defects. To address the limited bone regeneration associated with demineralized bone techniques, various synthetic

and raw materials, such as extracellular matrix (ECM) components, have been proposed for tissue regeneration such as hydroxyapatite (Hap), Bioglass, hyaluronic acid (HA), DBM, and decellularized cartilage (DCC).(104, 105) Growth factors such as bone morphogenetic protein (BMP)-2 and vascular endothelial growth factor (VEGF) have shown further promise in bone regeneration, and can be used both separately or by dual delivery.(106, 107) The majority of craniofacial skeleton forms by intramembranous (IM) ossification; however, leveraging endochondral (EC) ossification approaches for regeneration of craniofacial bone may provide novel medical treatment avenues.(108)

A clinical application that could greatly benefit from a medical product exhibiting paste-like rheological properties and bone regenerative potential is the surgical management of severe traumatic brain injury (TBI). TBI resulting from a severe closed head injury or stroke often causes life-threatening brain swelling.(109) Decompressive hemi-craniectomy is a life-saving treatment to alleviate brain swelling. In this procedure, approximately half of the patient's calvarial bone is removed allowing the brain to swell and herniate beyond the confines of the closed calvarial vault.(110) This skin is draped over the herniating brain and the skull is left removed for an average of 80 days before it is restored/replaced once swelling subsides in a second surgical procedure, cranioplasty.(111) This surgical procedure gained popularity with its utilization and proven beneficial outcomes in the treatment of active duty service who suffer severe head trauma in recent military conflicts. These soldiers represent a group that has been greatly impacted by TBI, referred to as the "invisible war on the

brain”(112) and accounting for 30% of military hospitalizations during modern warfare.(113)

A poorly understood neurologic condition termed “syndrome of the trephined” (SoT) often results in TBI patients who undergo hemi-craniectomy. SoT is also termed “sinking skin flap syndrome” as a result of the sunken, concave appearance of the skull at the sight of hemi-craniectomy that develops as TBI patients await cranioplasty.(114, 115) SoT is associated with symptoms such as mood changes, fatigue, headaches, dizziness, fine motor dexterity problems, and difficulties concentrating.(116) Interestingly, SoT neurologic deficits are immediately reversible with a cranioplasty procedure where the missing cranial bone is replaced/restored and the underlying sunken cerebral tissue is allowed to re-expand within the calvarial vault. The symptoms typically return should the cranioplasty reconstruction require future removal such as the case of infection.

Current surgical management of TBI requires a two staged procedure, the initial hemi-craniectomy and the reconstructive cranioplasty. They are typically performed months apart which delay recovery and rehabilitation and increasing cost and risk due to an additional surgery.(117, 118) Research on materials for TBI treatment has generally focused on reducing brain swelling(32, 119) or blocking tissue regeneration between the dura and periosteum for safer transition to cranioplasty.(111) Colloidal gel technology has the potential to provide a single surgical treatment for severe TBI cases in which the material is implanted with

the initial surgery, remain pliable during brain swelling, and provide a combination of materials and growth factors to regenerate bone over time.

To effectively develop a material capable of providing a single surgery for TBI treatment, we must first identify an effective colloidal gel formulation that can regenerate bone across a critical size calvarial defect. After identifying a colloidal gel that can regenerate bone in a critical size defect, the regeneration time can be tuned specifically for treatment of TBI. The objective of this work was to evaluate colloidal gels composed of natural materials and growth factors for regenerating calvarial bone in a critical size calvarial defect. The use of natural materials is our first attempt with this type of formulation, and represents a next generation colloidal gel from our previously published work by Wang *et al.(103)* Hap, DBM or DCC nanoparticles were evaluated in physically crosslinked colloidal gel formulations with HA to create paste-like materials with desirable yield stress for injection in a bone regeneration application. Colloidal gel material characterization studies have previously been published by Dennis *et al.(37)*, colloidal formulations with desirable mechanical properties were chosen for evaluation in the current study. Colloidal gels were loaded with or without BMP-2 and VEGF to evaluate the extent to which growth factors would facilitate bone regeneration. We hypothesized that the colloidal gel formulations would regenerate bone at the defect site, and that the addition of DCC particles would increase regenerative capabilities.

Materials and Methods

Materials

Hydroxyapatite (Hap) was purchased in powder form (D_{avg} ≤ 200 nm; Sigma-Aldrich, St. Louis, MO). Hyaluronic acid (HA, Mw = 1.01-1.8 Mda) (Lifecore Biomedical, Chaska, MN) was purchased as a sodium salt. Human demineralized bone matrix (DBM) was purchased from Biomet (Warsaw, IN). Human VEGF (Cat# 100-20) and human BMP-2 (Cat# 120-02) were purchased from PeproTech (Rocky Hill, NJ).

Preparation of Decellularized Cartilage (DCC)

Ten porcine knees were purchased from a local abattoir (Bichelmeyer Meats, Kansas City, KS). Articulating hyaline cartilage was harvested from mixed-breed, mixed-sex hogs 7-8 months of age. Harvested cartilage was coarse ground using a cryogenic tissue grinder (BioSpec Products, Bartlesville, OK) and packed into dialysis tubing (3500 MWCO) and decellularized using an adapted version of our previously established method using osmotic shock, detergent, and enzymatic washes.(120-122) Briefly, dialysis packets containing DCC were placed in a hypertonic salt solution (HSS) overnight at room temperature under agitation (70 rpm). The packets were then subjected to 220 rpm agitation and washed in triton X-100 (0.01 v/v) followed by HSS, with DI washes between each step, to permeabilize intact cellular membranes. Tissue packets were then treated with benzonase enzyme solution (0.0625 KU/mL) at 37°C overnight followed by DI washing, and then treated with sodium-lauroylsarcosine (NLS, 1%

v/v) overnight to lyse cells and denature proteins. After NLS treatment, the tissue was washed in DI water, and then in 40% (v/v) ethanol at 70 rpm. Tissue packets were then subjected to organic exchange resins and to remove organic material from solution. Tissue packets were then washed in a saline-mannitol solution at 70 rpm followed by 1 hour of DI washes. The tissue was then removed from the dialysis packets and frozen.

After the decellularization process, DCC particles were lyophilized and cryoground with a freezer-mill (SPEX, SamplePrep, Metuchen, NJ). Cryoground DCC was then sieved (Spectra/Mesh Woven Filters, Spectrum Laboratories, Inc., Rancho Dominguez, CA) ($D_{avg} \leq 200$ nm) and stored at -20 ºC for later use. Decellularization was confirmed by PicoGreen (Thermo Fisher Scientific, Waltham, MA, P7589) assay to determine DNA content. The particle size ranges of DCC and Hap were confirmed using dynamic light scattering (Brookhaven, ZetaPALS) as previously described.(34)

Preparation of Colloidal Gels

Colloidal gels were prepared as previously described.(34) Briefly, 20 mg of HA, 800 mg of Hap, and 150 mg of ECM (DCC or DBM) materials were weighed dry and combined. Dry combinations were dispersed in 1 mL of phosphate buffered saline (PBS, Sigma-Aldrich, P3813) solution. Dry powder formulations were sterilized using ethylene oxide gas prior to use *in vivo*. PBS and growth factors were mixed together (25 µg/mL) in select groups before dispersion of dry powder combinations. Samples were allowed to reach ambient

conditions for 2 hours before implanting. Formulations are reported as material components with the addition of growth factors in parentheses [e.g. HA-Hap (VEGF)].

Environmental Scanning Electron Microscopy (ESEM)

Colloidal gels were imaged using an FEI Quanta 200 scanning electron microscope (FEI Company, Hillsboro, OR) with a tungsten filament electron source. The gaseous secondary electron detector (GSED) was used in environmental mode. Samples were imaged at a magnification of approximately 500x, and an accelerating voltage of 15 kV.

Rheological Testing

Colloidal gel rheological properties were mapped using a controlled stress rheometer (TA-Instruments, AR2000). All measurements were performed at a gap distance of 500 μm using a 20 mm diameter roughened stainless steel plate geometry. Samples were tested at 37 °C. Initially, an oscillatory stress sweep from 1-10,000 Pa was performed at a constant frequency of 1 Hz to determine the linear viscoelastic (LVE) region for the colloidal formulations. The yield stress was defined as the oscillatory stress corresponding to a 15% departure of the storage modulus (G') from the LVE region.

Animal Model and Surgical Method

Mixed sex SAS Sprague Dawley rats were raised in house to an age of 7-10 weeks and randomly assigned to treatment groups prior to surgery. Animal experiments were approved by the Institutional Animal Care and Use Committee of the University of Kansas Medical Center (protocol #2015-2303). A posterior incision along the periphery of the skull was created to peel back and suture the skin and periosteum to the anterior portion of the skull. A single critical size 7.5 mm defect was created on the center of the calvarial bone using a cylindrical drill. The calvarial disk was carefully removed leaving the dura matter intact. After creation of the defect, approximately 50 µL of material was used to fill the site via syringe (Fig. 3.1A). The skin and periosteum were then draped over the defect site and sutured in place to hold the material during the healing process. The sham group received the same surgical procedure without the addition of any further treatment. Repaired tissue was harvested at 8 weeks' post-implantation and analyzed. A sample size of 5 rats was used in BMP-2 containing groups, and a sample size of 4 rats was used in all other groups.

Micro-computed Tomography (µCT)

Micro-computed tomography analysis was performed on explanted rat calvarial sections to visualize and quantify new bone formation. An Xradia MicroXCT-400 system was used with a 50 kV X-ray source at 7.9 W. µCT images were reconstructed to generate 3D models for analysis of new bone formation. Avizo-Fire computational software (FEI Company) was used to generate 3D

images and quantify volumes. New bone was confirmed using pre-existing calvarial bone as the threshold, separating original Hap from new bone formed. Hap nanoparticles were partitioned from bone on the basis that any material above the bone threshold must be original Hap. Quantified new bone volume is expressed as a total (mm^3) within the 7.5 mm diameter defect site.

Histology and Immunohistochemistry

Harvested calvarial bone samples were fixed in 10% phosphate buffered formalin for 48 hours then stored in 70% ethanol for long term. Tissue sections were then decalcified using Calrite media (Thermo Fisher Scientific, 22-046-339) for 3 weeks before dehydrating in a grade series of ethanol to xylenes, and then embedded in paraffin wax. Sections of 5 μm were obtained using a microtome (Thermo Fisher Scientific, HM 355S) and affixed to microscope slides. Before staining, tissue sections were dewaxed in xylene and rehydrated in graded (i.e., 100 to 70%) ethanol followed by deionized water. Slides were stained with hematoxylin and eosin (H&E) (Abcam, Cambridge, UK, H-3404) for cell infiltration and new bone formation.

Immunohistochemistry was employed to visualize the distribution of collagen I (Novus Biological, Littleton, CO, NB600-408, 10 μg/mL), collagen II (Novus Biological, NBP2-33343, 5 μg/mL), osteocalcin (Abcam, ab93876, 5 μg/mL), and α-smooth muscle actin (Abcam, ab5694, 10 μg/mL). Briefly, tissue sections were dewaxed in xylenes and rehydrated in a graded series of ethanol (100-70%) to DI water. Antigen retrieval was performed enzymatically with

proteinase K (Abcam, ab64220, 20 µg/mL) for 15 minutes at 37 °C. Following enzymatic retrieval, sections were blocked with 0.3% hydrogen peroxide (Abcam, ab94666) for 10 minutes, 10% normal horse serum (Vector Labs, Burlingame, CA, PK-6200) for 20 minutes, 5 % bovine serum albumin (Sigma, A9647) for 20 minutes, and avidin/biotin blocking (Vector Labs, SP-2001) for 15 minutes each. Sections were incubated in one of the aforementioned primary antibodies for 1 hour. Post-primary antibody incubation, sections were washed in PBS with Tween-20 (Sigma-Aldrich, P3563) solution for 5 minutes between each step. Sections were then incubated with biotinylated horse anti-mouse/rabbit IgG (Vector Labs, PK-6200) for 30 minutes. Sections were then incubated with VECTASTAIN Elite ABC solution (Vector Labs, PK-6200) for 30 minutes, before being developed using DAB (Vector Labs, SK-4100) for 2 minutes. DAB enhancing solution (Vector Labs, H-2200) was used for 10 seconds before counter-staining with hematoxylin QS (Vector Labs, H-3404) for 1 minute. Bluing solution (Thermo Fisher Scientific, 7301) was used for 3 minutes. Finally, sections were dehydrated in a grade series of ethanol (95-100%) to xylenes before mounting. Negative controls for each immunohistochemical staining batch were included.

Statistical Methods

GraphPad Prism (Graphpad Software Inc, La Jolla, CA) statistical software was used to conduct all statistical analyses. Groups were analyzed using a one-way analysis of variance with groups of factors. Dunnett's test was used to

compare groups to the sham control group. Tukey's HSD test was used for comparing between groups in the rheological analysis. Results were considered significant at a level of $p < 0.05$. Results are reported as the mean ± standard deviation.

Results

Rheological Analysis

Figure 3.1B shows colloidal material groups being shaped, and ESEM images of the gel microstructure. Colloidal material shaping demonstrated that all formulations exhibited some degree of yield stress. Representative rheometer traces for each colloidal formulation have been provided (Fig. 3.2A-C). The yield stress of the HA-Hap-DBM was 4.6 times higher than the HA-Hap formulation ($p < 0.01$) (Fig. 3.2D). Post-hoc analysis (Tukey's HSD) showed no statistically significant difference between HA-Hap and HA-Hap-DCC, or between HA-Hap-DBM and HA-Hap-DCC formulations.

Microcomputed Tomography (μCT) Analysis

The HA-Hap (BMP-2) and HA-Hap-DCC groups had 89 and 82% higher regenerated bone volume compared to the sham, respectively (Fig. 3.3A, $p < 0.01$). Peripheral bone growth was noted in all groups, and large peripheral bone growth into the defect site in the HA-Hap-DCC group without the addition of growth factors (Fig. 3.3B). Large bone island formation was noted in the sham and VEGF-containing groups, excluding the group containing DCC. Bone islands

observed in all groups were very thin compared to the native bone, and did not contribute significantly to regenerated bone volume.

Histological Analysis

A distinctive soft tissue formation spanning the defect site was observed in all colloidal gel formulations (Fig. 3.4). The presence of conglomerated colloidal particles was observed in all groups. Bone at the defect periphery was noted in all groups with new bone forming toward the dural side of the defect. The H&E stain confirmed the differences in new bone formation versus original colloidal particles identified from the μCT analysis. Histological analysis of all samples showed general trends of bone formation encapsulating conglomerated colloidal particles in HA-Hap groups with and without addition of growth factors. VEGF containing groups tended to have thicker soft tissue formation spanning the defect site compared to groups without the addition of growth factors and the sham. The HA-Hap-DCC group and the BMP-2 groups had more peripheral bone growth into the defect site compared to the sham and VEGF-containing groups.

Immunohistochemical (IHC) Analysis

Visual results of all samples stained for COL1 show substantial deposition of COL1 in the tissue spanning the defect site using peripheral bone for reference (Fig. 3.5). COL2 deposition in all groups was near non-existent in the tissue spanning the defect site, except for DCC groups with addition of growth factors, with the DCC (BMP-2) group in particular showing more regions of collagen II

than the DCC (VEGF) group. COL2 deposition in groups containing DCC and growth factors resulted in positive staining tissue pockets within the defect site; however, this was not seen in DCC samples without growth factors. OCN staining was similar to COL1 staining in that all groups showed positive antibody staining throughout the defect site using the peripheral bone as a reference. αSMA staining was positive only in the soft tissue spanning the defect site and no staining in the bone portion as expected.

Discussion

The current study was the first to use naturally derived decellularized cartilage extracellular matrix for regeneration of calvarial bone.(108) Colloidal gels formulated of naturally derived ECM materials were evaluated with and without growth factors to determine osteogenic potential *in vivo*. The focus of this work in developing colloidal gels with physical crosslinking properties for ease of placement and pliability during the healing process is ideally positioned for the treatment of TBI after hemi-craniectomy.(34, 35) The proposed work is one of the few to propose a material capable of providing a single-surgical method for severe TBI treatment, eliminating the need for a second surgery to reclose the cranial vault.(123) A single-surgical intervention for TBI has great implications for increasing the quality of life for the people suffering from this issue, and decreased time for rehabilitation. In developing these colloidal materials, our team has proposed the use of nanoparticle-size DBM and DCC as natural materials for the promotion of new bone growth.

Colloidal gels exhibiting a yield stress sufficient to create a paste-like consistency may have great clinical relevance for material placement and retention. Colloidal gels rely on physical interactions and the presence of a suitable yield stress in lieu of covalent crosslinking for material retention. The formulations presented in the current study were all capable of forming a paste-like material, and the addition of ECM materials further increased the yield stress observed. ESEM images of the gel microstructure indicated that the addition of ECM particles reduced cavitation, contributing to the mechanical stability. An increased yield stress in colloidal gels has implications for the improvement of mechanical performance in surgical placement and retention in the defect site.(35) Although rheological testing confirmed the existence of a noticeable yield stress in all formulations, challenges with material retention were observed in the current study. In all cases, the majority of migrated material had moved anteriorly, possibly due to the normal head grooming motion of rats. Alternatively, the migration of Hap particles can possibly be attributed to material disintegration due to the lack of gel crosslinking after placement. The post-μCT analysis allowed for the ability to better assess regenerative capabilities by quantifying the volume of bone excluding the colloidal material, while subsequently visualizing the two. Other groups have previously used similar techniques for eliminating the quantification of non-bone material;(124) however, it is not uncommon to report regenerated new bone volume including the added material.(3) The result of the DCC material group without growth factors supports the idea that cartilage can

be used as a raw material for use in a paste-like application for calvarial bone regeneration.

Aggregation of Hap particles was noted in all samples analyzed, suggesting interaction between Hap nanoparticles to form larger clusters. Bone growth around the Hap clusters was visualized by H&E stain, supporting the osteoconductive properties of Hap. Possible osteoinductive potential was observed in the form of new bone islands throughout the defect site without the presence of Hap particles; however, bone island formation was also noted in the sham group. In all samples, a noticeable tissue had formed throughout the defect site. Small pockets of positive COL2 staining was noted in the DCC group containing BMP-2, leading to the suggestion that growth factor addition had a negative role on cell differentiation in the presence of the material DCC. The result may potentially be attributed to competing effects of DCC and BMP-2, or a synergistic effect of chondrogenesis rather than osteogenesis leading to delayed bone regeneration. COL2 deposition was not observed in the group containing DCC without growth factors, suggesting that including DCC may have provided osteoinductive potential. Consistent positive staining in all groups for COL1 and OCN can most likely be attributed to the common material HA-Hap in all groups. Additionally, results of αSMA staining showed a positive response in the soft tissue portion of the defect site; however, increased blood vessel formation was not observed in VEGF treated groups. Addition of BMP-2 did not produce the bone regeneration that had been previously observed in similar studies in rat calvarial defects. Cowan *et al.*(125) observed a significant increase in bone

formation with the addition of 30 µg/mL of BMP-2 (0.59 µg total); however, this was not observed in the current study using 25 µg/mL of BMP-2 (1.25 µg total). The differences observed emphasize the value of future growth factor dose response studies. The low amount of new bone regeneration in growth factor-containing groups could possibly be due to a fast release from the defect site, causing a low response to available stem cells. Future studies including growth factors will include a controlled release mechanism for optimal delivery, and characterizing growth factor release *in-vitro*, as the release profile would have been of great value in the current study.

The addition of natural materials, i.e., DBM or DCC, had unexpected results in terms of bone regeneration potential. On average, the addition of DBM did not increase the regenerative potential compared to HA-Hap hydrogels, whereas addition of DCC had produced greater bone regeneration on average compared to DBM groups. DCC samples without growth factors were observed to have large amounts of peripheral bone growth, suggesting potential for DCC in calvarial bone regenerative approaches. Regenerated bone volumes of all groups tested in the current study were within the range of previously published studies in the area, and on average the HA-Hap (BMP-2) and HA-Hap-DCC group had more regenerated bone volume.(124, 126) Other groups studying the use of cartilage ECM for bone regeneration observed similar findings compared to the current study. In a study by Visser *et al.*(127) using decellularized cartilage ECM particles embedded in gelatin methacrylamide hydrogels found mineralized bone surrounding hypertrophic cartilage. Similarly, Gawlitta *et al.(128)* found that

bone formation was greatly enhanced by the presence of mesenchymal stem cells in decellularized cartilage ECM scaffolds. The collective results from the studies previously mentioned and the current study further support the use of DCC in bone regeneration applications. Caution should be taken in comparing the results of the current study due to the randomized sex study design. The National Institute of Health (NIH) notice (NOT-OD-102) “Consideration of Sex as a Biological Variable in NIH-funded Research” has identified an over-reliance on male animals and cells in research. The random use of both sexes in the current study attempts to follow NIH guidelines to eliminate sex as a variable.

Poor retention of growth factors and colloidal materials in the defect site was observed in the current study. Retention issues may be fixed by implementing a covalent crosslinking mechanism after material placement. A tunable crosslinking mechanism would effectively provide material stiffness and allow for recovery after non-plastic deformation. The crosslinking can be tuned accordingly to create hydrogels that remain pliable enough for application in the treatment of TBI. In future studies, colloidal materials encapsulated in covalently crosslinked hydrogels will be explored for application to craniofacial bone regeneration.

Conclusion

Colloidal gels composed of polymers and tissue particles represent a promising material for bone regenerative approaches, specifically in their ability

to exhibit paste-like properties for surgical placement. The study evaluated bone regeneration of critical size (7.5 mm) rat calvarial defects using colloidal gels comprised of hyaluronic acid, hydroxyapatite, and tissue particles (DCC or DBM) with and without the addition of growth factors (BMP-2 and/or VEGF). All colloidal formulations exhibited suitable yield stress for material placement, and an increased yield stress performance with the addition of DBM or DCC particles. Significant bone volume regeneration was observed in the HA-Hap (BMP-2) and HA-Hap-DCC group compared to the sham defect after 8 weeks. The results suggest that the material DCC has osteogenic potential for bone regeneration applications. Colloidal gels incorporating natural ECM materials have promise for calvarial bone regeneration applications.

Chapter 4: Decellularized Cartilage-Based Hydrogel Encapsulating Osteoconductive Particles for Calvarial Bone Regeneration[3]

Abstract

In the treatment of severe traumatic brain injury (TBI), decompressive craniectomy is commonly used to remove a large portion of calvarial bone to allow unimpeded brain swelling. Hydrogels have the potential to revolutionize TBI treatment by permitting a single-surgical intervention, remaining pliable during brain swelling, and tuned to regenerate bone after swelling has subsided. With this motivation, our goal is to present a pliable material capable of regenerating calvarial bone across a critical size defect. We therefore proposed the use of a methacrylated solubilized decellularized cartilage (MeSDCC) hydrogel encapsulating synthetic osteogenic particles of hydroxyapatite nanofibers (HAPnf), bioglass microparticles (BG), or added rat bone marrow-derived mesenchymal stem cells (rMSCs) for bone regeneration in critical-size rat calvarial defects. Fibrin hydrogels were employed as a control material for the study. MeSDCC hydrogels exhibited sufficient rheological performance for material placement before crosslinking (τ_y > 500 Pa), and sufficient compressive moduli post-crosslinking (E > 150 kPa). Bone regeneration was minimal in both

[3]Submitted as: Townsend JM, Zabel TA, Feng Y, Wang J, Andrews BT, Nudo RJ, Berkland CJ, Detamore MS. Decellularized Cartilage-Based Hydrogel Encapsulating Osteoconductive Particles for Calvarial Bone Regeneration. *Biomedical Materials*, 2017.

MeSDCC and fibrin groups, even with colloidal materials or added rMSCs. Minimal bone regeneration in the MeSDCC test groups may potentially be attributed to cartilage solubilization after decellularization, in which material signals may have degraded from enzymatic treatment. Looking to the future, an improvement in the bioactivity of the material will be crucial to the success of bone regeneration strategies for TBI treatment.

Introduction

Traumatic brain injury (TBI) is characterized by severe brain swelling commonly resulting from motor vehicle accidents, assaults, and stroke. Active duty military service members are especially vulnerable to this condition, as an estimated 22% of wounded soldiers evacuated from conflict zones have severe TBI.(113) The brain swelling that results from TBI can be life-threatening as the brain lies within a closed cranial vault incapable of expansion to mitigate rising intracranial pressures. Currently, severe TBI is treated by a two-stage surgical intervention. In the first stage, a large portion of calvarial bone is removed in a procedure termed decompressive craniectomy.(129) Decompressive craniectomy allows the brain to swell beyond the cranial vault and reduces dangerous intracranial pressure.(117) After brain swelling has sufficiently decreased, typically weeks to months later, a second procedure termed cranioplasty is performed to restore the skull anatomy and reclose the cranial vault.(111) Disadvantages of the current two-stage TBI surgical intervention are that it prolongs neurorehabilitation and recovery, increases medical costs, and is

associated with adverse neurologic symptoms termed syndrome of the trephined.(130) Syndrome of the trephined, also known as sinking skin flap syndrome, is manifested by symptoms such as headaches, unsteadiness, a feeling of apprehension, difficulties concentrating, and fine-motor dexterity concerns. Interestingly, these often debilitating neurologic symptoms of syndrome of the trephined are immediately reversible with a cranioplasty procedure to restore the cranial vault anatomy.(114, 116) Previous attempts to combine the two-stage TBI treatment into a single surgery have resulted in extremely high complication rates due to the inability of materials to expand as initial brain swelling occurs.(123) Current commercial bone products for cranioplasty have been unsuccessful in meeting the demand required for TBI treatment, in either single or two-stage surgical approaches.

Current materials used in commercially available cranioplasty products for bone repair include allogenic bone, synthetic calcium-apatite, and custom polymer/metallic implants.(131) Products that utilize allogenic bone, such as DBX® (MTF/Synthes) and AlloFuse® (AlloSource), have reported advantages of favorable material integration and low rejection; however, issues with batch variability have been noted as potential limitations of using human bone matrix.(16, 132) Current allogenic bone products have limited use in cranioplasty procedures with large cranial defects, termed critical size defects, resulting in reasonable bone regeneration at the defect periphery but minimal regeneration centrally. Synthetic calcium-apatite products, such as NovaBone Putty® (NovaBone Products), which utilize synthetic processes for high-reproducibility,

are reported to have acceptable osteoconductive material properties.(133) Similar issues using synthetic apatite approaches compared to allogenic bone products persist with regard to limited bone regeneration across large defect sizes. Cranioplasty approaches utilizing custom-made implants generated based on computed-tomography have gained popularity within the medical community for their patient-specificity.(131, 134) Although custom-made implants are attractive for repairing the cranial vault, they lack in their ability to regenerate calvarial bone, and cannot be implemented in a single surgery for TBI cases due to issues with material flexibility during brain swelling. Beyond commercial products, research avenues for TBI-related issues have generally focused on easing transition between decompressive craniectomy and cranioplasty,(111) or focused on intracerebral regenerative medicine.(119, 135-138) Major gaps in current knowledge exist regarding materials capable of regenerating bone in critical size defects, and in materials that can be implemented in a single surgery for treatment of TBI while avoiding syndrome of the trephined. The first step in meeting the overall goal of developing a single surgical intervention for the treatment of TBI is to first identify a pliable material capable of regenerating calvarial bone across a critical size defect. Once the first step has been achieved, the regenerative medicine community can focus on translating materials for treatment of TBI. Hydrogels are a promising class of materials for calvarial bone regeneration and future TBI application, offering the capability for *in situ* placement, allowing for application to any shape or size of defect,

photocrosslinking for user-defined material activation, and modulation of stiffness for material elasticity during brain swelling.(20)

The objective of the current study was to evaluate the use of a methacrylated solubilized decellularized cartilage (MeSDCC) hydrogel encapsulating synthetic osteogenic particles of hydroxyapatite nanofibers (HAPnf), bioglass microparticles (BG), or added rat bone marrow-derived mesenchymal stem cells (rMSCs) for bone regeneration in critical size rat calvarial defects. Fibrin hydrogels were used as a control material for the study. The combinational use of photo-crosslinking cartilage-based hydrogel matrix in combination with synthetic particles represents a next-generation approach from our previously published work in the area.(36) The choice of cartilage as a material to facilitate bone regeneration is inspired by the process of endochondral ossification during fracture healing. In a previous publication from our group, the three phases of endochondral ossification: inflammatory, reparative, and remodeling, were reviewed in detail.(108) During the reparative phase, a fibrous and cartilaginous tissue forms spanning the defect. The use of cartilage in the current study attempted to circumvent the initial phases of the endochondral ossification process to accelerate the formation of bone by delivering a similar tissue. Although the calvarium forms from intramembranous ossification, endochondral ossification can be leveraged as an attractive route to increase bone regeneration. Previous *in vitro* studies conducted by our group using rMSCs encapsulated in cartilage-based hydrogels demonstrated an initial increase of collagen I gene expression.(2) The combination of *in vitro* data regarding

cartilage-based hydrogels and *in vivo* results using cartilage as a biomaterial for bone regeneration inspired further evaluation of cartilage in calvarial bone regeneration. The addition of synthetic particles to the hydrogel matrix serves a dual purpose, to create a paste-like consistency to facilitate material placement by the surgeon, and to aid in bone regeneration by delivering osteogenic materials. We hypothesized that decellularized cartilage-based hydrogel would facilitate bone regeneration, and that the addition of synthetic osteogenic particles would further improve overall bone regeneration.

Materials and Methods

Preparation of Decellularized Cartilage (DCC)

Ten porcine knees were purchased from a local abattoir (Bichelmeyer Meats, Kansas City, KS). Hyaline cartilage was harvested from castrated male Berkshire hogs, 7-8 months of age and 120 kg in weight. The cartilage processing and decellularization protocol is described in our previous publication.(48) Briefly, harvested hyaline cartilage was rinsed, strained, then coarse-ground using a cryogenic tissue grinder (BioSpec Products, Bartlesville, OK). The coarse-ground cartilage was then packed into dialysis tubing (MWCO 3500) packets. Decellularization was achieved through a series of solution exchanges of osmotic shock, detergent, and enzymatic washes as described in our previously established protocols.(120-122) Dialysis packets containing cryoground cartilage were placed in hypertonic salt solution (HSS) at room temperature under agitation (70 rpm) overnight. Dialysis packets were then washed in triton X-100 (0.01 v/v)

at 220 rpm, followed by HSS, with DI washes between each step to permeabilize cellular membranes. Dialysis packets were then treated with benzonase enzyme solution (0.0625 KU/mL) at 37°C overnight followed by DI washing before treatment with sodium-lauroylsarcosine (NLS, 1% v/v) overnight for cell lysis and protein denaturation. Afterwards, dialysis packets were washed with DI water then 40% (v/v) ethanol at 70 rpm. Dialysis packets were then soaked in DI water with organic exchange resins to remove organic material from solution. Dialysis packets were then subjected to a saline-mannitol solution followed by DI washes. The tissue was then removed from the tissue packets, frozen, and lyophilized. After decellularization, DCC particles were cryoground using a freezer-mill (SPEX 6775, SamplePrep, Metuchen, NJ). Cryoground DCC was stored at -20°C for later use. The decellularization process was confirmed by PicoGreen assay (Thermo Fisher Scientific, Waltham, MA, P7589).

Synthesis of Methacrylated Solubilized Decellularized Cartilage (MeSDCC)

Solubilization and methacrylation of DCC was achieved using a protocol from our previously reported methods.(89) Briefly, solubilized DCC (sDCC) was created by mixing DCC powder in 0.1 M HCL at a concentration of 10 g/L. Pepsin (Cat# P7000, Sigma-Aldrich, St. Louis, MO) was then added to the DCC-HCL solution at a concentration of 1 g/L and stirred at 200 rpm for 48 hours at room temperature. The solution was then brought to physiological pH by adding 1 M NaOH. The solubilized DCC was then centrifuged at 7,000 x g for 5 min to pellet

any unsolubilized DCC particles. The supernatant was then retained, frozen, and lyophilized for later use as sDCC.

MeSDCC was synthesized by first dissolving sDCC in a 1:1 water:acetone mixture at a concentration of 10 g/L. sDCC was then reacted with 20-fold molar excess of glycidyl methacrylate (Cat# 779342, Sigma-Aldrich) in the presence of 62rimethylamine (Cat# T0886, Sigma-Aldrich) and tetrabutylammonium bromide (Cat# 426288, Sigma-Aldrich). The reaction was then stirred at 200 rpm for 6 days at room temperature. Afterward, MeSDCC was precipitated in an excess of acetone, then centrifuged at 3,000 x g for 3 min to pellet the MeSDCC. Pelleted MeSDCC was then dialyzed in DI water for 48 hours before freezing and lyophilizing for later use. The molar excess of glycidyl methacrylate to sDCC was approximated based on reacting one glycidyl methacrylate group to every monomer present in solution, assuming all monomers present were hyaluronic acid.

Rat Bone Marrow Harvest and Culture

rMSCs were harvested from the femurs of a male Sprague-Dawley rat (200-250 g) following an approved IACUC protocol at the University of Kansas (AUS #175-08). The rMSCs were cultured for 1 week in minimum essential medium-α (MEM-α, Cat# 12561072, Thermo Fisher Scientific, Waltham, MA) with 10% fetal bovine serum (FBS, Cat# 16000044, Thermo Fisher Scientific) and 1% antibiotic-antimyotic (Cat# 15240-062, Thermo Fisher Scientific) to ensure no contamination after harvest. After 1 week of culture, the antibiotic-antimyotic was

substituted for 1% penicillin/streptomycin (Cat# 15140-122, Thermo Fisher Scientific). Medium was exchanged every other day and cells were cultured until passage 3 before encapsulating the cells in material.

Hydrogel Preparation

MeSDCC hydrogels were prepared as previously described.(36) Briefly, 100 mg of MeSDCC and 100 mg of particles were weighed dry and combined. Hydroxyapatite nanofibers (HAPnf) were bestowed from Nanova Biomaterials, Inc. (Columbia, MO), and 1393-B3 bioglass (BG) microparticles (D_{avg} = 75 – 125 µm) were gifted from MO-SCI, Corp. (Rolla, MO). 1393-B3 BG is a borate glass containing 53% B_2O_3 (wt/wt). Dry material combinations were sterilized using ethylene oxide gas (AN74i, Anderson Anprolene, Haw River, NC) prior to use *in vivo*. Dry combinations were dispersed in 1 mL of phosphate buffered saline (PBS, Cat# P3813, Sigma-Aldrich) solution containing 0.05% 2-Hydroxy-4′-(2-hydroxyethoxy)-2-methylpropiophenone (I2959, Cat# 410896, Sigma-Aldrich) as the photo-initiator. The MeSDCC group with added rMSCs was made by making a 2x concentration of MeSDCC in PBS containing 0.1% I2959, and an equal volume of medium with cells was added to the 2x material and mixed, bringing the final rMSC concentration to 10^6 cells/mL. MeSDCC groups were loaded into 1 mL sterile syringes for later use.

Fibrin hydrogels were created using a dual syringe (2x2 mL, 1:1 ratio) and mixing tip (3x6 mm) purchased from Merlin Packaging Technologies (Gahanna, OH). Due to the quick setting time of enzymatically crosslinked fibrin hydrogels,

the dual syringe system was necessary to stop the material from prematurely crosslinking. In the first compartment, Human fibrinogen 1 (Cat# Fib1, Enzyme Research Labs, South Bend, IN) was dissolved in pooled normal plasma (Cat# 0010-5, George King Biomedical, Overland Park, KS) at a concentration of 10% (w/v). The second compartment contained a solution of 20 units/mL of human α-thrombin (Cat# HT1002A, Enzyme Research Labs) dissolved in a 40 mM $CaCl_2$ solution. After mixing, the final concentration was 5% fibrinogen, 10 units/mL of human α-thrombin, 20 mM $CaCl_2$, dissolved in a 50% (v/v) solution of normal human plasma. Fibrin groups with particles (HAPnf or BG) were added equally to both syringes of the dual mixing syringe at a concentration of 10% (w/v). The fibrin group with cells was achieved by mixing concentrated cells and medium with 20 units/mL human α-thrombin and 40 mM $CaCl_2$ in the dual syringe. The final concentration of components was the same as the other groups, with a final cell concentration of 10^6 cells/mL.

Rheological Testing of Hydrogel Precursor Solution

Hydrogel precursor solution yield stress was determined using an AR2000 controlled stress rheometer (TA-Instruments, New Castle, DE). Measurements were performed using a gap distance of 500 μm using a 20-mm diameter crosshatched stainless steel plate geometry and a crosshatched Peltier plate cover at 37°C (n = 5). Precursor yield stress was measured over an oscillatory shear stress sweep from 1-3000 Pa. The yield stress of each material was determined by the cross-over point of the storage (G') and loss modulus (G").

Hydrogel precursor solutions were prepared as previously described, with the exception that the fibrin groups were prepared without the enzymatic crosslinker α-thrombin.

Mechanical Testing of Crosslinked Hydrogel

The crosslinked hydrogel compressive modulus (n = 5) was determined using an RSA III dynamic mechanical analyzer (TA-Instruments). Hydrogels for mechanical testing were prepared as previously described.(35) Briefly, hydrogel precursor solution was loaded into a 2 mm thick Teflon mold sandwiched between glass microscope slides. MeSDCC hydrogels were crosslinked with a 312 nm UV-light at 9 mW/cm^2 for 10 min (EB-160C, Spectroline, Westbury, NY). Fibrin hydrogels were crosslinked by injecting the two precursor solutions into the mold space using the dual syringe with mixing tip, the fibrin mixture was allowed to set for 5 min. After crosslinking, circular hydrogels were cut using a sterile 3 mm biopsy punch. Hydrogels were pre-swollen in PBS for 24 hours before mechanical testing. The swollen hydrogel diameter was measured using a stereo microscope (20x magnification) and a micrometer, and the hydrogel height was measured using the RSA III. Hydrogels were compressed at a constant rate of 0.005 mm/s until mechanical failure.(139) The compressive modulus was calculated from the slope of the linear portion of the stress-strain curve between 10-20% strain.

Animal Model and Surgical Method

Animal experiments were approved by the Institutional Animal Care and Use Committee of the University of Kansas Medical Center (protocol #2015-2303). The animal model and surgical method was conducted as previously described.(36) Briefly, mixed-sex Sprague-Dawley rats were raised to an age of 7-10 weeks in-house and randomly assigned to treatment groups (n = 5). An incision was created on the posterior periphery of the skull to pull back the skin and periosteum exposing the calvarium. A critical-size (7.5 mm diameter) full thickness bone defect was created in the center of the calvarium (parietal bone) using a dental trephine. The circular piece of calvarial bone was removed, leaving the dura mater intact, and approximately 50 μL of material was syringed into the defect. MeSDCC groups were then crosslinked using a handheld 312 nm UV-light, and fibrin groups were allowed to enzymatically crosslink for 5 min after injection of material. The skin flap was then draped over the defect site and sutured to hold the material in place during the recovery period. The sham group, which has been republished from our previous study, received the same surgical method without the addition of material.(36) The DBX® group received approximately 50 μL of DBX® Putty. The treated and untreated calvarial bone defects were harvested with the surrounding bone at 8 weeks post-implantation.

Micro-computed Tomography (μCT)

Micro-computed tomography was performed on harvested rat calvarial bone after the 8-week recovery period to quantify new bone. A MicroXCT-400

(Carl Zeiss X-ray Microscopy, Pleasanton, CA) system with a 50-kV X-ray source at 7.9 W was used. Reconstructed µCT scans were analyzed using Avizo Fire computational software (FEI Company, Hillsboro, OR) to quantify new bone formation. New bone was confirmed using pre-existing bone as the threshold limit. Bone within the original 7.5 mm diameter defect was colored orange to indicate new bone formation. Quantified new bone is presented as the total (mm^3) within the 7.5 mm diameter defect.

Histology and Immunohistochemistry (IHC)

Explanted calvarial bone defect samples were fixed in 10% phosphate-buffered formalin for 48 hours then stored long term in 70% ethanol. Calvarial tissue samples were then decalcified in Calrite media (Cat# 22-046-339, Thermo Fisher Scientific) for 3 weeks before dehydrating in a grade series of ethanol to xylene, then to paraffin wax for embedding. Using a microtome (HM 355S, Thermo Fisher Scientific), 5 µm thick sections were taken and affixed to microscope slides. Tissue slides were heated to 60°C for 20 min to improve adhesion of tissue to slides, then stored long term at -20°C. Before staining, tissue slides were dewaxed in xylene then rehydrated in a graded series of ethanol (i.e., 100% to 70%) followed by PBS. Slides were stained with hematoxylin and eosin (H&E, Cat# H-3404, Abcam, Cambridge, UK) to visualize cell infiltration and new bone formation.

Immunohistochemistry (IHC) was used to visualize the deposition of collagen I (Cat# NB600-408, Novus Biologicals, Littleton, CO) and collagen II

(Cat# NBP2-33343, Novus Biologicals) within the defect site. An in-depth protocol of the IHC procedure has been previously published.(36) Briefly, after tissue dewaxing and rehydrating to PBS with Tween-20 (Cat# P3563, Sigma-Aldrich), antigen retrieval was performed using 20 µg/mL proteinase K (Cat# ab64220, Abcam) for 15 min at 37°C, then cooled at room temperature for 10 min. Sections were then blocked with 0.3% hydrogen peroxide (Cat# ab94666, Abcam) for 10 min, 10% normal horse serum (Cat# PK-6200, Vector Labs, Burlingame, CA) for 20 min, 5% bovine serum albumin (Cat# A9647, Sigma-Aldrich) for 20 min, and avidin/biotin blocking (Cat# SP-2001, Vector Labs) for 15 min each. Sections were then incubated with either 10 µg/mL of collagen I or 5 µg/mL of collagen II (100 µL volume) for 1 hour. After incubation of sections with the primary antibody, slides were washed between each following step using PBS with Tween-20 for 5 min. Sections were then incubated with biotinylated horse anti-mouse/rabbit IgG (Cat# PK-6200, Vector Labs) for 30 min, VECTASTAIN Elite ABC solution (Cat# PK-6200, Vector Labs) for 30 min, DAB solution (Cat# SK-4100, Vector Labs) for 2 min, DAB-enhancing solution (Cat# H-2200, Vector Labs) for 10 s, counterstained using hematoxylin QS (Cat# H-3404, Vector Labs) for 1 min, bluing solution (Cat# 7301, Thermo Fisher Scientific) for 3 min, then dehydrated in a graded series of ethanol (i.e., 70-100%) to xylene before mounting. Negative controls for each IHC batch were included to confirm negligible background staining.

Statistical Methods

Statistical analyses were conducted using the GraphPad Prism (Graphpad Software Inc, La Jolla, CA) statistical software. A one-way analysis of variance with groups of factors was used to analyze groups. Tukey's post-hoc test was used for comparing between groups. Rheological testing, mechanical testing, and μCT had n = 5 samples per group, and data are reported as the mean ± standard deviation.

Results

Rheological Analysis of Hydrogel Precursor

Representative rheometer traces are provided for each hydrogel precursor solution that exhibited a yield stress (Fig. 4.1A). Fibrin and fibrin-BG did not create a noticeable yield stress after being mixed. The yield stress of the MeSDCC-HAPnf group (1641 Pa) was 3.3 and 4.4 times greater than those of the MeSDCC and fibrin-HAPnf group, respectively (Fig. 4.1B, $p < 0.0001$). The yield stress of the MeSDCC-BG group (1456 Pa) was 2.9 and 3.9 times greater than those of the MeSDCC and fibrin-HAPnf group, respectively ($p < 0.0001$). No significant difference was observed between MeSDCC and fibrin-HAPnf, or between MeSDCC-HAPnf and MeSDCC-BG formulations.

Mechanical Analysis of Crosslinked Hydrogel

Representative stress-strain curves are provided for each material formulation post-crosslinking (Fig. 4.2A-B). The MeSDCC-HAPnf group (711

kPa) had a compressive modulus that was 4, 26.4, 45.7, and 29.4 times greater than the compressive moduli of the MeSDCC, fibrin, fibrin-HAPnf, and fibrin-BG groups, respectively (Fig. 4.2C, $p < 0.01$). The MeSDCC-BG group (989 kPa) had a compressive modulus 5.5, 36.7, 63.6, and 40.9 times greater than those of the MeSDCC, fibrin, fibrin-HAPnf, and fibrin-BG groups, respectively ($p < 0.01$). No other differences in modulus were statistically significant.

Micro-computed Tomography (μCT) Analysis

Large bone islands were observed in both the sham and DBX group; however, bone islands observed in the sham group were thin and did not significantly contribute to overall total regenerated bone volume (Fig. 4.3A). Small bone island formation was observed in all samples except the MeSDCC group and groups containing HAPnf. Peripheral bone growth was observed in all samples. The DBX group (8.94 mm^3) had 2.1, 2.7, 2.8, 4.3, 5.5, 3.1, 3.0, 3.1, and 2.6 times greater bone regeneration compared to the sham, fibrin, fibrin+Cells, fibrin-HAPnf, fibrin-BG, MeSDCC, MeSDCC+Cells, MeSDCC-HAPnf, and MeSDCC-BG groups, respectively (Fig. 4.3B, $p < 0.05$). No significant difference was observed among any other group.

Histological and Immunohistochemistry (IHC) Analysis

Soft tissue formation spanning the defect site was observed in all samples (Fig. 4.4). Peripheral bone growth was observed in all samples and tended to form toward the dural side of the defect. No differences were noted among the

MeSDCC or Fibrin groups with or without the addition of rMSCs. Groups with exogenously added cells did not appear to have a higher number of stained nuclei within the defect. Groups containing HAPnf had leftover material within the defect site after the 8-week recovery period, and in some samples, cells were unable to migrate to the center of the material. Leftover MeSDCC hydrogel was observed in the MeSDCC-BG group based on collagen II deposition. Leftover BG particles were observed in both MeSDCC and Fibrin hydrogels and tended to migrate to the periphery of the defect site in all samples.

Collagen I staining showed substantial deposition throughout the defect site, including the soft tissue portion (Fig. 4.5). Native peripheral bone was used as the reference for comparison. In groups containing HAPnf, minimal deposition of collagen I was observed toward the center of the defect. Staining for collagen II showed almost no collagen II deposition within the defect site, except for the MeSDCC-BG group, where small tissue pockets positively staining for collagen II deposition were observed.

Discussion

The current study was the first to use an *in situ* crosslinking hydrogel comprised of naturally-derived decellularized cartilage-based matrix for calvarial bone regeneration *in vivo*. The use of a cartilage-based hydrogel for bone regeneration follows our previous work using micronized decellularized hyaline-cartilage particles and hydroxyapatite colloidal gels for bone regeneration *in vivo*.(36) In designing hydrogels with potential for TBI treatment in mind, the

mechanical performance of the material before and after UV-crosslinking was identified as a crucial aspect for clinical translation.(20) All MeSDCC hydrogels tested exhibited sufficient yield stress (τ_y > 500 Pa) for material placement, and addition of HAPnf or BG particles significantly increased the yield stress of the material to a range of 1400 to 1600 Pa. For context, the yield stress of mayonnaise is approximately 200 Pa, and the yield stress of Play-Doh is approximately 3000 Pa.(67) The potential reason that only the fibrin-HAPnf led to a detectable yield stress may have been that the fibers would conceivably interact more with their surrounding environment than a sphere due to the randomized fiber orientation distribution, and a changing microstructure from fiber-fiber and fiber-medium interactions.(140) Although the calvarium is a non-load bearing bone, sufficient material mechanical performance is necessary to remain in place during healing, and provide a barrier between the brain and scalp. Due to stiffness being an important parameter for material success, the compressive modulus of hydrogels was characterized. After crosslinking of the hydrogel precursor, MeSDCC hydrogels with colloids had considerably higher compressive moduli compared to fibrin groups; however, no significant difference was observed among the MeSDCC group and the fibrin groups. The addition of colloids in fibrin groups did not increase the compressive modulus as observed in the MeSDCC groups. Comparing fibrin and MeSDCC without particles, MeSDCC on average had a higher compressive modulus, potentially due to a greater crosslinking density. The difference in compressive modulus could be in part due to limited initial crosslinking in fibrin groups compared to MeSDCC, and

thus the added colloids were not sufficiently encapsulated in the matrix, or that the MeSDCC material interacted with the particles to a greater extent. Additionally, Although the compressive modulus of native bone is on the magnitude of Gpa, hydrogels do not necessarily need to match the compressive modulus of native bone in the calvarium due to the non-load bearing nature.(141) The elastic nature of a hydrogel would also be beneficial for future TBI application allowing pliability during brain swelling. For these reasons, we have identified a minimum compressive modulus of 100 kPa, similar to human skin tissue to maintain shape while remaining pliable.(142)

In vivo bone tissue formation within the defect for both fibrin and MeSDCC groups was minimal. No difference in bone formation was observed among any fibrin or MeSDCC formulation. The DBX® group was the only group to outperform the sham control in regenerated bone volume, showing increased bone formation spanning into the defect. Sham groups had noticeable bone island formation covering an ample area; however, the bone formed was especially thin and did not contribute significantly to the overall bone volume. Sporadic small bone island formation was observed in all groups, with the exception of the HAPnf-containing groups. H&E staining revealed a large amount of leftover HAPnfs in both fibrin and MeSDCC formulations. The HAPnf appeared to perhaps inhibit cell migration toward the center of the material. Cell migration issues with HAPnf were especially problematic in combination with MeSDCC, potentially due to the high compressive modulus and yield stress of the material during hydrogel degradation for cellular infiltration. Collagen I deposition was homogeneous

throughout all samples except the HAPnf containing groups, where there was minimal positive staining for collagen I in the center of the material, most likely due to the lack of cellular infiltration into the material. The only material to have leftover hydrogel matrix inside the defect after the 8-week period was the MeSDCC-BG group; however, the remaining volume was especially small and not apparent in all samples. Collagen II deposition was not detected in all samples except for the MeSDCC-BG group, in which the leftover MeSDCC hydrogel positively stained for collagen II. One may argue that the incorporation enzymatically degradable sequences or a material porogen may enhance regenerative capabilities by facilitating cellular infiltration and remodeling. However, the observation of remaining MeSDCC in only one group, juxtaposed with the limited capacity of regeneration even with rMSCs present, leads to the conclusion that the inherent material bioactivity is the primary focus for future improvement becomes, with cell infiltration and migration being relegated to a secondary issue.

Although our group was the first to use naturally derived cartilage for calvarial bone regeneration, other groups have studied the use of cartilage matrix (naturally derived or tissue engineered) for bone formation. Cunniffe *et al*.(143) studied the use of chondrogenically-primed rMSCs encapsulated in alginate hydrogels to partially mimic the endochondral ossification healing process in rat critical-size femur and calvarial defects. The rMSC-alginate hydrogels appeared to support bone formation at the hydrogel surface, and comparable bone regeneration to the current study was observed. In another study from that same

group, a decellularized tissue engineered cartilage scaffold was studied for use in long bone defect healing.(144) The tissue engineered cartilage scaffold promoted more bone regeneration on average compared to the sham group; however, a considerable amount of deviation was observed within the group. Both studies by Cunniffe *et al*. illustrated promise for the use of cartilage-derived matrix/cells in promoting bone regeneration by recapitulating part of the endochondral ossification process. In a study using DCC scaffolds to promote endochondral bone formation, collagen I deposition was observed after 22 days of subcutaneous implantation in a rat model.(128) Similarly, in another study, collagen I deposition and mineralization was observed in gelatin methacrylamide hydrogels encapsulating DCC particles after 8 weeks of *in vivo* rat subcutaneous implantation.(145) Both studies supported the use of DCC as a material for bone regeneration. In comparing the referred studies to the current study, limited bone regeneration with MeSDCC hydrogels in the current study may potentially have been attributed to the processing of DCC. The further processing of DCC to create MeSDCC may potentially have contributed to a lower bioactivity and subsequent lower bone formation. DCC solubilization is speculated to have been the major contributing factor in the reduction of material bioactivity, as potential signals may have been affected by the process. Reduced bioactivity due to tissue decellularization has been previously discussed, in which devitalized cartilage (DVC) had greater bioactivity than DCC potentially due to altering matrix architecture and a reduction of important growth factors from decellularization.(48) DVC is cartilage extracellular matrix that has only

undergone physical processing (i.e., granulating) without the additional step of chemical decellularization.(7) In another study from our group evaluating methacrylated solubilized devitalized cartilage (MeSDVC) loaded with DVC particles, increased gene expression was observed in MeSDVC hydrogels with DVC particles compared to MeSDVC alone.(2) Therefore, both decellularization and solubilization could potentially contribute to lower bioactivity. Future studies using cartilage will focus on minimizing the processing of cartilage to retain material activity, in which the use of DVC may be of interest for enhancing endochondral bone formation. Further research is necessary to fully characterize the use of cartilage in bone regeneration in general, and in calvarial defect regeneration in particular.

Conclusion

MeSDCC hydrogels composed entirely of naturally-derived DCC demonstrated desirable handling properties in the pre-crosslinked form, and appropriate mechanical performance post-crosslinking for a cranioplasty application. The addition of synthetic particles (HAPnf or BG) increased the mechanical stiffness of MeSDCC hydrogels several fold, approaching the 1 Mpa mark in compressive modulus, which may be desirable in a TBI application. *In vivo* testing in an 8-week rat calvarial defect model demonstrated minimal bone formation in both MeSDCC and fibrin groups containing osteoconductive particles. Encapsulated rMSCs did not appear to influence bone formation in either fibrin or MeSDCC hydrogels, and significant bone formation was only

observed in the DBX® group, suggesting that material bioactivity may be the governing limitation beyond cell infiltration. Minimal bone formation using MeSDCC compared to other published studies potentially suggests that DCC solubilization may have potentially reduced material activity in this application. Further research is necessary to determine the full capacity of cartilage (DCC and DVC) as a material to promote bone regeneration.

Chapter 5: Superior Calvarial Bone Regeneration with Pentenoate-Functionalized Hyaluronic Acid Hydrogels with Devitalized Tendon Particles[4]

Abstract

Traumatic brain injury (TBI) is a life-threatening condition defined by internal brain herniation. Severe TBI is commonly treated by a two-stage surgical intervention, where decompressive craniectomy is first conducted to remove a large portion of calvarial bone and allow unimpeded brain swelling. In the second surgery, spaced weeks to months after the first, cranioplasty is performed to restore the cranial bone. Hydrogels with paste-like precursor solutions for surgical placement may potentially revolutionize TBI treatment by permitting a single-stage surgical intervention, capable of being implanted with the initial surgery, remaining pliable during brain swelling, and tuned to regenerate calvarial bone after brain swelling has subsided. The current study evaluated the use of photocrosslinkable pentenoate-functionalized hyaluronic acid (PHA) and non-crosslinking hyaluronic acid (HA) hydrogels encapsulating naturally derived tissue particles of demineralized bone matrix (DBM), devitalized cartilage (DVC), devitalized meniscus (DVM), or devitalized tendon (DVT) for bone regeneration in critical-size rat calvarial defects. The commercial product DBX® was used as

[4]Submitted as: Townsend JM, Andrews BT, Feng Y, Wang J, Nudo RJ, Van Kampen E, Gehrke SH, Berkland CJ, Detamore MS. Superior Calvarial Bone Regeneration using Pentenoate-Functionalized Hyaluronic Acid Hydrogels with Devitalized Tendon Particles. *Acta Biomaterialia*, 2017.

the positive control for the study. The HA-DBM (4-30%), PHA (4%), and PHA-DVT (4-30%) groups had 5 ($p < 0.0001$), 3.1, and 3.2 ($p < 0.05$) times greater regenerated bone volume compared to the sham (untreated defect) group, respectively. *In vitro* cell studies suggested that the PHA-DVT (4-10%) group would have the most desirable performance. Overall, hydrogels containing DVT particles outperformed other materials in terms of bone regeneration *in vivo* and calcium deposition *in vitro*. Hydrogels containing DVT will be further evaluated in future rat TBI studies.

Introduction

Traumatic brain injury (TBI) is a life-threatening condition characterized by internal brain swelling, the degree of which can vary greatly. TBI inflicted by a closed head injury or stroke can result in severe brain swelling requiring surgical intervention.(109) The current surgical procedure to treat severe TBI involves a two-stage surgery. In the first surgery, decompressive craniectomy (DC) is performed to remove a large portion of the calvarial bone and allow un-impeded brain swelling.(146) The size of calvarial bone removed during DC is considered a critical size defect as the bone will not naturally heal by itself. After brain swelling has subsided, a second surgery—termed cranioplasty—is performed to close the cranial vault.(131) The average time between DC and cranioplasty has been reported up to 80 days; during this time the brain is left unprotected. Syndrome of the trephined (SoT), also known as sinking skin flap syndrome, is a severe neurological condition associated with mood changes, fatigue, dizziness, motor skill problems, and concentration issues.(116) The occurrence of SoT has

been connected to patients following DC for the treatment of TBI.(114) The cause of SoT has been attributed to various factors such as changing intracranial pressure,(147) and physical distortion of the brain from the weight of the scalp.(148) Immediate relief from SoT has been observed directly after cranioplasty,(114) and it is recommended that cranioplasty be performed as soon as clinically possible to mitigate the occurrence of SoT.(148) The current two-stage surgical treatment is non-advantageous as it prolongs patient recovery by requiring two separate surgeries and potentially results in the neurological condition SoT.

Various research groups have reported new approaches to treat TBI. Martin *et al*.(123) previously studied the effect of a single-surgical approach combining DC and autologous bone flap cranioplasty in a pediatric patient population and found high complication rates. A potential issue with combining DC and cranioplasty in a single surgical intervention is that current methods, such as autologous bone flap cranioplasty, do not allow the brain to swell as the constructs are rigid bodies. Currently there is an unmet need for a material that can be implemented in a single-stage surgery to treat TBI, capable of remaining flexible during brain swelling, then transitioning to bone after brain swelling has ceased. Most research into TBI treatment has focused on methods to improve brain tissue healing(119, 135-138) or blocking tissue growth to ease the transition between DC and cranioplasty.(111) Currently available commercial bone void fillers cannot be used for cranioplasty following DC as the treatments are unable to regenerate sufficient bone across the critical size defect and do not remain

pliable after implantation. The first step in designing a material for TBI treatment after DC is to identify a pliable material capable of regenerating bone across a critical size defect. Once a pliable material that can sufficiently regenerate bone has been identified, the next logical step would be testing in a TBI animal model.

The objective of the current study was to evaluate the use of a photocrosslinking hyaluronic acid (HA) hydrogel encapsulating devitalized tissue particles for calvarial bone regeneration in a critical size calvarial defect. The use of a photocrosslinking hydrogel for calvarial bone regeneration represents a next-generation biomaterial following our previous work.(36, 103) In the current study, hydrogels encapsulating tissue particles were created by combining pentenoate functionalized hyaluronic acid (PHA) or non-crosslinking hyaluronic acid (HA) with demineralized bone matrix (DBM), devitalized cartilage (DVC), devitalized meniscus (DVM), or devitalized tendon (DVT) particles. PHA hydrogels are an attractive material choice as the crosslinking time is on the range of 1-2 minutes. Compared to other options like methacrylated HA, which has a crosslinking time on the range of 5-10 minutes, a faster crosslinking time is desirable for the addition of cells or for surgical use.(149-153) The use of hydrogels by surgeons is often overlooked during the hydrogel design process. Hydrogel precursor handling properties can be tuned specifically with the surgeon in mind, developing paste-like precursor solutions to aid in material placement to ease clinical translation.(35)

The use of different extracellular matrix (ECM) materials for calvarial bone regeneration attempts to apply and recapitulate part of the endochondral

ossification process by delivering an intermediate material to accelerate healing.(108) Cartilage, meniscus, and tendon tissues were selected as they are comprised of varying amounts of collagen I or collagen II and may provide additional bioactive signals to promote healing. Crosslinking (i.e., PHA) and non-crosslinking (i.e., HA) tissue hydrogels with a single colloidal loading of 30% were evaluated in a critical size rat calvarial defect model and groups with significant bone regeneration were refined explored *in vitro*. We hypothesized that ECM from sources other than bone would promote comparable or superior bone regeneration in a critical-size calvarial defect.

Materials and Methods

Preparation of Devitalized Tissue

Cartilage, meniscus, and tendon tissues were harvested from the knees of 10 castrated male Berkshire hogs (7-8 months of age, 120 kg) purchased from the local abattoir (Bichelmeyer Meats, Kansas City, KS). Tissue devitalization was described in our previous publication.(48) Briefly, harvested tissues were rinsed, strained, and chopped into small pieces. Tissues were coarse ground using a cryogenic tissue grinder (BioSpec Products, Bartlesville, OK) then frozen and lyophilized. Tissues were then cryoground using a freezer-mill (SPEX 6775, SamplePrep, Metuchen, NJ). Devitalized cartilage (DVC), devitalized meniscus (DVM), and devitalized tendon (DVT) particles were stored at -20°C for later use.

Synthesis of Pentenoate Functionalized Hyaluronic Acid (PHA)

Pentenoate functionalized hyaluronic acid (PHA) was synthesized as previously described.(154, 155) hyaluronic acid (HA, Mw = 1.01-1.8 MDa, Lifecore Biomedical, Chaska, MN) was dissolved in DI water at a concentration of 0.5% (w/v). Once fully dissolved, DMF was slowly added to the solution to achieve a final ratio of 3:2 (water:DMF). The pH of the solution was then adjusted to 9.5 using 1M NaOH. Pentenoic anhydride (Cat# 471801, Sigma-Aldrich, St. Louis, MO) was added in 5 M excess relative to HA and the pH was maintained between 8-9 for approximately 2 hours. Afterwards, NaCl was added to the solution to achieve a final concentration of 0.5 M. The PHA was then precipitated in four volumes of acetone and centrifuged at 7,000 x g to separate the PHA from solution. PHA pellets were then dissolved in DI water and transferred to dialysis packets (MWCO: 6-8 kDa). PHA was dialyzed against DI water for 48 hours, performing DI water exchanges every 12 hours. After dialysis, the PHA solution was frozen and lyophilized. Dry PHA was stored at -20°C for later use.

Hydrogel Preparation

Hydrogels were prepared as previously described.(36) Briefly, HA or PHA and tissue particles were weighed dry and combined. HA groups were resuspended in phosphate buffered saline (PBS, Cat# P3813, Sigma-Aldrich) solution, and PHA groups were resuspended in PBS solution containing 2.3 mM of 2-Hydroxy-4′-(2-hydroxyethoxy)-2-methylpropiophenone (Irgacure 2959, Cat# 410896, Sigma-Aldrich) and 1% dithiothreitol (DTT, Cat# D0632, Sigma-Aldrich).

Dry material combinations were sterilized using ethylene oxide gas (AN74i, Anderson Anprolene, Haw River, NC) and the PBS-I2959-DTT solution was sterile-filtered prior to resuspending PHA groups for use *in vivo* or *in vitro*. Hydrogel precursor solutions were allowed to reach ambient conditions for 2 h before implanting. Groups are presented as the material contents followed by weight per volume (in PBS) percentages of each in parentheses (i.e. PHA-DVC (4-30%) = 4% PHA + 30% DVC in PBS).

Rheological Testing of Hydrogel Precursor

Hydrogel precursor yield stress (n = 3) was determined using a DHR-2 controlled stress rheometer (TA Instruments, New Castle, DE). Measurements were performed using a 20-mm diameter crosshatched stainless steel plate geometry and a crosshatched Peltier plate cover at 37°C and a gap distance of 500 µm. The Peltier solvent trap was used to ensure the material did not dehydrate during testing. An oscillatory shear stress sweep from 10-5000 Pa was used to measure hydrogel precursor yield stress. Material yield stress was defined as the cross-over point of the storage (G') and loss modulus (G").(2)

Mechanical Testing of Crosslinked Hydrogel

Crosslinked hydrogel compressive moduli (n = 5) were determined using an RSA III dynamic mechanical analyzer (TA Instruments). Crosslinked hydrogels were prepared using a previously published protocol.(35) Briefly, hydrogel precursor solutions were loaded into 2-mm thick Teflon molds

sandwiched between glass microscope slides and secured using clamps. Hydrogels were then crosslinked using a 312 nm UV-light at 9 mW/cm^2 for 2 minutes (EB-160C, Spectroline, Westbury, NY). Post-crosslinking, circular hydrogels cylinders were cut using a sterile 3 mm punch and swelled in PBS for 24 hours before proceeding with mechanical testing. Swollen hydrogels were measured using a stereomicroscope and micrometer to determine the diameter (3.75 ± 0.1 mm), and hydrogel height (2.75 ± 0.1 mm) was measured using the RSA III. Hydrogels were compressed at a constant rate of 0.005 mm/s until 30% strain. The compressive modulus was calculated from the linear portion slope of the stress-strain curve between 5-15% strain.

Animal Model and Surgical Method

Animal experiments were approved by the Institutional Animal Care and Use Committee of the University of Kansas Medical Center (protocol #2015-2303). Male Sprague-Dawley rats were purchased from Charles River Laboratories (Wilmington, MA) at an age of 7-8 weeks; surgeries were conducted between 8-9 weeks of age. The calvarial bone was exposed by creating an incision on the posterior periphery of the skull to pull back the skin and periosteum. Using a dental trephine, a critical-size 7.5 mm diameter defect was created on the center of the calvarial bone. The circular piece of calvarial bone was carefully removed, leaving the dura mater intact. Approximately 50 µL of hydrogel paste was then syringed into the space and smoothed/shaped to the defect using a sterile spatula. Groups containing PHA hydrogel were then

crosslinked using a handheld 312 nm UV-light using a 312 nm UV-light at 9 mW/cm^2 for 2 minutes (EB-160C, Spectroline). The skin and periosteum were carefully draped over the defect site and sutured in place. The sham (untreated defect) group received the same surgical procedure without the addition of material, the DBX® group received approximately 50 µL of DBX® Putty, and the uninjured group received no surgical intervention. Calvarial bone was harvested after 8 weeks post-implantation (n = 5).

Micro-Computed Tomography (µCT)

Micro-computed Tomography was performed using a Quantum FX imaging system (PerkinElmer, Waltham, MA) with a 50-kV X-ray source at 160 µA. µCT imaging was conducted on harvested rat calvarial bone after 8 weeks post-implantation (n = 5). Scans were analyzed using Avizo computational software (FEI Company, Hillsboro, OR) to quantify regenerated bone volume. Regenerated bone was confirmed using pre-existing peripheral bone as the threshold. Total bone was determined using uninjured rat calvarial bone for determination of total bone regeneration percentage.

Histology and Immunohistochemistry (IHC)

After fixing in 10% phosphate-buffered formalin for 48 hours and µCT imaging, explanted cranial bone samples were submerged in 70% ethanol for long-term storage. Embedding, sectioning, and staining of tissue was performed by the Stephenson Cancer Tissue Pathology Core at the University of Oklahoma

Health Sciences Center. Briefly, cranial implants with surrounding host bone were embedded in paraffin and sectioned in the sagittal plane following a standard protocol. Paraffin blocks were cut to a thickness of 4 μm and affixed to glass microscope slides. The SelecTech hematoxylin and eosin (H&E) staining system (Leica Biosystems, Wetzlar, Germany) was performed using a Leica ST5020 multistainer (Leica Biosystems) following the manufacturer's protocol (n = 5).

In Vitro Cell Culture and Experimental Design

Pre-osteoblast mouse calvarial cells (MC3T3-E1, ATCC, Manassas, VA) were cultured in minimum essential medium-α (Cat# 12561072, Thermo Fisher Scientific, Waltham, MA) supplemented with 10% fetal bovine serum (FBS, Cat# 16000044, Thermo Fisher Scientific) and 1% penicillin/streptomycin (Cat# 15140-122, Thermo Fisher Scientific). Medium was exchanged every other day and cells were cultured to a passage number of 2 before being used in the study. Experimental groups from the 8-week *in vivo* study that significantly outperformed the negative control ($p < 0.05$) were chosen to be refined *in vitro* to determine the minimum tissue particle concentration to achieve a desirable cellular response. Following the results of the *in vivo* study; PHA, PHA-DBM, and PHA-DVT groups were selected to evaluate the tissue particle concentration from 10 to 30%. Approximately 50 μL of material was injected by syringe into each well of a 96-well plate, centrifuged at 1000 x g for 5 minutes to evenly coat the bottom of the well, then crosslinked using the handheld UV light for 2 minutes. MC3T3-E1 cells

were seeded at a concentration of 10^4 cells per well (150 μL volume) directly on top of the crosslinked material in each well of the 96-well plate (n = 5).

Biochemical Assays

After 2 and 10 days of cell culture, seeded cells were lysed with 200 μL of lysis buffer (Cat# R1060-1-50, Zymo Research, Irvine, CA) and DNA content was determined using the Quant-iT™ PicoGreen™ assay (Cat# P7589, Thermo Fisher Scientific) according to the manufacturer's protocol (n = 5). Hydrogels without seeded MC3T3 cells served as controls for the study, designated as the tissue culture plastic (TCP) group. Hydrogel constructs were then dissolved in 100 μL of 1M hydrochloric acid to determine the amount of deposited calcium. Calcium was assayed using the QuantiChrom™ calcium assay kit (BioAssay Systems, Hayward, CA) according to the manufacturer's protocol (n = 5).

Statistical Methods

GraphPad Prism (GraphPad Software Inc, La Jolla, CA) software was used to conduct all statistical analyses. A one-way analysis of variance with groups of factors was used for analyzing mechanical testing and μCT results, and a two-way analysis of variance with groups of factors was used to analyze biochemical assays. Tukey's post-hoc analysis was used to compare between groups. Yield stress testing had n = 3 samples per group. Compressive modulus, μCT, DNA, and calcium testing had n = 5 samples per group; all data are reported as the mean ± the standard deviation.

Results

Rheological Analysis of Hydrogel Precursor

All material formulations tested exhibited a yield stress (τ_y > 200 Pa, Fig. 1A). The addition of ECM particles to PHA significantly increased the material yield stress in all groups except for the PHA-DVT (4-10%) group. PHA-DVC (4-30%), PHA-DVM (4-30%), PHA-DBM (4-30%), PHA-DVT (4-20%), and PHA-DVT (4-30%) had 23.1, 12.8, 14.8, 8.4, and 10.4 times greater yield stresses compared to the control PHA (4%) group (206 Pa) ($p < 0.0001$). PHA-DBM (4-10%) and PHA-DBM (4-20%) had 6.3 and 5.8 times greater yield stresses compared to the PHA (4%) group ($p < 0.05$). The PHA-DVC (4-30%) group (4760 Pa) had the highest yield stress, which was 1.8, 3.7, 4.0, 1.6, 5.3, 2.8, and 2.2 times greater than those of the PHA-DVM (4-30%), PHA-DBM (4-10%), PHA-DBM (4-20%), PHA-DBM (4-30%), PHA-DVT (4-10%), PHA-DVT (4-20%), and PHA-DVT (4-30%) groups, respectively ($p < 0.0001$). The PHA-DVM (4-30%) group (2644 Pa) had a yield stress that was 2.0, 2.2, and 2.9 times greater than those of the PHA-DBM (4-10%), PHA-DBM (4-20%), and PHA-DVT (4-10%) groups, respectively ($p < 0.0001$), and 1.5 times greater than that of the PHA-DVT (4-20%) group ($p < 0.05$). The PHA-DBM (4-30%) group (3060 Pa) had a yield stress that was 2.4, 2.6, and 3.4, times greater than those of the PHA-DBM (4-10%), PHA-DBM (4-20%), and PHA-DVT (4-30%) groups, respectively ($p < 0.0001$), and 1.8 times greater than that of the PHA-DVM (4-20%) group ($p < 0.001$), and 1.4 times greater than that of the PHA-DVT (4-30%) group ($p < 0.05$).

The PHA-DVT (4-30%) group (2154 Pa) had a yield stress 1.7, 1.8, and 2.4 times greater than that of the PHA-DBM (4-10%), PHA-DBM (4-20%), and PHA-DVT (4-10%) groups, respectively ($p < 0.05$).

Mechanical Analysis of Crosslinked Hydrogel

The addition of ECM particles increased the average compressive modulus of all hydrogels tested (Fig. 1B). The PHA-DVC (4-30%), PHA-DVT (4-20%), and PHA-DVT (4-30%) groups respectively had 7.6, 3.2, and 2.5 times greater compressive moduli compared to the PHA (4%) group (7.4 kPa) without ECM particle ($p < 0.01$). PHA-DVC (4-30%) had a compressive modulus that was 2.5 times greater than that of the PHA-DVM (4-30%) group ($p < 0.05$), and 4, 2.7, and 3 times greater than those of the PHA-DVT (4-10%), PHA-DBM (4-10%), and PHA-DBM (4-30%) groups, respectively ($p < 0.001$), and 2.4 times greater than that of the PHA-DBM (4-20%) group($p<0.01$). The PHA-DVT (4-20%) group had a compressive modulus that was 3.2 times greater than that of the PHA-DVT (4-10%) group ($p < 0.05$). The addition of ECM particles in DBM groups did not significantly increase the compressive modulus; however, a statistically significant increase in compressive modulus was observed in PHA-DVT groups with increasing ECM particles.

Micro-computed Tomography (μCT) Analysis

Significant bone regeneration was not observed in non-crosslinking HA-ECM formulations, except for the HA-DBM (4-30%) group (Fig. 2). Large bone

island formation was observed in all PHA groups; however, minimal bone-bridging was observed. The HA-DBM (4-30%) group (67.1%) had 5, 4.2, 6.4, 6.3, 3.6, and 2.9 times greater percent bone volume regeneration compared to the sham, HA-DVC (4-30%), HA-DVM (4-30%), HA-DVT (4-30%), PHA-DVC (4-30%), and PHA-DVM (4-30%) groups, respectively ($p < 0.0001$). HA-DBM (4-30%) also had 2.4 times ($p < 0.01$) and 1.8 times ($p < 0.05$) times greater percent bone volume regeneration compared to the DBX® and PHA-DBM (4-30%) groups, respectively. The PHA (4%) group (41.9%) had 3.1, 4, and 3.9 times greater percent bone volume regeneration compared to the sham, HA-DVM (4-30%), and HA-DVT (4-30%), respectively ($p < 0.05$). The PHA-DVT (4-30%) group (42.4%) had 3.2, 4.1, and 4 times greater percent bone volume regeneration compared to the sham, HA-DVM (4-30%), and HA-DVT (4-30%), respectively ($p < 0.05$).

Histological Analysis

Bone growth at the defect periphery was observed in all samples and formed toward the dural side of the defect (Fig. 3). A noticeable soft tissue formation was observed in the defect space where bone formation was absent. Thicker bone formation was observed in hydrogel groups with PHA compared to HA groups. Peripheral bone growth spanning into the defect site was observed at a higher rate in PHA hydrogel groups. Disjoined DBM particles were observed in the defect space for both the HA and PHA hydrogels and did not appear to

integrate with the regenerated bone. DVC, DVM, and DVT tissue particles were not observed in any group after the 8 week recovery time.

Biochemical Analysis from *In Vitro* Study

After 2 days of cell growth, DNA content was by far the highest for the PHA-DVT (4-30%) group (14.2 µg/mL), significantly outperforming all other groups (Fig. 4A). Specifically, this PHA-DVT (4-30%) group at day 2 had 6.9, 18.1, 19, 15.6, 13, 6.4, and 3.5 times greater DNA content compared to the TCP, PHA (4%), PHA-DBM (4-10%), PHA-DBM (4-20%), PHA-DBM (4-30%), PHA-DVT (4-10%), and PHA-DVT (4-20%) groups at day 2, respectively ($p < 0.0001$). After 10 days of cell culture on hydrogel groups, the only group with a significant increase in DNA content was the TCP group. The TCP group (12.7 µg/mL) at day 10 had had 6.1 times greater DNA content compared to TCP at day 2 ($p < 0.0001$). The TCP group at day 10 had 21.5, 19.3, 11.7, 10.6, 17.5, and 3.9 times greater DNA content compared to the PHA (4%), PHA-DBM (4-10%), PHA-DBM (4-20%), PHA-DBM (4-30%), PHA-DVT (4-10%), and PHA-DVT (4-20%) groups, respectively ($p < 0.001$). The PHA-DVT (4-30%) group (18.4 µg/mL) at day 10 had 31.2, 28, 16.9, 15.4, 25.4, and 5.6 times greater DNA content compared to the PHA (4%), PHA-DBM (4-10%), PHA-DBM (4-20%), PHA-DBM (4-30%), PHA-DVT (4-10%), and PHA-DVT (4-20%) groups, respectively ($p < 0.0001$).

Calcium assayed at days 2 and 10 showed a significant increase of calcium content in hydrogels containing devitalized tendon. The TCP group had a near zero result (Fig. 4B). PHA-DVT (4-10%) (8.44 mg/dL), PHA-DVT (4-20%)

(8.78 mg/dL), and PHA-DVT (4-30%) (6.82 mg/dL) at day 10 had increases of 2.8, 2.7, and 3.3 times compared to day 2, respectively ($p < 0.0001$). At day 10, The PHA-DVT (4-10%) group had 2.2, 1.6, 3.1, and 6.3 times greater calcium content compared to the PHA (4%), PHA-DBM (4-10%), PHA-DBM (4-20%), and PHA-DBM (4-30%), respectively ($p<0.0001$). The PHA-DVT (4-20%) group at day 10 had 2.3, 1.7, 3.2, and 6.6 times greater calcium content compared to PHA (4%), PHA-DBM (4-10%), PHA-DBM (4-20%), and PHA-DBM (4-30%), respectively ($p < 0.0001$). The PHA-DVT (4-30%) group at day 10 had 1.8, 2.5, and 5.1 times greater calcium content compared to the PHA (4%), PHA-DBM (4-20%), and PHA-DBM (4-30%) groups, respectively ($p < 0.05$). The PHA-DBM (4-10%) group (5.17 mg/dL) at day 10 had 3.9 times greater calcium content compared to the PHA-DBM (4-30%) group ($p < 0.001$). No significant differences were observed among day 2 groups.

Discussion

The current study was the first to evaluate multiple sources of extracellular matrix materials for bone regeneration in a critical size calvarial defect. Hydrogels presented in the current study demonstrated desirable paste-like handling properties for surgical placement and fast crosslinking times. The current study represents the next generation of materials following our previous work using micron-sized decellularized cartilage and hydroxyapatite for calvarial bone regeneration *in vivo*.(36, 37) In designing hydrogels for the current study, aspects such as mechanical performance, both solid (post-crosslinking) and fluid (pre-

crosslinking), were determined to be of great importance for clinical translation and future application to TBI treatment.(20) Mechanical performance of the hydrogel precursor solution and the crosslinked hydrogel, specifically the precursor solution yield stress and the crosslinked hydrogel compressive modulus, respectively, were determined to be vital parameters to demonstrate feasibility for material placement and retention. All hydrogel precursors (prior to crosslinking) exhibited adequate yield stress (τ_y > 200 Pa) for material placement, and the addition of tissue particles increased the average yield stress of all groups. For context, the yield stress of common household items such as mayonnaise and Play-Doh are 200 and 3000 Pa, respectively.(67) The addition of 30% cartilage particles had the greatest effect on material yield stress, potentially due to the presence of the charged proteoglycan, aggrecan.(156) Only PHA-containing groups were evaluated for yield stress as the rheological differences between HA and PHA were assumed to be negligible. After material crosslinking to form hydrogels, the average compressive modulus increased for the groups containing particles; however, the result was only significant in the DCC and some DVT-containing groups. The significant increase in compressive modulus for the DVC and DVT groups was speculated to be attributed to material interaction between the PHA hydrogel and the tissue particle. Although the compressive moduli of the hydrogels tested in the current study were relatively low, the stiffness does not necessarily need to meet that of native bone (i.e., GPa) due to the TBI application requiring flexibility of the biomaterial.(141)

One of the more striking results of the current study was that *in vivo* bone formation differed greatly between the HA- and PHA-containing groups. Both HA and PHA were evaluated due to the speculation that hydrogel crosslinking may influence cellular infiltration. For every group besides the DBM containing group, average bone formation was greater when the tissue was combined with PHA rather than non-crosslinking HA. Due to the aforementioned observation, hydrogel formation may potentially aid in regeneration by providing a three-dimensional framework; however, the hydrogel may also impede access to the colloidal material as demonstrated by the μCT results. The speculation that the PHA hydrogel crosslinking may potentially impede cellular infiltration was debunked for the PHA hydrogels in the current study as demonstrated by H&E staining. Interestingly, the positive control of DBX® had less bone regeneration compared to both HA-DBM and PHA-DBM. DBX® contains approximately 31% cortical bone and 4% hyaluronic acid (M_w = 1 MDa) by weight and would be expected to have similar bone regeneration compared to the non-crosslinking HA-DBM (4-30%) group that had approximately 22% cortical bone by weight.(157) The major difference of DBX® comparatively to HA-DBM (4-30%) and PHA-DBM (4-30%) being the hyaluronic acid molecular weight and bone concentration. The PHA (4%) control group similarly demonstrated greater average bone regeneration compared to DBX®; however, the finding was not significant. Another study used an 80 kDa, 30 wt% maleimide-modified HA (MaHA) hydrogel tested in a critical size rat calvarial defect and reported less bone regeneration on average compared to the current study.(87) Noting

differences of the MaHA hydrogel compared to the current study of HA molecular weight, concentration, and crosslinking mechanism, histological analysis demonstrated that the MaHA gel remained after 8 weeks of recovery. No hydrogel persisted after 8 weeks of recovery in the current study as demonstrated by H&E staining. Further investigation into the relationship between hyaluronic acid molecular weight and bone regeneration is recommended to fully understand the use of the polymer in bone regeneration.

Other groups have evaluated the use of different extracellular matrices for bone regeneration. One such group demonstrated desirable bone regeneration in a mouse calvarial defect model using scaffolds derived from decellularized bovine Achilles tendon seeded with human adipose-derived stem cells.(158) Another group proposed the use of different ECM materials for general hydrogel applications, in which photocrosslinking hydrogels composed of methacrylated gelatin and solubilized-methacrylated-ECM (i.e., cartilage, meniscus, and tendon) were created and tested for *in vitro* gene expression.(145) Perhaps the majority of focus into new ECM materials for bone regeneration has been targeted at using cartilage as a material for bone regeneration.(36, 128, 143, 144) Although other groups have demonstrated promise for cartilage as a material to facilitate bone regeneration, including our own group, the current study demonstrated minimal regeneration compared to previous studies as indicated by µCT and H&E staining.

Groups with significantly greater bone regeneration compared to the sham were selected for further refinement *in vitro* to determine the most attractive tissue

particle concentration for future application to TBI treatment. PHA (4%), PHA-DBM (4-30%), and PHA-DVT (4-30%) were selected for further refinement. Although the HA-DBM (4-30%) group had the largest bone regeneration in the current study, a crosslinking hydrogel is necessary for application to TB treatment, thus the PHA-DBM (4-30%) group was included due to the large bone regeneration observed in the HA-DBM (4-30%) group. Material crosslinking is necessary for potential application to a single surgical intervention to treat TBI, thus refining the material to determine the minimum particle concentration to achieve maximum crosslinking was explored. *In vitro* studies demonstrated significantly greater proliferation on the PHA-DVT (4-30%) group, potentially attributed to greater initial cellular adhesion during seeding. Interestingly, cellular number did not significantly change over 10 days on the hydrogel groups. Initial calcium deposition was relatively the same for hydrogel groups after 2 days of culture, but significantly increased on hydrogels containing DVT by 10 days. Overall, DVT hydrogels outperformed other crosslinked hydrogels and calcium deposition suggested that the most desirable particle concentration would be 10%. Future studies will focus on using the refined particle concentration in a rat TBI model.

Conclusion

The current study demonstrated the feasibility of PHA hydrogels encapsulating ECM tissue particles for use in calvarial bone regeneration. Desirable paste-like handling properties of the pre-crosslinked hydrogels, and

mechanical performance after crosslinking was demonstrated in the current study for relevance to TBI. The addition of tissue particles increased both the yield stress and compressive modulus of the material on average, with the cartilage particles leading to the greatest yield stress. The PHA (4%) and PHA-DVT (4-30%) groups led to the greatest bone regeneration, and the tendon particles likewise demonstrated superior calcium deposition by MC3T3 cells *in vitro*, with 10% DVT appearing to be the most desirable concentration. Future studies will attempt to evaluate leading materials in an *in vivo* rat TBI model.

Chapter 6: Conclusion

The current dissertation has successfully identified a pliable hydrogel material capable of regenerating bone in a critical size calvarial defect with potential application to the treatment of traumatic brain injury (TBI). Hydrogels are an attractive choice for regenerative medicine approaches, highlighting their capability for *in situ* placement to fill any size or shape of tissue defect, a secondary crosslinking mechanism to ensure retention at the site of application, pliability after crosslinking for tailored application such as TBI, and the inherent ability to encapsulate other materials or biosignals for specific tissue regeneration. The hydrogel precursor performance can be further tailored with clinical translation in mind, creating precursor solutions that exhibit paste-like or putty-like handling properties for ease of placement. For the aforementioned reasons, hydrogels were selected for application in calvarial bone regeneration and treatment of TBI.

To successfully create a hydrogel material for application to a single-stage TBI treatment the material must remain pliable after initial implantation to allow un-impeded brain swelling, prevent the manifestation of neurological conditions, and regenerate bone spanning a critical size defect. Hydrogels are inherently pliable after crosslinking, thus the first step in designing hydrogels for TBI application is to create a hydrogel that can adequately regenerate bone in a critical size defect. Predecessors of the current dissertation have evaluated the use of physical “colloidal gels” comprised of synthetic particles capable of tailored biosignal release to promote calvarial bone regeneration.(31, 32, 34, 37, 103,

108) The colloidal gels were capable of exhibiting desirable paste-like handling properties for placement and demonstrated promising *in* vitro cell response. The encouraging results from predecessors using colloidal gels prompted their use in the current dissertation, marking the beginning of the research presented.

Colloidal hydrogels comprised of hyaluronic acid (HA), hydroxyapatite nanoparticles (HAp), and extracellular matrix (ECM) materials of demineralized bone matrix (DBM) or decellularized cartilage (DCC) exhibited ideal handling performance for implantation. Comparing the use of ECM materials to growth factors such as bone morphogenetic protein-2 (BMP-2) or vascular endothelial growth factor (VEGF), similar bone regeneration was observed between the HA-HAp (BMP-2) group and the HA-HAp-DCC group. DBM containing groups on average had lower bone regeneration compared to the HA-HAp-DCC group, suggesting that materials other than the traditional DBM could be used for bone regeneration. The aforementioned findings suggested that ECM materials could be used in place of costly growth factors to create clinically translatable products and prompted additional research using DCC in bone regeneration. One major down-fall of the colloidal gels used in Aim 1 was the lack of a crosslinking mechanism, which resulted in material retention issues, which I believe may have led to diminished regenerative potential. To circumvent the material retention issue observed and further evaluate the use of cartilage ECM as a material for bone regeneration, a crosslinking hydrogel material was selected for subsequent studies.

Predecessors of this work had previously developed a crosslinking hydrogel matrix comprised of naturally derived decellularized cartilage matrix for use in cartilage regenerative medicine.(48, 89) The methacrylated solubilized decellularized cartilage (MeSDCC) hydrogel exhibited desirable handling performance prior to crosslinking, high mechanical stiffness after crosslinking, and the ability to encapsulate nano- and micron-size particles. The MeSDCC hydrogels were an attractive material choice to address material retention issues while expanding upon the use of cartilage ECM for bone regeneration in aim 2 studies.

MeSDCC could be further refined for bone regeneration by the addition of rat mesenchymal stem cells, or synthetic osteoconductive particles of bioglass microparticles or hydroxyapatite nanofibers. MeSDCC results following the 8 week *in vivo* study were lackluster in terms of bone regeneration. Clear differences in average bone regeneration were observed between the use of DCC and MeSDCC, prompting speculation into why these potential differences may exist. Tissue processing was speculated to be the major contributing factor, as tissue solubilization using protein digestion most likely diminished ECM bioactivity by degrading the ECM into unrecognizable components. For future studies, utilizing cartilage it is highly recommended to minimize tissue processing to retain material bioactivity, thus cartilage devitalization is an attractive approach. Devitalization, which is similar to decellularization, only incorporates physical processing (i.e., granulating) methods without the additional step of chemical decellularization. To retain material bioactivity, both tissue

decellularization and solubilization were excluded from future studies to retain material bioactivity. One major drawback associated with the exclusion of tissue decellularization was that there could now be potential for an immune response due to foreign tissue. Although this concern was noted at the time, ECM sources selected were generally acellular and did not require decellularization during allogenic tissue implantation.

In moving forward, the objective was to combine the bone regeneration observed in aim 1 with the crosslinking of aim 2. Additionally, ECM sources such as demineralized bone matrix (DBM), devitalized cartilage (DVC), devitalized meniscus (DVM), and devitalized tendon (DVT) were included to expand the evaluation of different ECM materials for bone regeneration. Both non-crosslinking HA and crosslinking HA hydrogels were evaluated for *In vivo* bone regeneration after 8 weeks. Significant bone regeneration was observed for the HA-DBM (4-30%), PHA (4%), and PHA-DVT (4-30%) groups compared to the sham. I then sought to refine the colloidal particle concentration to determine the minimum concentration required to achieve the highest crosslinking density for application to TBI and the most economically feasible formulation for clinical translation and affordability. Due to the HA-DBM (4-30%) group not being able to crosslink, the PHA-DBM (4-30%) group was included in the *in vitro* colloidal refinement study. Calcium deposition suggested superior bone regeneration from the PHA-DVT (4-10%) group, and overall the most attractive material for application to a single-stage surgical intervention to treat TBI. In hindsight, further *in vitro* analysis and refinement of groups following the *in vivo* study would have

increased confidence in the colloidal refinement. Multiple time points, and a longer overall study time may have helped reassure and better pinpoint the most attractive colloidal concentration. Before additional *in vivo* work is conducted, it is strongly recommended that the *in vitro* study is repeated with time points of 14 and 21 days to better observe deposited calcium and include ELISA testing for osteogenic markers such as osteocalcin release.

In vivo testing prior to *in vitro* refinement was beneficial to the study as the *in vivo* animal model served as a reliable method to evaluate various osteogenic materials. The *in vitro* model, which provides less confidence compared to an *in vivo* animal model, acted to refine the superior groups rather than exclude groups. The route of performing *in vivo* before *in vitro* is uncommon within the field, potentially due to the associated monetary cost for animal studies. Although *in vitro* studies can be a cost-effective method for eliminating a large number of potential options, the reality persists that the *in vitro* model may not accurately depict the *in vivo* environment. For the aforementioned reasons, an iterative design between *in vitro* and *in vivo* models is recommended for future experimental designs.

A limitation of the current dissertation was the lack of physical evaluation of regenerated calvarial bone following the *in vivo* rat study. Various methods exist to mechanically characterize the regenerated bone such as indentation testing, which is used to determine the stiffness, or push-out testing, which is used to evaluate the interfacial strength. Although the mechanical characterization would be of potential value for comparing different materials in a

research setting, a clinician may be more interested in the extent of regenerated bone across the entire defect to ensure patient safety. Indentation mapping of the entire defect space may be the most relevant test to satisfy both scientists and medical professionals. Although indentation mapping would not provide information on the defect interfacial strength, it would provide information on the degree of bone stiffness at various points of the defect.

Although the greatest crosslinking hydrogel bone regeneration was observed using DVT, impressive bone regeneration was also observed in the control PHA hydrogel without the addition of ECM particles. Comparing to another study using a similar HA based hydrogel, which utilized a lower molecular weight (80 kDa), the average bone regeneration was greater for the higher molecular weight HA based hydrogel used in the current dissertation.(87) The difference in observed bone regeneration suggests further research is needed in the evaluation of HA as a material for bone regeneration. Publications utilizing HA based hydrogels rarely provide background information into the selection process for hydrogel characteristics such as the choice of molecular weight, concentration, and compressive modulus. The current dissertation is in part at fault for the same aforementioned reasons, and further research is necessary to understand how molecular weight, concentration, and hydrogel stiffness effects cellular response. Although the physical material component may only be a piece of the larger puzzle, a better understanding of how HA properties effect cellular response can lead to enhanced regenerative potential.

The current dissertation has successfully identified a hydrogel material capable of regenerating bone in a critical size calvarial defect, utilizing natural materials as an affordable alternative to growth factors such as BMP-2, and capable of remaining pliable after initial implantation. Future studies will be conducted to evaluate the use of the PHA hydrogels encapsulating tendon ECM in a rat TBI model. At the time of writing the current dissertation, the rat TBI model was still under development. After successful development of the model by Dr. Brian Andrew's team at the University of Kansas Medical Center, the hydrogel will be evaluated for application of the material for the treatment of TBI following decompressive craniectomy.

References

1. Klouda L, Mikos AG. Thermoresponsive hydrogels in biomedical applications. Eur J Pharm Biopharm. 2008;68(1):34-45. doi: 10.1016/j.ejpb.2007.02.025. PubMed PMID: 17881200; PMCID: PMC3163097.

2. Beck EC, Barragan M, Tadros MH, Kiyotake EA, Acosta FM, Kieweg SL, Detamore MS. Chondroinductive Hydrogel Pastes Composed of Naturally Derived Devitalized Cartilage. Ann Biomed Eng. 2016;44(6):1863-80. doi: 10.1007/s10439-015-1547-5. PubMed PMID: 26744243; PMCID: PMC5209355.

3. Ferreira JR, Padilla R, Urkasemsin G, Yoon K, Goeckner K, Hu WS, Ko CC. Titanium-enriched hydroxyapatite-gelatin scaffolds with osteogenically differentiated progenitor cell aggregates for calvaria bone regeneration. Tissue Eng Part A. 2013;19(15-16):1803-16. doi: 10.1089/ten.TEA.2012.0520. PubMed PMID: 23495972; PMCID: PMC3700087.

4. Lu HD, Soranno DE, Rodell CB, Kim IL, Burdick JA. Secondary photocrosslinking of injectable shear-thinning dock-and-lock hydrogels. Adv Healthc Mater. 2013;2(7):1028-36. doi: 10.1002/adhm.201200343. PubMed PMID: 23299998.

5. Visser J, Levett PA, te Moller NC, Besems J, Boere KW, van Rijen MH, de Grauw JC, Dhert WJ, van Weeren PR, Malda J. Crosslinkable hydrogels derived from cartilage, meniscus, and tendon tissue. Tissue Eng Part A. 2015;21(7-8):1195-206. doi: 10.1089/ten.TEA.2014.0362. PubMed PMID: 25557049; PMCID: PMC4394887.

6. Sridharan B, Sharma B, Detamore MS. A Road Map to Commercialization of Cartilage Therapy in the United States of America. Tissue Eng Part B Rev. 2015. doi: 10.1089/ten.TEB.2015.0147. PubMed PMID: 26192161; PMCID: PMC4753577.

7. Sutherland AJ, Converse GL, Hopkins RA, Detamore MS. The bioactivity of cartilage extracellular matrix in articular cartilage regeneration. Adv Healthc Mater. 2015;4(1):29-39. doi: 10.1002/adhm.201400165. PubMed PMID: 25044502; PMCID: PMC4286437.

8. Brown TE, Marozas IA, Anseth KS. Amplified Photodegradation of Cell-Laden Hydrogels via an Addition-Fragmentation Chain Transfer Reaction. Adv Mater. 2017. doi: 10.1002/adma.201605001. PubMed PMID: 28112845.

9. Peak CW, Wilker JJ, Schmidt G. A review on tough and sticky hydrogels. Colloid and Polymer Science. 2013;291(9):2031-47. doi: 10.1007/s00396-013-3021-y.

10. Rosiak JM, Yoshii F. Hydrogels and their medical applications. Nuclear Instruments and Methods in Physics Research Section B: Beam Interactions with Materials and Atoms. 1999;151(1-4):56-64. doi: 10.1016/s0168-583x(99)00118-4.

11. Peppas NA. Hydrogels and drug delivery. Curr Opin Colloid In. 1997;2(5):531-7. doi: 10.1016/s1359-0294(97)80103-3.

12. Shewan HM, Stokes JR. Review of techniques to manufacture micro-hydrogel particles for the food industry and their applications. Journal of Food Engineering. 2013;119(4):781-92. doi: 10.1016/j.jfoodeng.2013.06.046.

13. Di Giuseppe E, Corbi F, Funiciello F, Massmeyer A, Santimano TN, Rosenau M, Davaille A. Characterization of Carbopol® hydrogel rheology for experimental tectonics and geodynamics. Tectonophysics. 2015;642:29-45. doi: 10.1016/j.tecto.2014.12.005.

14. Hu X, Hao L, Wang H, Yang X, Zhang G, Wang G, Zhang X. Hydrogel Contact Lens for Extended Delivery of Ophthalmic Drugs. International Journal of Polymer Science. 2011;2011:1-9. doi: 10.1155/2011/814163.

15. Omidian H, Rocca JG, Park K. Advances in superporous hydrogels. J Control Release. 2005;102(1):3-12. doi: 10.1016/j.jconrel.2004.09.028. PubMed PMID: 15653129.

16. Gruskin E, Doll BA, Futrell FW, Schmitz JP, Hollinger JO. Demineralized bone matrix in bone repair: history and use. Adv Drug Deliv Rev. 2012;64(12):1063-77. doi: 10.1016/j.addr.2012.06.008. PubMed PMID: 22728914.

17. Peppas N. Hydrogels in pharmaceutical formulations. European Journal of Pharmaceutics and Biopharmaceutics. 2000;50(1):27-46. doi: 10.1016/s0939-6411(00)00090-4.

18. Murphy PS, Evans GR. Advances in wound healing: a review of current wound healing products. Plast Surg Int. 2012;2012:190436. doi: 10.1155/2012/190436. PubMed PMID: 22567251; PMCID: PMC3335515.

19. Hunziker EB, Lippuner K, Keel MJ, Shintani N. An educational review of cartilage repair: precepts & practice--myths & misconceptions--progress & prospects. Osteoarthritis Cartilage. 2015;23(3):334-50. doi: 10.1016/j.joca.2014.12.011. PubMed PMID: 25534362.

20. Kretlow JD, Young S, Klouda L, Wong M, Mikos AG. Injectable biomaterials for regenerating complex craniofacial tissues. Adv Mater. 2009;21(32-33):3368-93. doi: 10.1002/adma.200802009. PubMed PMID: 19750143; PMCID: PMC2742469.

21. Hoffman AS. Hydrogels for biomedical applications. Advanced Drug Delivery Reviews. 2012;64:18-23. doi: 10.1016/j.addr.2012.09.010.

22. D'Este M, Eglin D. Hydrogels in calcium phosphate moldable and injectable bone substitutes: Sticky excipients or advanced 3-D carriers? Acta Biomater. 2013;9(3):5421-30. doi: 10.1016/j.actbio.2012.11.022. PubMed PMID: 23201020.

23. DePuy Synthes Website [cited 2016 August]. Available from: www.synthes.com.

24. Salgado CL, Sanchez EM, Zavaglia CA, Almeida AB, Granja PL. Injectable biodegradable polycaprolactone-sebacic acid gels for bone tissue engineering. Tissue Eng Part A. 2012;18(1-2):137-46. doi: 10.1089/ten.TEA.2011.0294. PubMed PMID: 21902607.

25. Yu L, Ding J. Injectable hydrogels as unique biomedical materials. Chem Soc Rev. 2008;37(8):1473-81. doi: 10.1039/b713009k. PubMed PMID: 18648673.

26. Wang H, Hansen MB, Lowik DW, van Hest JC, Li Y, Jansen JA, Leeuwenburgh SC. Oppositely charged gelatin nanospheres as building blocks for injectable and biodegradable gels. Adv Mater.

2011;23(12):H119-24. doi: 10.1002/adma.201003908. PubMed PMID: 21394793.

27. Gratson G, Xu M, Lewis JA. Direct writing of three- dimensional webs. Nature. 2004;428:386.

28. Smay JE, Gratson GM, Shepherd RF, Cesarano J, Lewis JA. Directed Colloidal Assembly of 3D Periodic Structures. Advanced Materials. 2002;14(18):1279-83.

29. Arimura H, Ohya Y, Ouchi T, Yamada H. Preparation of a biodegradable matrix through polyion complex formation by mixing polylactide-based microspheres having oppositely charged surfaces. Journal of Colloid and Interface Science. 2004;270(2):299-303. doi: http://dx.doi.org/10.1016/j.jcis.2003.10.010.

30. Van Tomme SR, van Steenbergen MJ, De Smedt SC, van Nostrum CF, Hennink WE. Self-gelling hydrogels based on oppositely charged dextran microspheres. Biomaterials. 2005;26(14):2129-35. doi: http://dx.doi.org/10.1016/j.biomaterials.2004.05.035.

31. Wang Q, Wang L, Detamore MS, Berkland C. Biodegradable Colloidal Gels as Moldable Tissue Engineering Scaffolds. Advanced Materials. 2008;20(2):236-9. doi: 10.1002/adma.200702099.

32. Wang Q, Wang J, Lu Q, Detamore MS, Berkland C. Injectable PLGA based colloidal gels for zero-order dexamethasone release in cranial defects. Biomaterials. 2010;31(18):4980-6. doi: 10.1016/j.biomaterials.2010.02.052. PubMed PMID: 20303585; PMCID: PMC2856787.

33. Fakhari A, Phan Q, Thakkar SV, Middaugh CR, Berkland C. Hyaluronic Acid Nanoparticles Titrate the Viscoelastic Properties of Viscosupplements. Langmuir. 2013;29(17):5123-31. doi: 10.1021/la304575x.

34. Dennis SC, Detamore MS, Kieweg SL, Berkland CJ. Mapping glycosaminoglycan-hydroxyapatite colloidal gels as potential tissue defect fillers. Langmuir. 2014;30(12):3528-37. doi: 10.1021/la4041985. PubMed PMID: 24606047; PMCID: PMC3974614.

35. Beck EC, Lohman BL, Tabakh DB, Kieweg SL, Gehrke SH, Berkland CJ, Detamore MS. Enabling Surgical Placement of Hydrogels Through Achieving Paste-Like Rheological Behavior in Hydrogel Precursor Solutions. Ann Biomed Eng. 2015;43(10):2569-76. doi: 10.1007/s10439-015-1277-8. PubMed PMID: 25691398; PMCID: PMC4540702.

36. Townsend JM, Dennis SC, Whitlow J, Feng Y, Wang J, Andrews B, Nudo RJ, Detamore MS, Berkland CJ. Colloidal Gels with Extracellular Matrix Particles and Growth Factors for Bone Regeneration in Critical Size Rat Calvarial Defects. The AAPS Journal. 2017;19(3):703-11. doi: 10.1208/s12248-017-0045-0.

37. Dennis SC, Whitlow J, Detamore MS, Kieweg SL, Berkland CJ. Hyaluronic-Acid-Hydroxyapatite Colloidal Gels Combined with Micronized Native ECM as Potential Bone Defect Fillers. Langmuir. 2017;33(1):206-18. doi: 10.1021/acs.langmuir.6b03529. PubMed PMID: 28005380.

38. Wilson CB. Adoption of new surgical technology. BMJ. 2006;332(7533):112-4. doi: 10.1136/bmj.332.7533.112. PubMed PMID: 16410591; PMCID: PMC1326944.

39. Fernandez-Moure JS. Lost in Translation: The Gap in Scientific Advancements and Clinical Application. Front Bioeng Biotechnol. 2016;4:43. doi: 10.3389/fbioe.2016.00043. PubMed PMID: 27376058; PMCID: PMC4891347.

40. Ibrahim AM, Varban OA, Dimick JB. Novel Uses of Video to Accelerate the Surgical Learning Curve. J Laparoendosc Adv Surg Tech A. 2016;26(4):240-2. doi: 10.1089/lap.2016.0100. PubMed PMID: 27031876; PMCID: PMC4845634.

41. Bruns NE, Irtan S, Rothenberg SS, Bogen EM, Kotobi H, Ponsky TA. Trans-Atlantic Telementoring with Pediatric Surgeons: Technical Considerations and Lessons Learned. J Laparoendosc Adv Surg Tech A. 2016;26(1):75-8. doi: 10.1089/lap.2015.0131. PubMed PMID: 26698191.

42. Kwon JS, Yoon SM, Kwon DY, Kim DY, Tai GZ, Jin LM, Song B, Lee B, Kim JH, Han DK, Min BH, Kim MS. Injectable in situ-forming hydrogel for cartilage tissue engineering. Journal of Materials Chemistry B. 2013;1(26):3314. doi: 10.1039/c3tb20105h.

43. Spicer PP, Kretlow JD, Young S, Jansen JA, Kasper FK, Mikos AG. Evaluation of bone regeneration using the rat critical size calvarial defect. Nat Protoc. 2012;7(10):1918-29. doi: 10.1038/nprot.2012.113. PubMed PMID: 23018195; PMCID: PMC3513397.

44. Dumas JE, Zienkiewicz K, Tanner SA, Prieto EM, Bhattacharyya S, Guelcher SA. Synthesis and characterization of an injectable allograft bone/polymer composite bone void filler with tunable mechanical properties. Tissue Eng Part A. 2010;16(8):2505-18. doi: 10.1089/ten.TEA.2009.0672. PubMed PMID: 20218874.

45. Geisler IM, Schneider JP. Evolution-Based Design of an Injectable Hydrogel. Advanced Functional Materials. 2012;22(3):529-37. doi: 10.1002/adfm.201102330.

46. Glassman MJ, Chan J, Olsen BD. Reinforcement of Shear Thinning Protein Hydrogels by Responsive Block Copolymer Self-Assembly. Adv Funct Mater. 2013;23(9):1182-93. doi: 10.1002/adfm.201202034. PubMed PMID: 25568642; PMCID: PMC4283780.

47. Lu HD, Charati MB, Kim IL, Burdick JA. Injectable shear-thinning hydrogels engineered with a self-assembling Dock-and-Lock mechanism. Biomaterials. 2012;33(7):2145-53. doi: 10.1016/j.biomaterials.2011.11.076. PubMed PMID: 22177842.

48. Beck EC, Barragan M, Libeer TB, Kieweg SL, Converse GL, Hopkins RA, Berkland CJ, Detamore MS. Chondroinduction from Naturally Derived Cartilage Matrix: A Comparison Between Devitalized and Decellularized Cartilage Encapsulated in Hydrogel Pastes. Tissue Eng Part A. 2016;22(7-8):665-79. doi: 10.1089/ten.TEA.2015.0546. PubMed PMID: 27001140; PMCID: PMC4840832.

49. Fakhari A, Phan Q, Berkland C. Hyaluronic acid colloidal gels as self-assembling elastic biomaterials. J Biomed Mater Res B Appl Biomater. 2014;102(3):612-8. doi: 10.1002/jbm.b.33041. PubMed PMID: 24124008.

50. Tsaryk R, Gloria A, Russo T, Anspach L, De Santis R, Ghanaati S, Unger RE, Ambrosio L, Kirkpatrick CJ. Collagen-low molecular weight hyaluronic acid semi-interpenetrating network loaded with gelatin microspheres for cell and growth factor delivery for nucleus pulposus

regeneration. Acta Biomater. 2015;20:10-21. doi: 10.1016/j.actbio.2015.03.041. PubMed PMID: 25861947.

51. Beck E, Berkland C, Gehrke S, Detamore M, editors. Novel hyaluronic acid nanocomposite hydrogel for cartilage tissue engineering: utilizing yield stress for ease of implantation. Summer Bioengineering Conference; 2013; Sunriver, Oregon, USA: ASME.
52. Guvendiren M, Lu HD, Burdick JA. Shear-thinning hydrogels for biomedical applications. Soft Matter. 2012;8(2):260-72. doi: 10.1039/c1sm06513k.

53. Wagner NJ, Brady JF. Shear thickening in colloidal dispersions. Physics Today. 2009;62(10):27-32. doi: 10.1063/1.3248476.

54. Barbucci R, Leone G, Lamponi S. Thixotrophy property of hydrogels to evaluate the cell growing on the inside of the material bulk (Amber effect). J Biomed Mater Res B Appl Biomater. 2006;76(1):33-40. doi: 10.1002/jbm.b.30390. PubMed PMID: 16240431.

55. Barnes HA. Thixotropy - A review. J Non-Newton Fluid. 1997;70(1-2):1-33. doi: Doi 10.1016/S0377-0257(97)00004-9. PubMed PMID: WOS:A1997XB14900001.

56. Lee CH, Moturi V, Lee Y. Thixotropic property in pharmaceutical formulations. J Control Release. 2009;136(2):88-98. doi: 10.1016/j.jconrel.2009.02.013. PubMed PMID: 19250955.

57. Dennis SC, Whitlow J, Detamore MS, Kieweg SL, Berkland CJ. Hyaluronic-Acid–Hydroxyapatite Colloidal Gels Combined with Micronized Native ECM as Potential Bone Defect Fillers. Langmuir. 2016. doi: 10.1021/acs.langmuir.6b03529.

58. Hao X, Liu H, Lu Z, Xie Y, Yang H. Endowing the conventional HMPAM hydrogel with pH-responsive and self-healing properties. Journal of Materials Chemistry A. 2013;1(23):6920. doi: 10.1039/c3ta10285h.

59. Gaharwar AK, Avery RK, Assmann A, Paul A, McKinley GH, Khademhosseini A, Olsen BD. Shear-thinning nanocomposite hydrogels for the treatment of hemorrhage. ACS Nano. 2014;8(10):9833-42. doi: 10.1021/nn503719n. PubMed PMID: 25221894; PMCID: PMC4212795.

60. Olsen BD, Kornfield JA, Tirrell DA. Yielding Behavior in Injectable Hydrogels from Telechelic Proteins. Macromolecules. 2010;43(21):9094-9. doi: 10.1021/ma101434a. PubMed PMID: 21221427; PMCID: PMC3017468.

61. Liu Q, Zhan C, Barhoumi A, Wang W, Santamaria C, McAlvin JB, Kohane DS. A Supramolecular Shear-Thinning Anti-Inflammatory Steroid Hydrogel. Adv Mater. 2016;28(31):6680-6. doi: 10.1002/adma.201601147. PubMed PMID: 27214390.

62. Gao L, Gao Y, Lin Y, Ju Y, Yang S, Hu J. A Charge-Transfer-Induced Self-Healing Supramolecular Hydrogel. Chem Asian J. 2016;11(23):3430-5. doi: 10.1002/asia.201601216. PubMed PMID: 27685710.

63. Yu H, Liu Y, Yang H, Peng K, Zhang X. An Injectable Self-Healing Hydrogel Based on Chain-Extended PEO-PPO-PEO Multiblock Copolymer. Macromol Rapid Commun. 2016;37(21):1723-8. doi: 10.1002/marc.201600323. PubMed PMID: 27633950.

64. Dumas JE, BrownBaer PB, Prieto EM, Guda T, Hale RG, Wenke JC, Guelcher SA. Injectable reactive biocomposites for bone healing in critical-size rabbit calvarial defects. Biomed Mater. 2012;7(2):024112. doi: 10.1088/1748-6041/7/2/024112. PubMed PMID: 22456057.

65. Osswald T, Rudolph N. Polymer Rheology - Fundamentals and Applications. Hanser Publishers.

66. Wang Q, Jamal S, Detamore MS, Berkland C. PLGA-chitosan/PLGA-alginate nanoparticle blends as biodegradable colloidal gels for seeding human umbilical cord mesenchymal stem cells. J Biomed Mater Res A. 2011;96(3):520-7. doi: 10.1002/jbm.a.33000. PubMed PMID: 21254383; PMCID: PMC3080015.

67. Samaniuk JR, Shay TW, Root TW, Klingenberg DJ, Scott CT. A novel rheometer design for yield stress fluids. AIChE Journal. 2014;60(4):1523-8. doi: 10.1002/aic.14329.

68. Priyadarshani P, Li Y, Yang S, Yao L. Injectable hydrogel provides growth-permissive environment for human nucleus pulposus cells. J Biomed Mater Res A. 2016;104(2):419-26. doi: 10.1002/jbm.a.35580. PubMed PMID: 26422588.

69. Ballios BG, Cooke MJ, Donaldson L, Coles BL, Morshead CM, van der Kooy D, Shoichet MS. A Hyaluronan-Based Injectable Hydrogel Improves the Survival and Integration of Stem Cell Progeny following Transplantation. Stem Cell Reports. 2015;4(6):1031-45. doi: 10.1016/j.stemcr.2015.04.008. PubMed PMID: 25981414; PMCID: PMC4471829.

70. Su WY, Chen YC, Lin FH. Injectable oxidized hyaluronic acid/adipic acid dihydrazide hydrogel for nucleus pulposus regeneration. Acta Biomater. 2010;6(8):3044-55. doi: 10.1016/j.actbio.2010.02.037. PubMed PMID: 20193782.

71. Vadala G, Russo F, Di Martino A, Denaro V. Intervertebral disc regeneration: from the degenerative cascade to molecular therapy and tissue engineering. J Tissue Eng Regen Med. 2015;9(6):679-90. doi: 10.1002/term.1719. PubMed PMID: 23512973.

72. Xie B, Jin L, Luo Z, Yu J, Shi S, Zhang Z, Shen M, Chen H, Li X, Song Z. An injectable thermosensitive polymeric hydrogel for sustained release of Avastin(R) to treat posterior segment disease. Int J Pharm. 2015;490(1-2):375-83. doi: 10.1016/j.ijpharm.2015.05.071. PubMed PMID: 26027491.

73. Zeng Y, Chen C, Liu W, Fu Q, Han Z, Li Y, Feng S, Li X, Qi C, Wu J, Wang D, Corbett C, Chan BP, Ruan D, Du Y. Injectable microcryogels reinforced alginate encapsulation of mesenchymal stromal cells for leak-proof delivery and alleviation of canine disc degeneration. Biomaterials. 2015;59:53-65. doi: 10.1016/j.biomaterials.2015.04.029. PubMed PMID: 25956851.

74. Koreen IV, McClintic EA, Mott RT, Stanton C, Yeatts RP. Evisceration with Injectable Hydrogel Implant in a Rabbit Model. Ophthal Plast Reconstr Surg. 2016. doi: 10.1097/IOP.0000000000000679. PubMed PMID: 27015238.

75. Suenaga H, Furukawa KS, Suzuki Y, Takato T, Ushida T. Bone regeneration in calvarial defects in a rat model by implantation of human bone marrow-derived mesenchymal stromal cell spheroids. J Mater Sci Mater Med. 2015;26(11):254. doi: 10.1007/s10856-015-5591-3. PubMed PMID: 26449444; PMCID: PMC4598349.

76. Oliveira SM, Barrias CC, Almeida IF, Costa PC, Ferreira MR, Bahia MF, Barbosa MA. Injectability of a bone filler system based on hydroxyapatite microspheres and a vehicle with in situ gel-forming ability. J Biomed Mater Res B Appl Biomater. 2008;87(1):49-58. doi: 10.1002/jbm.b.31066. PubMed PMID: 18437700.

77. Herschel WH, Bulkley R. Konsistenzmessungen von Gummi-Benzollösungen. Kolloid-Zeitschrift. 1926;39(4):291-300. doi: 10.1007/bf01432034.

78. Ahmad NH, Ahmed J, Hashim DM, Manap YA, Mustafa S. Oscillatory and steady shear rheology of gellan/dextran blends. J Food Sci Technol. 2015;52(5):2902-9. doi: 10.1007/s13197-014-1330-x. PubMed PMID: 25892789; PMCID: PMC4397348.

79. Aktas S, Kalyon DM, Marín-Santibáñez BM, Pérez-González J. Shear viscosity and wall slip behavior of a viscoplastic hydrogel. Journal of Rheology. 2014;58(2):513-35. doi: 10.1122/1.4866295.

80. Albu MG, Ghica MV, Popa L, Leca M, Trandafir V. Kinetics of in Vitro Release of Doxycycline Hyclate from Collagen Hydrogels. Rev Roum Chim. 2009;54(5):373-+. PubMed PMID: WOS:000270468200007.

81. Francisco AT, Hwang PY, Jeong CG, Jing L, Chen J, Setton LA. Photocrosslinkable laminin-functionalized polyethylene glycol hydrogel for intervertebral disc regeneration. Acta Biomater. 2014;10(3):1102-11. doi: 10.1016/j.actbio.2013.11.013. PubMed PMID: 24287160; PMCID: PMC3969710.

82. Li B, Wang L, Xu F, Gang X, Demirci U, Wei D, Li Y, Feng Y, Jia D, Zhou Y. Hydrosoluble, UV-crosslinkable and injectable chitosan for patterned cell-laden microgel and rapid transdermal curing hydrogel in vivo. Acta Biomater. 2015;22:59-69. doi: 10.1016/j.actbio.2015.04.026. PubMed PMID: 25917845.

83. Chuang CH, Lin RZ, Tien HW, Chu YC, Li YC, Melero-Martin JM, Chen YC. Enzymatic regulation of functional vascular networks using gelatin hydrogels. Acta Biomater. 2015;19:85-99. doi: 10.1016/j.actbio.2015.02.024. PubMed PMID: 25749296; PMCID: PMC4589259.

84. Duffy CV, David L, Crouzier T. Covalently-crosslinked mucin biopolymer hydrogels for sustained drug delivery. Acta Biomater. 2015;20:51-9. doi: 10.1016/j.actbio.2015.03.024. PubMed PMID: 25818947.

85. Choi B, Kim S, Lin B, Li K, Bezouglaia O, Kim J, Evseenko D, Aghaloo T, Lee M. Visible-light-initiated hydrogels preserving cartilage extracellular signaling for inducing chondrogenesis of mesenchymal stem cells. Acta Biomater. 2015;12:30-41. doi: 10.1016/j.actbio.2014.10.013. PubMed PMID: 25462526.

86. Kumar D, Gerges I, Tamplenizza M, Lenardi C, Forsyth NR, Liu Y. Three-dimensional hypoxic culture of human mesenchymal stem cells encapsulated in a photocurable, biodegradable polymer hydrogel: a potential injectable cellular product for nucleus pulposus regeneration. Acta Biomater. 2014;10(8):3463-74. doi: 10.1016/j.actbio.2014.04.027. PubMed PMID: 24793656.

87. Holloway JL, Ma H, Rai R, Hankenson KD, Burdick JA. Synergistic Effects of SDF-1alpha and BMP-2 Delivery from Proteolytically Degradable Hyaluronic Acid Hydrogels for Bone Repair. Macromol Biosci. 2015;15(9):1218-23. doi: 10.1002/mabi.201500178. PubMed PMID: 26059079; PMCID: PMC4558375.

88. Levett PA, Melchels FP, Schrobback K, Hutmacher DW, Malda J, Klein TJ. A biomimetic extracellular matrix for cartilage tissue engineering centered on photocurable gelatin, hyaluronic acid and chondroitin sulfate. Acta Biomater. 2014;10(1):214-23. doi: 10.1016/j.actbio.2013.10.005. PubMed PMID: 24140603.

89. Beck EC, Barragan M, Tadros MH, Gehrke SH, Detamore MS. Approaching the compressive modulus of articular cartilage with a decellularized cartilage-based hydrogel. Acta Biomater. 2016;38:94-105. doi: 10.1016/j.actbio.2016.04.019. PubMed PMID: 27090590; PMCID: PMC4903909.

90. Jin R, Teixeira LS, Dijkstra PJ, van Blitterswijk CA, Karperien M, Feijen J. Enzymatically-crosslinked injectable hydrogels based on biomimetic dextran-hyaluronic acid conjugates for cartilage tissue engineering. Biomaterials. 2010;31(11):3103-13. doi: 10.1016/j.biomaterials.2010.01.013. PubMed PMID: 20116847.

91. Yuan L, Li B, Yang J, Ni Y, Teng Y, Guo L, Fan H, Fan Y, Zhang X. Effects of Composition and Mechanical Property of Injectable Collagen I/II Composite Hydrogels on Chondrocyte Behaviors. Tissue Eng Part A. 2016;22(11-12):899-906. doi: 10.1089/ten.TEA.2015.0513. PubMed PMID: 27221620.

92. Ghosh K, Shu XZ, Mou R, Lombardi J, Prestwich GD, Rafailovich MH, Clark RA. Rheological characterization of in situ cross-linkable hyaluronan hydrogels. Biomacromolecules. 2005;6(5):2857-65. doi: 10.1021/bm050361c. PubMed PMID: 16153128.

93. DeVolder RJ, Kong HJ. Three dimensionally flocculated proangiogenic microgels for neovascularization. Biomaterials. 2010;31(25):6494-501. doi: 10.1016/j.biomaterials.2010.05.016. PubMed PMID: 20538334.

94. Ruel-Gariépy E, Shive M, Bichara A, Berrada M, Le Garrec D, Chenite A, Leroux J-C. A thermosensitive chitosan-based hydrogel for the local delivery of paclitaxel. European Journal of Pharmaceutics and Biopharmaceutics. 2004;57(1):53-63. doi: 10.1016/s0939-6411(03)00095-x.

95. Tadier S, Galea L, Charbonnier B, Baroud G, Bohner M. Phase and size separations occurring during the injection of model pastes composed of beta-tricalcium phosphate powder, glass beads and aqueous solutions. Acta Biomater. 2014;10(5):2259-68. doi: 10.1016/j.actbio.2013.12.018. PubMed PMID: 24361425.

96. Kovtun A, Goeckelmann MJ, Niclas AA, Montufar EB, Ginebra MP, Planell JA, Santin M, Ignatius A. In vivo performance of novel soybean/gelatin-based bioactive and injectable hydroxyapatite foams. Acta Biomater. 2015;12:242-9. doi: 10.1016/j.actbio.2014.10.034. PubMed PMID: 25448348; PMCID: PMC4298359.

97. Zhu L, Yang J, Zhang J, Lei D, Xiao L, Cheng X, Lin Y, Peng B. In vitro and in vivo evaluation of a nanoparticulate bioceramic paste for dental pulp repair. Acta Biomater. 2014;10(12):5156-68. doi: 10.1016/j.actbio.2014.08.014. PubMed PMID: 25182220.

98. Rughani RV, Branco MC, Pochan D, Schneider JP. De Novo Design of a Shear-Thin Recoverable Peptide-Based Hydrogel Capable of Intrafibrillar Photopolymerization. Macromolecules. 2010;43(19):7924-30. doi: 10.1021/ma1014808. PubMed PMID: WOS:000282478500011.

99. Ekenseair AK, Boere KW, Tzouanas SN, Vo TN, Kasper FK, Mikos AG. Structure-property evaluation of thermally and chemically gelling injectable hydrogels for tissue engineering. Biomacromolecules. 2012;13(9):2821-30. doi: 10.1021/bm300797m. PubMed PMID: 22881074; PMCID: PMC3448273.

100. Chang CC, Boland ED, Williams SK, Hoying JB. Direct-write bioprinting three-dimensional biohybrid systems for future regenerative therapies. J Biomed Mater Res B Appl Biomater. 2011;98(1):160-70. doi: 10.1002/jbm.b.31831. PubMed PMID: 21504055; PMCID: PMC3772543.

101. Chien KB, Makridakis E, Shah RN. Three-dimensional printing of soy protein scaffolds for tissue regeneration. Tissue Eng Part C Methods. 2013;19(6):417-26. doi: 10.1089/ten.TEC.2012.0383. PubMed PMID: 23102234.

102. Mouser VH, Melchels FP, Visser J, Dhert WJ, Gawlitta D, Malda J. Yield stress determines bioprintability of hydrogels based on gelatin-methacryloyl and gellan gum for cartilage bioprinting. Biofabrication. 2016;8(3):035003. doi: 10.1088/1758-5090/8/3/035003. PubMed PMID: 27431733; PMCID: PMC4954607.

103. Wang Q, Gu Z, Jamal S, Detamore MS, Berkland C. Hybrid hydroxyapatite nanoparticle colloidal gels are injectable fillers for bone tissue engineering. Tissue Eng Part A. 2013;19(23-24):2586-93. doi: 10.1089/ten.TEA.2013.0075. PubMed PMID: 23815275; PMCID: PMC3856930.

104. Renth AN, Detamore MS. Leveraging "raw materials" as building blocks and bioactive signals in regenerative medicine. Tissue Eng Part B Rev. 2012;18(5):341-62. doi: 10.1089/ten.TEB.2012.0080. PubMed PMID: 22462759; PMCID: PMC3458620.

105. Wu Z, Fan L, Xu B, Lin Y, Zhang P, Wei X. Use of decellularized scaffolds combined with hyaluronic acid and basic fibroblast growth factor for skin tissue engineering. Tissue Eng Part A. 2015;21(1-2):390-402. doi: 10.1089/ten.TEA.2013.0260. PubMed PMID: 25167809; PMCID: PMC4293131.

106. Patel ZS, Young S, Tabata Y, Jansen JA, Wong ME, Mikos AG. Dual delivery of an angiogenic and an osteogenic growth factor for bone

regeneration in a critical size defect model. Bone. 2008;43(5):931-40. doi: 10.1016/j.bone.2008.06.019. PubMed PMID: 18675385; PMCID: PMC3014108.

107. Young S, Patel ZS, Kretlow JD, Murphy MB, Mountziaris PM, Baggett LS, Ueda H, Tabata Y, Jansen JA, Wong M, Mikos AG. Dose effect of dual delivery of vascular endothelial growth factor and bone morphogenetic protein-2 on bone regeneration in a rat critical-size defect model. Tissue Eng Part A. 2009;15(9):2347-62. doi: 10.1089/ten.tea.2008.0510. PubMed PMID: 19249918; PMCID: PMC2792218.

108. Dennis SC, Berkland CJ, Bonewald LF, Detamore MS. Endochondral ossification for enhancing bone regeneration: converging native extracellular matrix biomaterials and developmental engineering in vivo. Tissue Eng Part B Rev. 2015;21(3):247-66. doi: 10.1089/ten.TEB.2014.0419. PubMed PMID: 25336144; PMCID: PMC4442558.

109. Omary R, Chernoguz D, Lasri V, Leker RR. Decompressive hemicraniectomy reduces mortality in an animal model of intracerebral hemorrhage. J Mol Neurosci. 2013;49(1):157-61. doi: 10.1007/s12031-012-9922-2. PubMed PMID: 23152135.

110. Marquez-Rivas J, Rivero-Garvia M, Mayorga-Buiza MJ, Rodriguez-Boto G. Craniectomy. J Neurosurg. 2013;119(6):1657. Epub 2013 Oct 11. doi: 10.3171/2013.5.JNS131034. PubMed PMID: 24116719.

111. Oladunjoye AO, Schrot RJ, Zwienenberg-Lee M, Muizelaar JP, Shahlaie K. Decompressive craniectomy using gelatin film and future bone flap replacement. J Neurosurg. 2013;118(4):776-82. doi: 10.3171/2013.1.JNS121475. PubMed PMID: 23394343.

112. Alexander C. The Invisible War On the Brain. National Geographic. 2015;1.

113. Risdall JE, Menon DK. Traumatic brain injury. Philos Trans R Soc Lond B Biol Sci. 2011;366(1562):241-50. doi: 10.1098/rstb.2010.0230. PubMed PMID: 21149359; PMCID: PMC3013429.

114. Dujovny M, Agner C, Aviles A. Syndrome of the trephined: theory and facts. Crit Rev Neurosurg. 1999;9(5):271-8. PubMed PMID: 10525845; PMCID: 10525845.

115. Bijlenga P, Zumofen D, Yilmaz H, Creisson E, de Tribolet N. Orthostatic mesodiencephalic dysfunction after decompressive craniectomy. J Neurol Neurosurg Psychiatry. 2007;78(4):430-3. doi: 10.1136/jnnp.2006.099242. PubMed PMID: 17119005; PMCID: PMC2077792.

116. Schiffer J, Gur R, Nisim U, Pollak L. Symptomatic patients after craniectomy. Surgical Neurology. 1997;47(3):231-7. doi: 10.1016/s0090-3019(96)00376-x.

117. Yang XF, Wen L, Shen F, Li G, Lou R, Liu WG, Zhan RY. Surgical complications secondary to decompressive craniectomy in patients with a head injury: a series of 108 consecutive cases. Acta Neurochir (Wien). 2008;150(12):1241-7; discussion 8. doi: 10.1007/s00701-008-0145-9. PubMed PMID: 19005615.

118. Stiver SI. Complications of decompressive craniectomy for traumatic brain injury. Neurosurg Focus. 2009;26(6):E7. doi: 10.3171/2009.4.FOCUS0965. PubMed PMID: 19485720.

119. Tian WM, Hou SP, Ma J, Zhang CL, Xu QY, Lee IS, Li HD, Spector M, Cui FZ. Hyaluronic acid-poly-D-lysine-based three-dimensional hydrogel for traumatic brain injury. Tissue Eng. 2005;11(3-4):513-25. doi: 10.1089/ten.2005.11.513. PubMed PMID: 15869430.

120. Sutherland AJ, Beck EC, Dennis SC, Converse GL, Hopkins RA, Berkland CJ, Detamore MS. Decellularized cartilage may be a chondroinductive material for osteochondral tissue engineering. PLoS One. 2015;10(5):e0121966. doi: 10.1371/journal.pone.0121966. PubMed PMID: 25965981; PMCID: PMC4428768.

121. Sutherland AJ, Detamore MS. Bioactive Microsphere-Based Scaffolds Containing Decellularized Cartilage. Macromol Biosci. 2015;15(7):979-89. doi: 10.1002/mabi.201400472. PubMed PMID: 25821206; PMCID: PMC4504825.

122. Converse GL, Armstrong M, Quinn RW, Buse EE, Cromwell ML, Moriarty SJ, Lofland GK, Hilbert SL, Hopkins RA. Effects of cryopreservation,

decellularization and novel extracellular matrix conditioning on the quasi-static and time-dependent properties of the pulmonary valve leaflet. Acta Biomater. 2012;8(7):2722-9. doi: 10.1016/j.actbio.2012.03.047. PubMed PMID: 22484150.

123. Martin KD, Franz B, Kirsch M, Polanski W, von der Hagen M, Schackert G, Sobottka SB. Autologous bone flap cranioplasty following decompressive craniectomy is combined with a high complication rate in pediatric traumatic brain injury patients. Acta Neurochir (Wien). 2014;156(4):813-24. doi: 10.1007/s00701-014-2021-0. PubMed PMID: 24532225.

124. Vo TN, Shah SR, Lu S, Tatara AM, Lee EJ, Roh TT, Tabata Y, Mikos AG. Injectable dual-gelling cell-laden composite hydrogels for bone tissue engineering. Biomaterials. 2016;83:1-11. doi: 10.1016/j.biomaterials.2015.12.026. PubMed PMID: 26773659; PMCID: PMC4754149.

125. Cowan CM, Aghaloo T, Chou YF, Walder B, Zhang X, Soo C, Ting K, Wu B. MicroCT evaluation of three-dimensional mineralization in response to BMP-2 doses in vitro and in critical sized rat calvarial defects. Tissue Eng. 2007;13(3):501-12. doi: 10.1089/ten.2006.0141. PubMed PMID: 17319794.

126. Vo TN, Ekenseair AK, Spicer PP, Watson BM, Tzouanas SN, Roh TT, Mikos AG. In vitro and in vivo evaluation of self-mineralization and biocompatibility of injectable, dual-gelling hydrogels for bone tissue engineering. J Control Release. 2015;205:25-34. doi: 10.1016/j.jconrel.2014.11.028. PubMed PMID: 25483428; PMCID: PMC4395531.

127. Visser J, Gawlitta D, Benders KEM, Toma SMH, Pouran B, van Weeren PR, Dhert WJA, Malda J. Endochondral bone formation in gelatin methacrylamide hydrogel with embedded cartilage-derived matrix particles. Biomaterials. 2015;37:174-82. doi: http://dx.doi.org/10.1016/j.biomaterials.2014.10.020.

128. Gawlitta D, Benders KE, Visser J, van der Sar AS, Kempen DH, Theyse LF, Malda J, Dhert WJ. Decellularized cartilage-derived matrix as substrate for endochondral bone regeneration. Tissue Eng Part A. 2015;21(3-4):694-703. doi: 10.1089/ten.TEA.2014.0117. PubMed PMID: 25316202.

129. Cushing H. The establishment of cerebral hernia as a decompressive measure for inaccessible brain tumors: with the description of intermuscular methods of making the bone defect in temporal and occipital regions1905.

130. Grant FC, Norcross NC. Repair of cranial defects by cranioplasty. Annals of surgery. 1939;110(4):488.

131. Khader BA, Towler MR. Materials and techniques used in cranioplasty fixation: A review. Mater Sci Eng C Mater Biol Appl. 2016;66:315-22. doi: 10.1016/j.msec.2016.04.101. PubMed PMID: 27207068.

132. NaPier Z, Kanim LEA, Thordarson S, Kropf MA, Cuéllar JM, Glaeser JD, Bae HW. Demineralized Bone Matrix Bone Biology and Clinical Use. Seminars in Spine Surgery. 2016;28(4):196-216. doi: 10.1053/j.semss.2016.08.003.

133. Schallenberger MA, Rossmeier K, Lovick HM, Meyer TR, Aberman HM, Juda GA. Comparison of the osteogenic potential of OsteoSelect demineralized bone matrix putty to NovaBone calcium-phosphosilicate synthetic putty in a cranial defect model. J Craniofac Surg. 2014;25(2):657-61. doi: 10.1097/SCS.0000000000000610. PubMed PMID: 24577306; PMCID: PMC3958491.

134. O'Reilly EB, Barnett S, Madden C, Welch B, Mickey B, Rozen S. Computed-tomography modeled polyether ether ketone (PEEK) implants in revision cranioplasty. J Plast Reconstr Aesthet Surg. 2015;68(3):329-38. doi: 10.1016/j.bjps.2014.11.001. PubMed PMID: 25541423.

135. Choy DK, Nga VD, Lim J, Lu J, Chou N, Yeo TT, Teoh SH. Brain tissue interaction with three-dimensional, honeycomb polycaprolactone-based scaffolds designed for cranial reconstruction following traumatic brain injury. Tissue Eng Part A. 2013;19(21-22):2382-9. doi: 10.1089/ten.TEA.2012.0733. PubMed PMID: 23691928; PMCID: PMC3807547.

136. Tate M. Biocompatibility of methylcellulose-based constructs designed for intracerebral gelation following experimental traumatic brain injury. Biomaterials. 2001;22(10):1113-23. doi: 10.1016/s0142-9612(00)00348-3.

137. Wong DY, Hollister SJ, Krebsbach PH, Nosrat C. Poly(epsilon-caprolactone) and poly (L-lactic-co-glycolic acid) degradable polymer sponges attenuate astrocyte response and lesion growth in acute traumatic brain injury. Tissue Eng. 2007;13(10):2515-23. doi: 10.1089/ten.2006.0440. PubMed PMID: 17655492.

138. Zhang T, Yan Y, Wang X, Xiong Z, Lin F, Wu R, Zhang R. Three-dimensional Gelatin and Gelatin/Hyaluronan Hydrogel Structures for Traumatic Brain Injury. Journal of Bioactive and Compatible Polymers. 2007;22(1):19-29. doi: 10.1177/0883911506074025.

139. Rennerfeldt DA, Renth AN, Talata Z, Gehrke SH, Detamore MS. Tuning mechanical performance of poly(ethylene glycol) and agarose interpenetrating network hydrogels for cartilage tissue engineering. Biomaterials. 2013;34(33):8241-57. doi: 10.1016/j.biomaterials.2013.07.052. PubMed PMID: 23932504; PMCID: PMC3773240.

140. Eberle APR, Baird DG, Wapperom P. Rheology of Non-Newtonian Fluids Containing Glass Fibers: A Review of Experimental Literature. Industrial & Engineering Chemistry Research. 2008;47(10):3470-88. doi: 10.1021/ie070800j.

141. Motherway JA, Verschueren P, Van der Perre G, Vander Sloten J, Gilchrist MD. The mechanical properties of cranial bone: the effect of loading rate and cranial sampling position. J Biomech. 2009;42(13):2129-35. doi: 10.1016/j.jbiomech.2009.05.030. PubMed PMID: 19640538.

142. Yeung CC, Holmes DF, Thomason HA, Stephenson C, Derby B, Hardman MJ. An ex vivo porcine skin model to evaluate pressure-reducing devices of different mechanical properties used for pressure ulcer prevention. Wound Repair Regen. 2016;24(6):1089-96. doi: 10.1111/wrr.12481. PubMed PMID: 27717144.

143. Cunniffe GM, Vinardell T, Thompson EM, Daly AC, Matsiko A, O'Brien FJ, Kelly DJ. Chondrogenically primed mesenchymal stem cell-seeded alginate hydrogels promote early bone formation in critically-sized defects. European Polymer Journal. 2015;72:464-72. doi: 10.1016/j.eurpolymj.2015.07.021.

144. Cunniffe GM, Vinardell T, Murphy JM, Thompson EM, Matsiko A, O'Brien FJ, Kelly DJ. Porous decellularized tissue engineered hypertrophic cartilage as a scaffold for large bone defect healing. Acta Biomater. 2015;23:82-90. doi: 10.1016/j.actbio.2015.05.031. PubMed PMID: 26038199.

145. Visser J, Gawlitta D, Benders KE, Toma SM, Pouran B, van Weeren PR, Dhert WJ, Malda J. Endochondral bone formation in gelatin methacrylamide hydrogel with embedded cartilage-derived matrix particles. Biomaterials. 2015;37:174-82. doi: 10.1016/j.biomaterials.2014.10.020. PubMed PMID: 25453948.

146. Kurland DB, Khaladj-Ghom A, Stokum JA, Carusillo B, Karimy JK, Gerzanich V, Sahuquillo J, Simard JM. Complications Associated with Decompressive Craniectomy: A Systematic Review. Neurocrit Care. 2015;23(2):292-304. doi: 10.1007/s12028-015-0144-7. PubMed PMID: 26032808; PMCID: PMC4704457.

147. Láng J, Ganau M, Prisco L, Bozsik K, Banczerowski P. Syndrome of Trephined-Underestimated and Poorly Understood Complication after Decompressive Craniectomy. Ideggyógyászati szemle. 2016;69(7-8):227-32. doi: 10.18071/isz.69.0227.

148. Honeybul S. Neurological dysfunction due to large skull defect: Implications for physiotherapists. J Rehabil Med. 2017;49(3):204-7. doi: 10.2340/16501977-2209. PubMed PMID: 28233013.

149. Bencherif SA, Srinivasan A, Horkay F, Hollinger JO, Matyjaszewski K, Washburn NR. Influence of the degree of methacrylation on hyaluronic acid hydrogels properties. Biomaterials. 2008;29(12):1739-49. doi: 10.1016/j.biomaterials.2007.11.047. PubMed PMID: 18234331.

150. Burdick JA, Chung C, Jia X, Randolph MA, Langer R. Controlled degradation and mechanical behavior of photopolymerized hyaluronic acid networks. Biomacromolecules. 2005;6(1):386-91. doi: 10.1021/bm049508a. PubMed PMID: 15638543; PMCID: PMC2678566.

151. Chung C, Burdick JA. Influence of three-dimensional hyaluronic acid microenvironments on mesenchymal stem cell chondrogenesis. Tissue Eng Part A. 2009;15(2):243-54. doi: 10.1089/ten.tea.2008.0067. PubMed PMID: 19193129; PMCID: PMC2678568.

152. Oudshoorn MHM, Rissmann R, Bouwstra JA, Hennink WE. Synthesis of methacrylated hyaluronic acid with tailored degree of substitution. Polymer. 2007;48(7):1915-20. doi: 10.1016/j.polymer.2007.01.068.

153. Poldervaart MT, Goversen B, de Ruijter M, Abbadessa A, Melchels FPW, Oner FC, Dhert WJA, Vermonden T, Alblas J. 3D bioprinting of methacrylated hyaluronic acid (MeHA) hydrogel with intrinsic osteogenicity. PLoS One. 2017;12(6):e0177628. doi: 10.1371/journal.pone.0177628. PubMed PMID: 28586346; PMCID: PMC5460858.

154. Van Kampen E. Controlling Protein Permeability in Hydrogels for Drug Delivery Applications: University of Kansas; 2016.

155. Mergy J, Fournier A, Hachet E, Auzély-Velty R. Modification of polysaccharides via thiol-ene chemistry: A versatile route to functional biomaterials. Journal of Polymer Science Part A: Polymer Chemistry. 2012;50(19):4019-28.

156. Roughley PJ, Mort JS. The role of aggrecan in normal and osteoarthritic cartilage. J Exp Orthop. 2014;1(1):8. doi: 10.1186/s40634-014-0008-7. PubMed PMID: 26914753; PMCID: PMC4648834.

157. Gertzman AA, Sunwoo MH, inventors; Google Patents, assignee. Malleable paste with allograft bone reinforcement for filling bone defects patent US 6,458,375. 2002.

158. Ko E, Alberti K, Lee JS, Yang K, Jin Y, Shin J, Yang HS, Xu Q, Cho SW. Nanostructured Tendon-Derived Scaffolds for Enhanced Bone Regeneration by Human Adipose-Derived Stem Cells. ACS Appl Mater Interfaces. 2016;8(35):22819-29. doi: 10.1021/acsami.6b05358. PubMed PMID: 27502160.

159. Avery RK, Albadawi H, Akbari M, Zhang YS, Duggan MJ, Sahani DV, Olsen BD, Khademhosseini A, Oklu R. An injectable shear-thinning biomaterial for endovascular embolization. Sci Transl Med. 2016;8(365):365ra156. doi: 10.1126/scitranslmed.aah5533. PubMed PMID: 27856795.

160. Diba M, An J, Schmidt S, Hembury M, Ossipov D, Boccaccini AR, Leeuwenburgh SC. Exploiting Bisphosphonate-Bioactive-Glass Interactions for the Development of Self-Healing and Bioactive

Composite Hydrogels. Macromol Rapid Commun. 2016;37(23):1952-9. doi: 10.1002/marc.201600353. PubMed PMID: 27643998.

161. Li Y, Zhang Y, Shi F, Tao L, Wei Y, Wang X. Modulus-regulated 3D-cell proliferation in an injectable self-healing hydrogel. Colloids Surf B Biointerfaces. 2017;149:168-73. doi: 10.1016/j.colsurfb.2016.10.021. PubMed PMID: 27756013.

162. Rodell CB, Kaminski AL, Burdick JA. Rational design of network properties in guest-host assembled and shear-thinning hyaluronic acid hydrogels. Biomacromolecules. 2013;14(11):4125-34. doi: 10.1021/bm401280z. PubMed PMID: 24070551; PMCID: PMC3851010.

163. Rodell CB, MacArthur JW, Dorsey SM, Wade RJ, Wang LL, Woo YJ, Burdick JA. Shear-Thinning Supramolecular Hydrogels with Secondary Autonomous Covalent Crosslinking to Modulate Viscoelastic Properties In Vivo. Adv Funct Mater. 2015;25(4):636-44. doi: 10.1002/adfm.201403550. PubMed PMID: 26526097; PMCID: PMC4624407.

164. Townsend JM, Dennis SC, Whitlow J, Feng Y, Wang J, Andrews B, Nudo RJ, Detamore MS, Berkland CJ. Colloidal Gels with Extracellular Matrix Particles and Growth Factors for Bone Regeneration in Critical Size Rat Calvarial Defects. AAPS J. 2017. doi: 10.1208/s12248-017-0045-0. PubMed PMID: 28138909.

165. Vulpe R, Le Cerf D, Dulong V, Popa M, Peptu C, Verestiuc L, Picton L. Rheological study of in-situ crosslinkable hydrogels based on hyaluronanic acid, collagen and sericin. Mater Sci Eng C Mater Biol Appl. 2016;69:388-97. doi: 10.1016/j.msec.2016.07.003. PubMed PMID: 27612727.

Appendix A: Figures

Chapter 1: Figures 1.1-1.2

Chapter 2: Figures 2.1-2.4

Chapter 3: Figures 3.1-3.5

Chapter 4: Figures 4.1-4.5

Chapter 5: Figures 5.1-5.4

Chapter 6: No Figures

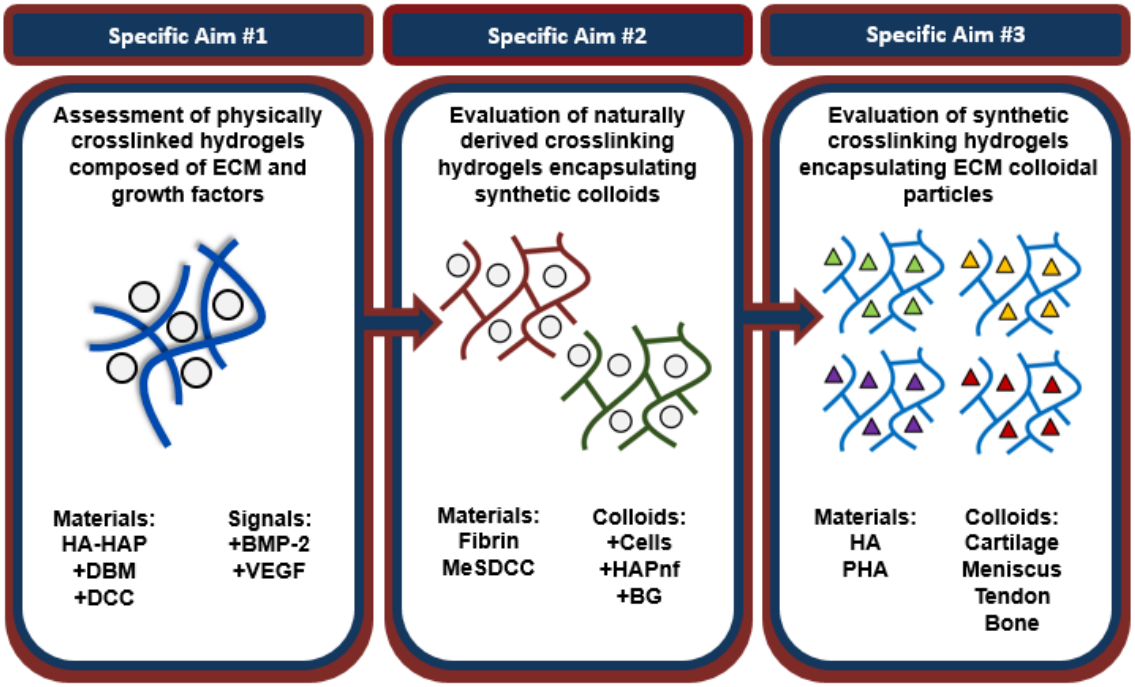


Figure 1.1: Illustration of Dissertation Aims

Graphical illustration of the three specific aims evaluated in chronological order.



Figure 1.2: Illustration of Implanted Hydrogel Pliability

Graphical illustration of an implanted hydrogel for treatment of traumatic brain injury following decompressive craniectomy. Note the pliability of the hydrogel to allow brain herniation during initial implantation.

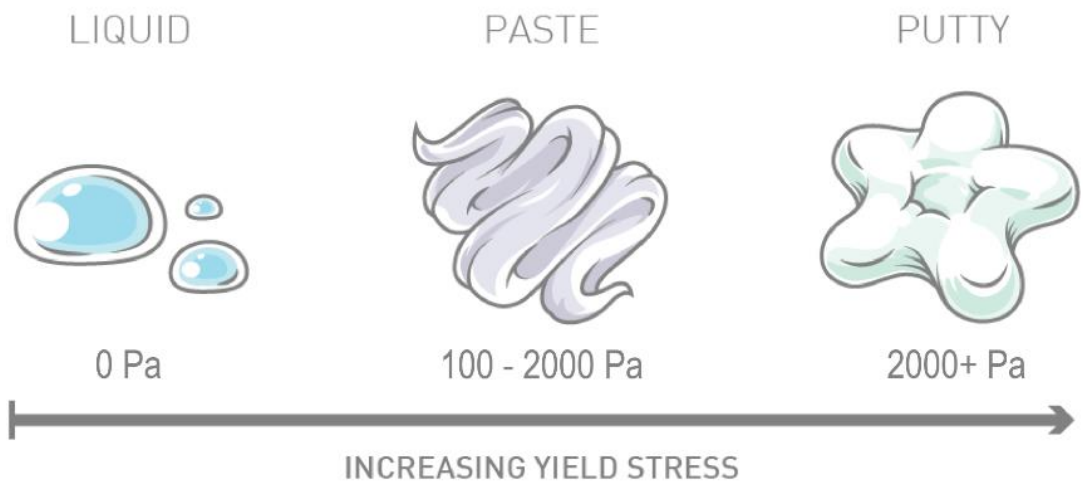


Figure 2.1: Liquid, paste, and Putty Precursor Solutions

Illustration of increasing precursor yield stress to achieve different material consistencies. Precursor materials with no yield stress exhibit liquid properties, and materials with increasing yield stress exhibit paste and putty hydrogel precursor properties.

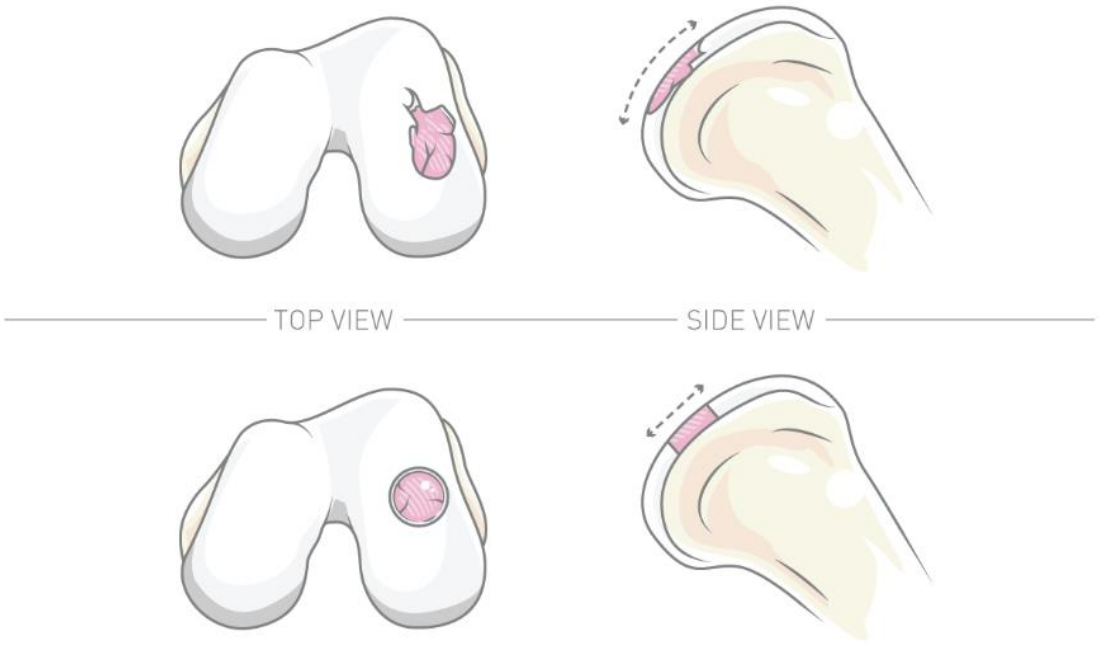


Figure 2.2: Illustration of Real and Induced Defects

Illustration depicting the difference between defects observed in patient populations (top) compared to defects used for *in vivo* studies (bottom). Common differences between actual injuries and defects used for research include shape, size, and orientation, and emphasize the clinical requirement of a hydrogel precursor solution that can be carefully molded as a paste and contoured to fit the defect site prior to crosslinking.

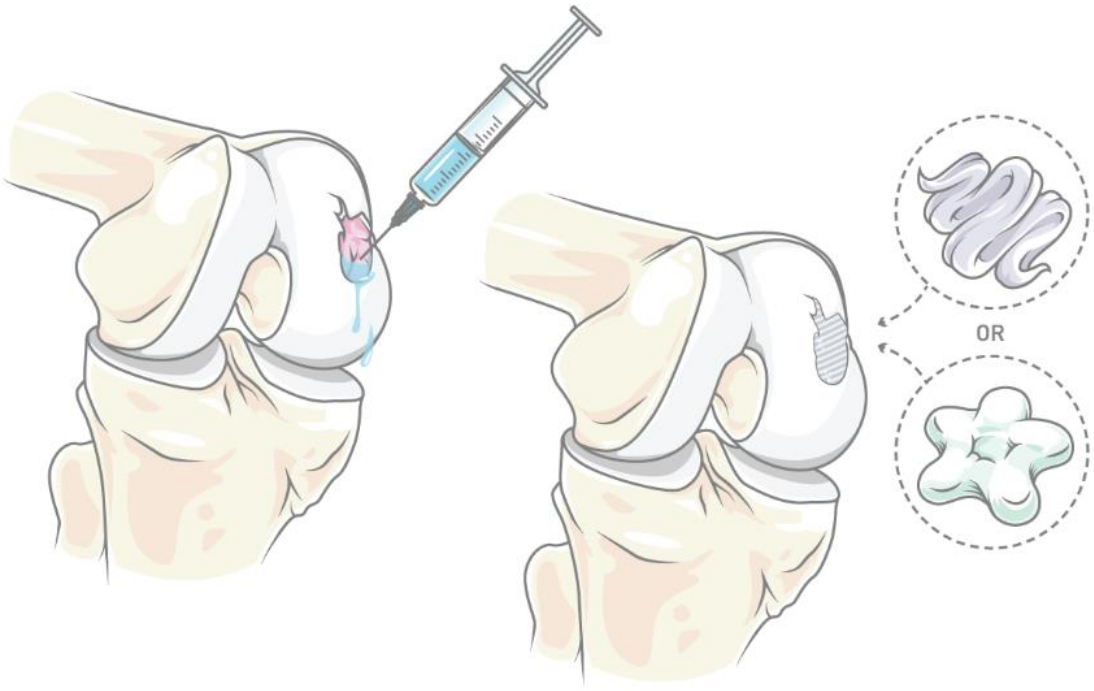


Figure 2.3. Defect Retention of Liquid Compared to Paste or Putty

Illustration of how achieving paste or putty rheological properties in hydrogel precursor solutions can aid in material placement. (Left) Lack of material retention using an *in situ* liquid hydrogel precursor solution compared to (Right) precursor materials exhibiting desirable paste and putty behavior.

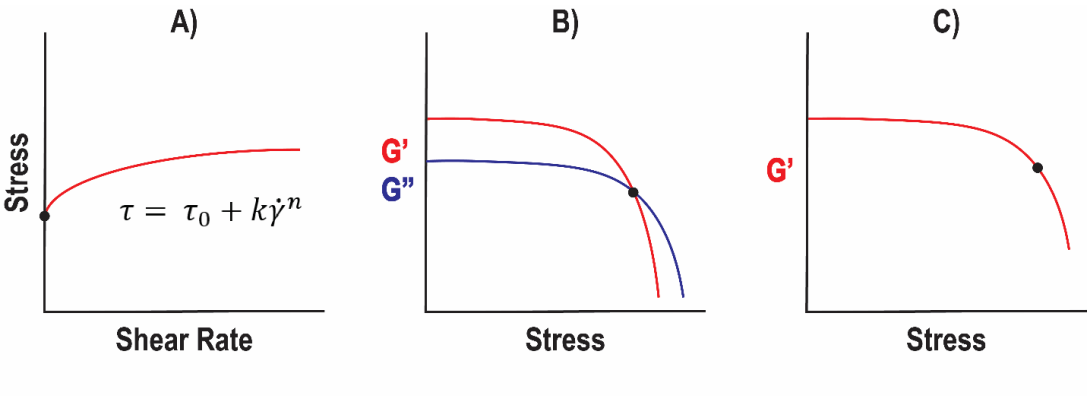


Figure 2.4: Methods to Determine Yield Stress

Graph illustrations of methods to determine the yield stress of a material, black dots correspond to the yield stress. A) Theoretical model fitting using the Herschel-Bulkley (HB) model as an example. B) Determining the shear stress at the crossover point of the storage and loss modulus (G'/G"). C) Determining the shear stress related to a pre-determined deviation of the storage modulus from linearity (i.e. 85% deviation). As a general rule, we recommend the HB model to calculate the yield stress (τ_0).

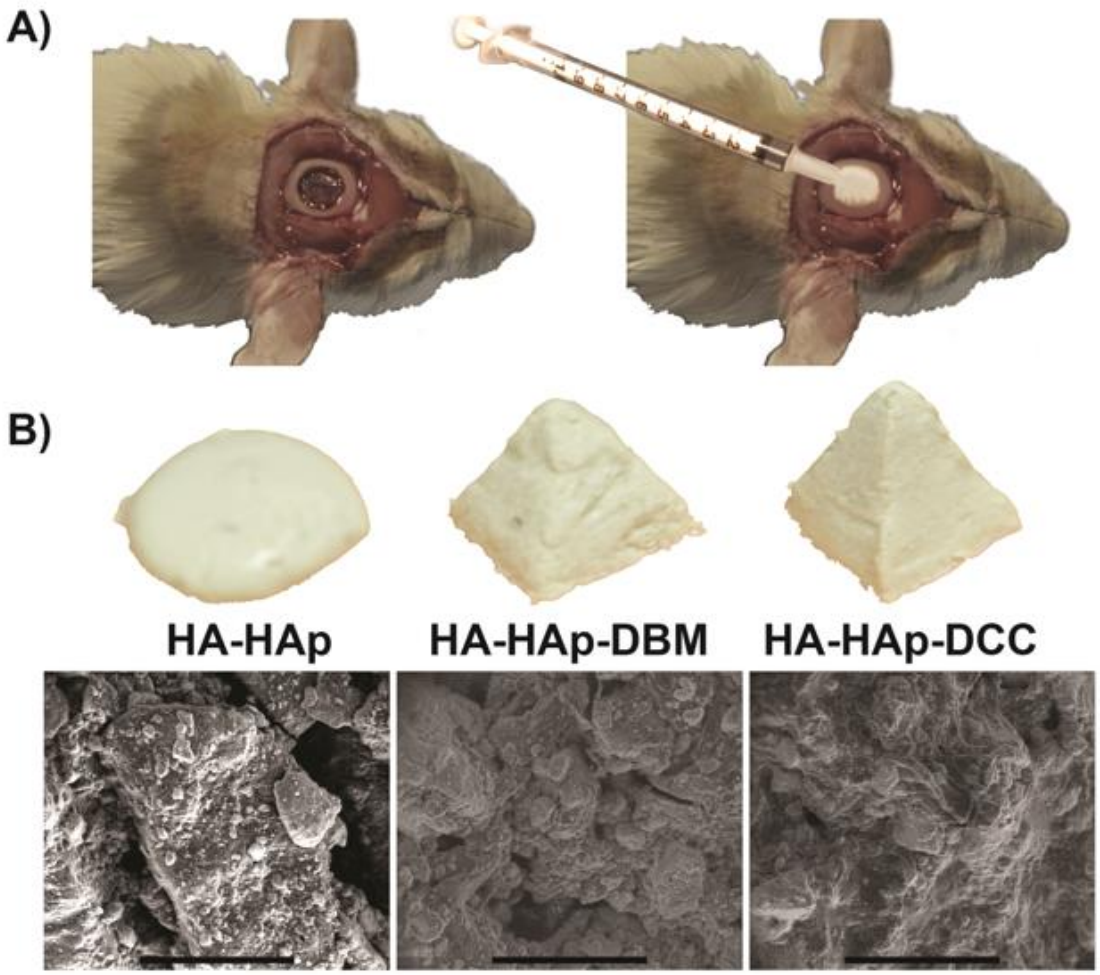


Figure 3.1: Surgical Method and Material ESEM Images

A) Surgical method illustration shown in two steps, in the first (left) step the scalp is opened and a 7.5 mm cylindrical bone section is removed. The following step (right) involves filling the defect gap using a syringe loaded with one of the material groups and smoothing into place, before suturing the scalp back in place. B) Extruded and shaped material groups of HA-HAp, HA-HAp-DBM, and HA-HAp-DCC. Material yield stress allowed for retention after shaping using a surgical spatula. Environmental scanning electron microscope images provide insight into the gel microstructure. Scale bars = 200 μm.

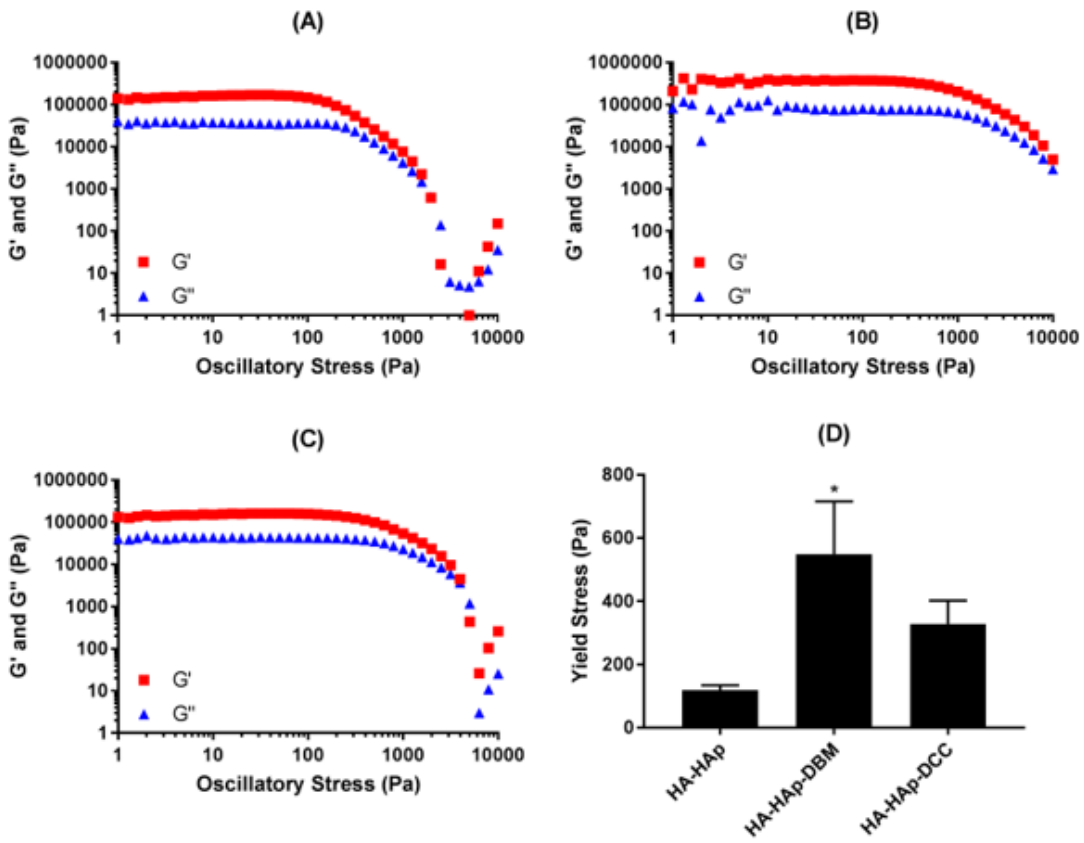


Figure 3.2: Aim 1 Hydrogel Precursor Yield Stress

A-C) Representative rheometer traces for HA-HAp, HA-HAp-DBM, and HA-HAp-DCC, respectively. D) Colloidal gel yield stress corresponding to a 15% deviation of G' from linearity. Addition of DBM significantly increased the yield stress of the material compared to HA-HAp as indicated by an asterisk ($p<0.01$).

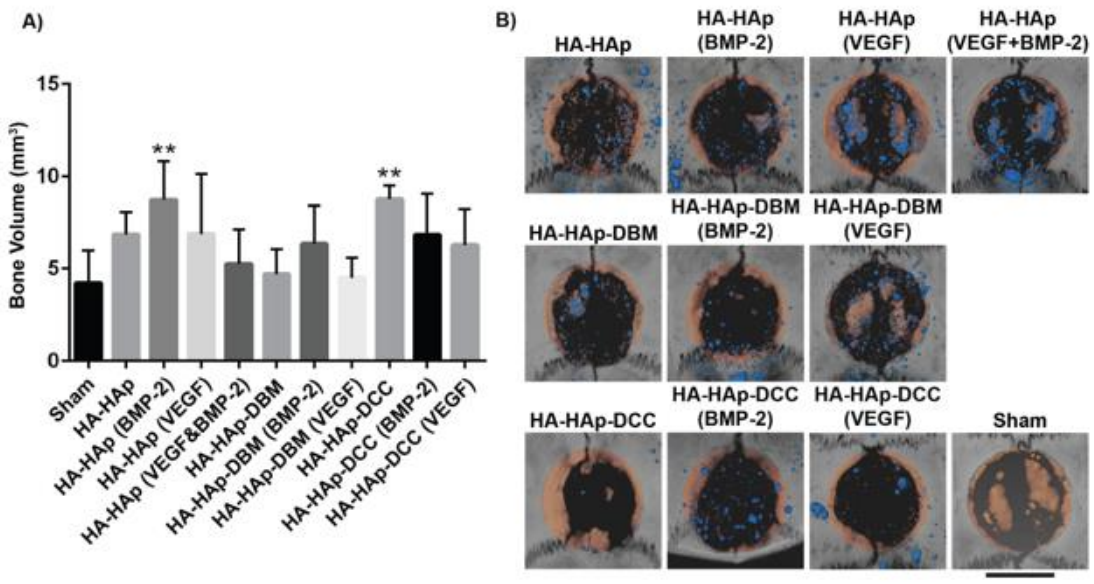


Figure 3.3: Aim 1 Regenerated Bone Volume and μCT Imaging

A) *In vivo* regenerated bone volume. Bone regeneration was evaluated after 8 weeks using micro-computed tomography (μCT) analysis. Asterisks (**) represent statistically significant results ($P<0.01$) compared to the sham. Error bars represent standard deviations. B) μCT analysis using Avizo Fire software. Orange coloring indicating the regenerated bone, and blue coloring defining original colloidal particles. Scale bar represents 5 mm in length.

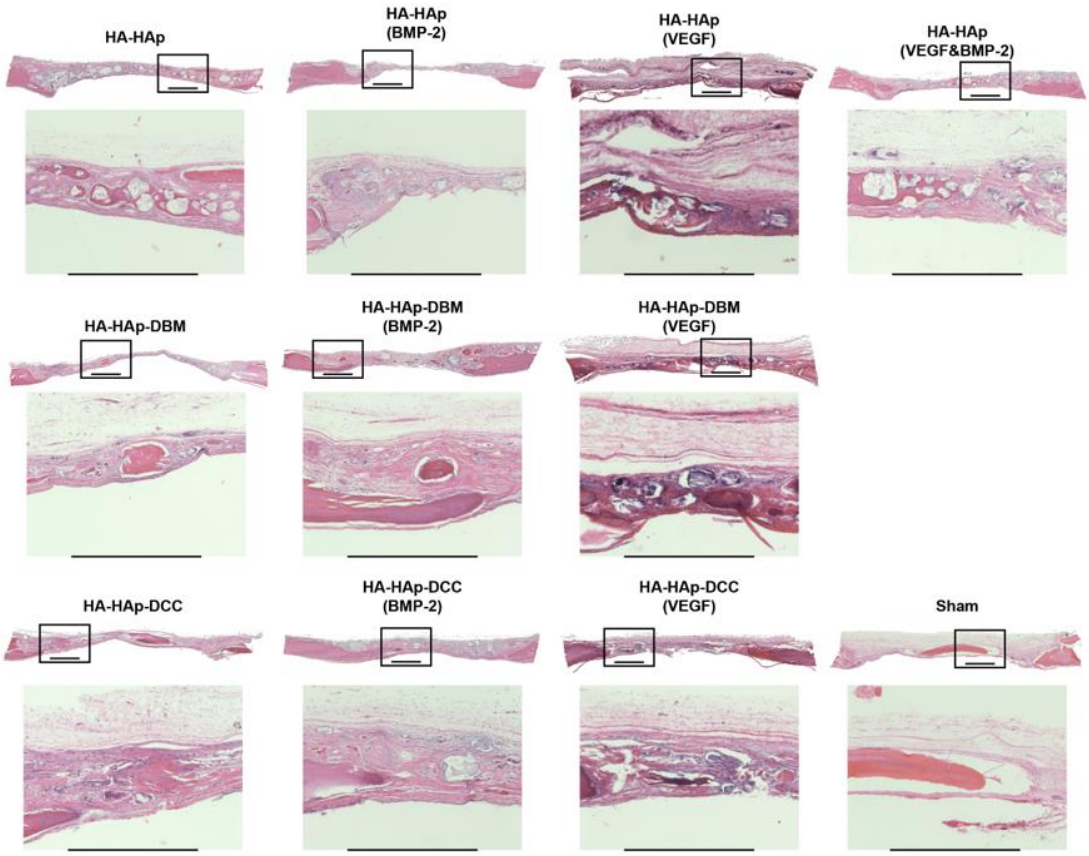


Figure 3.4: Aim 1 H&E Staining

Histological analysis of critical size (7.5 mm) rat calvarial defects after 8 weeks post-implantation. Sections were taken in the sagittal plane with the dural side of the calvaria as the bottom of the image. Groups were analyzed using hematoxylin and eosin (H&E) to highlight new bone formation versus original colloidal material. Zoomed images correspond to the boxed area on the total defect area. scale bars = 1 mm

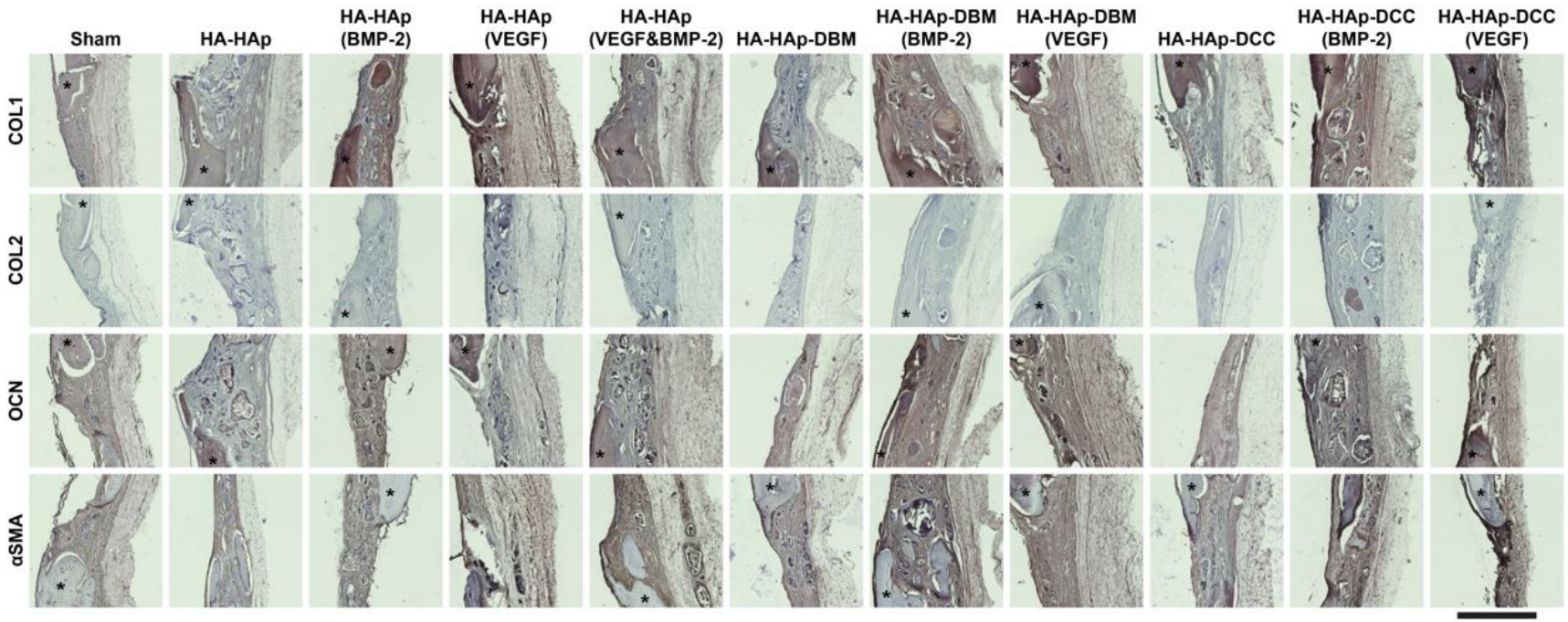


Figure 3.5: Aim 1 Immunohistochemistry

Immunohistochemistry (IHC) results for collagen 1 (COL1), collagen 2 (COL2), Osteocalcin (OCN), and alpha-smooth muscle actin (αSMA). Brown coloring represents positive presence for the selected antibody, where blue staining represents negative antibody presence. All images represent *in vivo* healing of material groups after 8 weeks post-implantation. (*) corresponds to defect bone edge, scale bar = 1 mm.

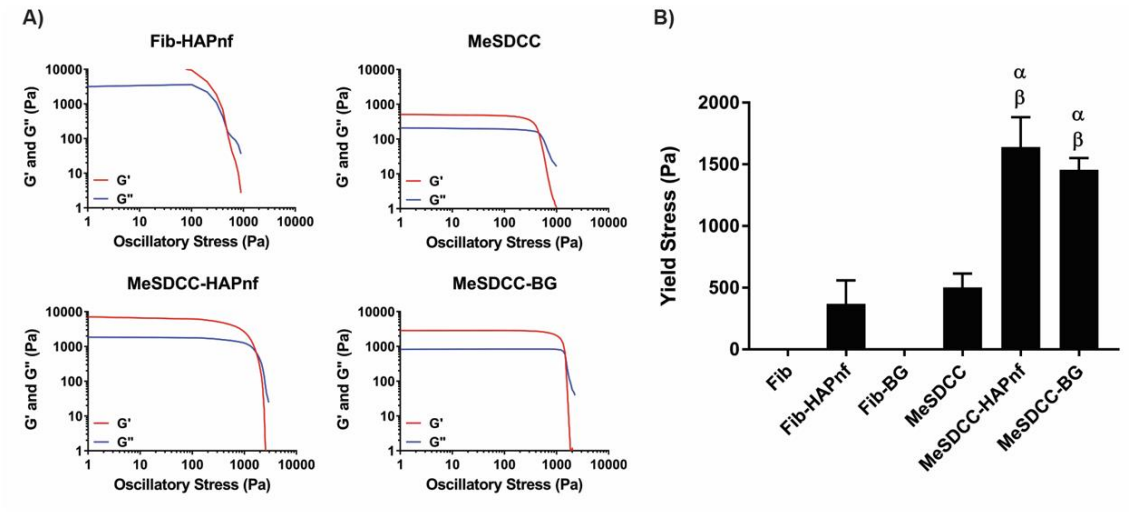


Figure 4.1: Aim 2 Hydrogel Precursor Yield Stress

A) Representative rheometer traces for Fib-HAPnf, MeSDCC, MeSDCC-HAPnf, and MeSDCC-BG hydrogel precursor solutions. B) Hydrogel yield stress determined by the crossover point of the storage (G') and loss (G") moduli. α = significant increase compared to MeSDCC ($p<0.0001$) and β = significantly larger value compared to the Fib-HAPnf group ($p<0.0001$). Addition of colloidal particles to MeSDCC significantly increased the yield stress by a factor of ~3. n = 5, values represent the mean ± standard deviation. Fib = Fibrin, MeSDCC = Methacrylated Solubilized Decellularized Cartilage, HAPnf = Hydroxyapatite Nanofibers, BG = Bioglass.

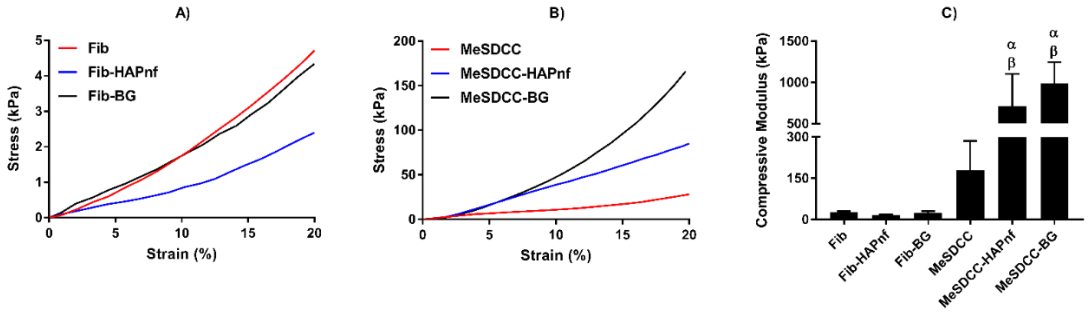


Figure 4.2: Aim 2 Hydrogel Compressive Modulus

A-B) Representative stress-strain curves for crosslinked hydrogel groups. C) Compressive modulus determined by the slope of the stress-strain curve between 10 and 20% strain. α = significant increase compared to the MeSDCC group ($p<0.01$) and β = significantly larger than Fib, Fib-HAPnf, and Fib-BG ($p<0.0001$). Addition of colloidal particles to MeSDCC significantly increased the compressive modulus by a factor of 4 to 5.5. n = 5, values represent the mean ± standard deviation. Fib = Fibrin, MeSDCC = Methacrylated Solubilized Decellularized Cartilage, HAPnf = Hydroxyapatite Nanofibers, BG = Bioglass.

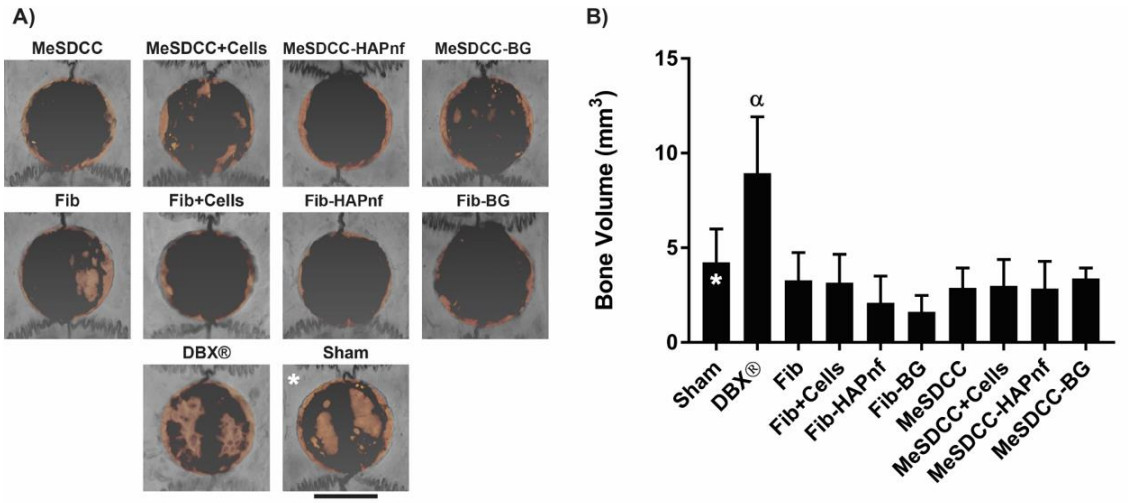


Figure 4.3: Aim 2 Regenerated Bone Volume and μCT Imaging

Microcomputed tomography (μCT) analysis using Avizo software 8 weeks after implantation. A) Reconstructed μCT scans of calvarial defects. Orange coloring indicates regenerated bone to distinguish from existing bone. B) Regenerated bone volume determined by μCT. α = significantly greater bone volume compared to all other groups ($p<0.05$). Note that only the DBX® treatment group had a significantly larger bone volume compared to the sham. Scale bar = 5 mm. Asterisks (*) represent our previously published data (i.e., sham group).(36) n = 5, values represent the mean ± standard deviation. Fib = Fibrin, MeSDCC = Methacrylated Solubilized Decellularized Cartilage, HAPnf = Hydroxyapatite Nanofibers, BG = Bioglass.

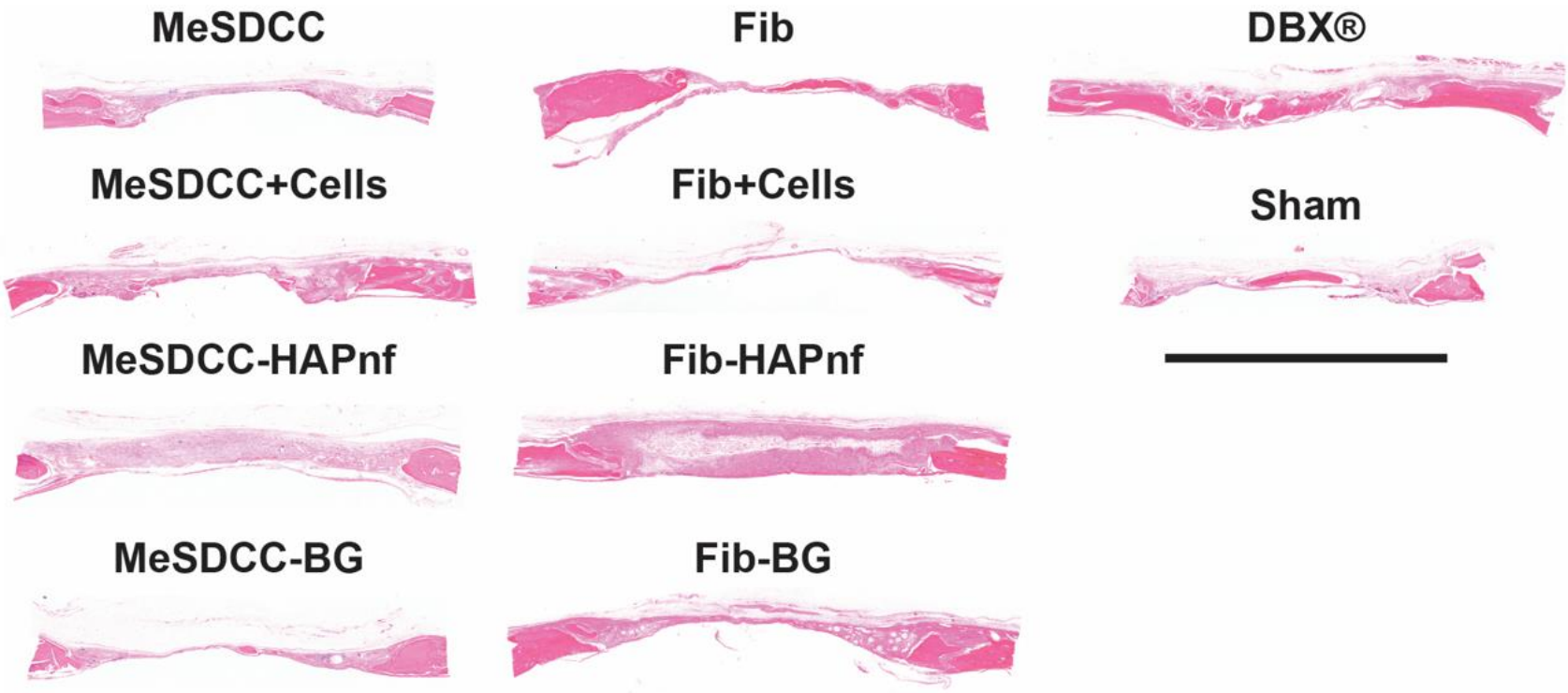


Figure 4.4: Aim 2 H&E Staining

Hematoxylin and eosin (H&E) histological analysis of critical size (7.5 mm) rat calvarial defects 8 weeks after implantation. Sections were taken in the sagittal plane with the dural side of the calvarium as the bottom of each image. Note that regeneration was limited in all groups except the DBX® group. Scale bar = 5 mm. Fib = Fibrin, MeSDCC = Methacrylated Solubilized Decellularized Cartilage, HAPnf = Hydroxyapatite Nanofibers, BG = Bioglass.

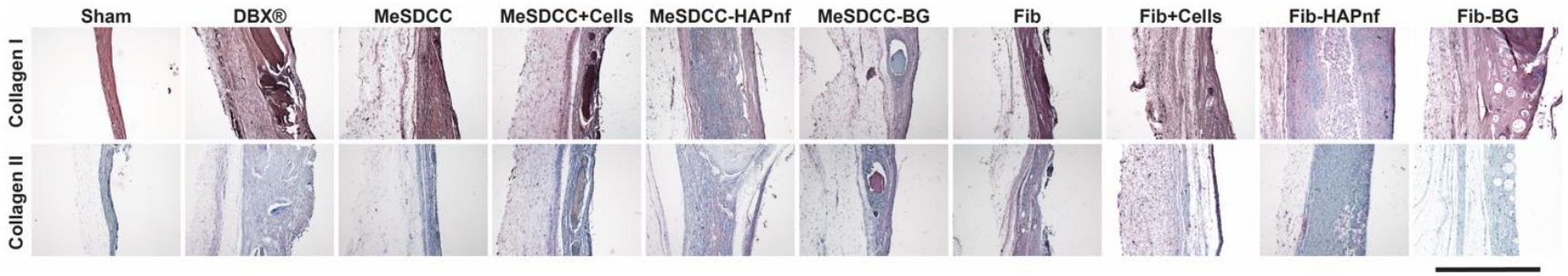


Figure 4.5: Aim 2 Immunohistochemistry

Immunohistochemical (IHC) staining for collagen I and collagen II. Brown coloring indicates positive presence for the selected antibody, and the blue staining represents the hematoxylin counterstain. Note the positive collagen II staining in the MeSDCC-BG group, indicating leftover hydrogel after the 8-week recovery period. Scale bar = 500 µm. Fib = Fibrin, MeSDCC = Methacrylated Solubilized Decellularized Cartilage, HAPnf = Hydroxyapatite Nanofibers, BG = Bioglass.

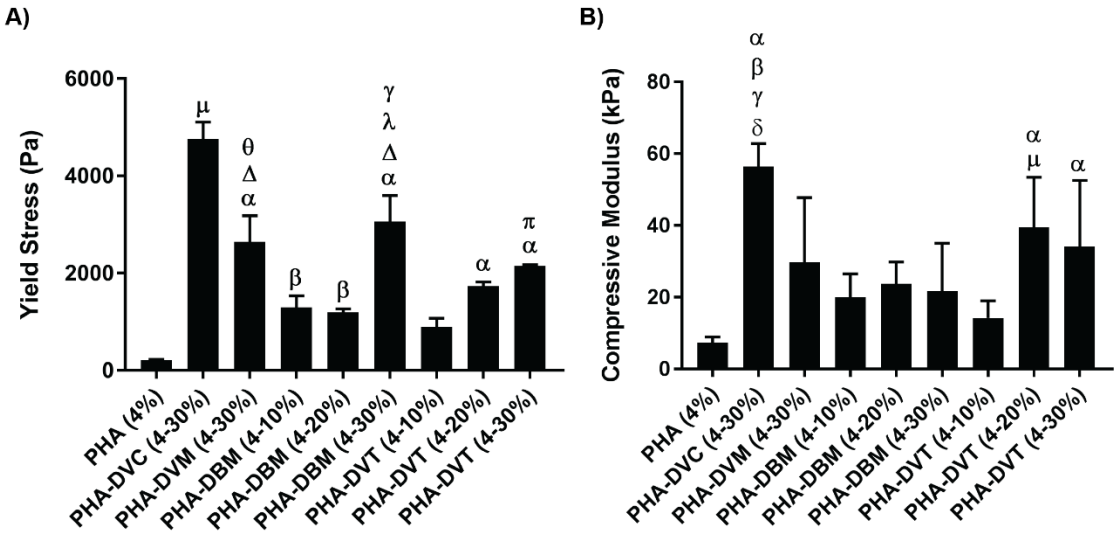


Figure 5.1: Aim 3 Mechanical Characterization

A) Hydrogel precursor yield stress determined by the crossover point of the storage (G') and loss (G") modulus (n = 3). Note increasing yield stress with DVT concentration. The highest yield stress observed in the DVC group. α = significantly larger value compared to PHA (4%) ($p < 0.0001$). β = significantly larger value compared to PHA (4%) ($p < 0.05$). μ = significantly larger value compared to all other groups ($p < 0.0001$). Δ = significantly larger value compared to PHA-DBM (4-10%), PHA-DBM (4-20%), and PHA-DVT (4-10%) ($p < 0.0001$). θ = significantly larger value compared to PHA-DVT (4-20%) ($p < 0.05$). λ = significantly larger value compared to PHA-DVT (4-20%) ($p < 0.001$). γ = significantly larger value compared to PHA-DVT (4-30%) ($p < 0.05$). π = significantly larger value compared to PHA-DBM (4-10%), PHA-DBM (4-20%), and PHA-DVT (4-10%) ($p < 0.05$). B) Crosslinked hydrogel compressive modulus determined by the slope of the stress-strain curve between 5-15% (n = 5). Note higher compressive moduli for hydrogels containing DVT or DVC. α = significantly larger value compared to PHA (4%) ($p < 0.01$). β = significantly larger value compared to PHA-DVM (4-30%) ($p < 0.05$). γ = significant larger value compared to PHA-DVT (4-10%), PHA-DBM (4-10%), and PHA-DBM (4-30%) ($p < 0.01$). δ = significantly larger value compared to PHA-DBM (4-20%) ($p < 0.05$). μ = significantly larger value compared to PHA-DVT (4-10%) ($p < 0.05$). PHA = pentanoate-functionalized hyaluronic acid, DBM = demineralized bone matrix, DVC = devitalized cartilage, DVM = devitalized meniscus, DVT = devitalized tendon.

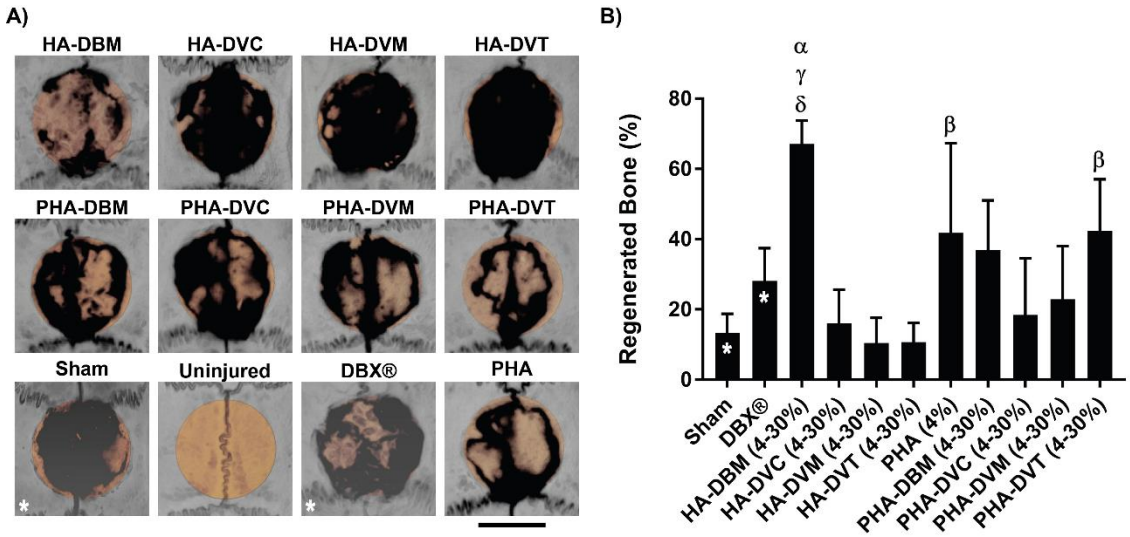


Figure 5.2: Aim 3 Regenerated Bone Volume and µCT Imaging

Microcomputed tomography (µCT) analysis using Avizo software after 8 weeks post hydrogel implantation (n = 5). A) Representative µCT scans of calvarial defect groups. Orange coloring indicates the space in which the original defect was created. Scale bar = 5 mm. Note greater bone regeneration for PHA hydrogel groups. B) Percent regenerated bone volume determined by µCT. α = significantly larger value compared to the sham, HA-DVC (4-30%), HA-DVM (4-30%), HA-DVT (4-30%), PHA-DVC (4-30%), and PHA-DVM (4-30%) ($p < 0.0001$). β = significantly larger value compared to the sham, HA-DVM (4-30%), and HA-DVT (4-30%) ($p < 0.05$). γ = significantly larger value compared to DBX® ($p < 0.01$). δ = significantly larger value compared to PHA-DBM (4-30%) ($p < 0.05$). HA = Hyaluronic acid, PHA = pentanoate-functionalized hyaluronic acid, DBM = demineralized bone matrix, DVC = devitalized cartilage, DVM = devitalized meniscus, DVT = devitalized tendon.

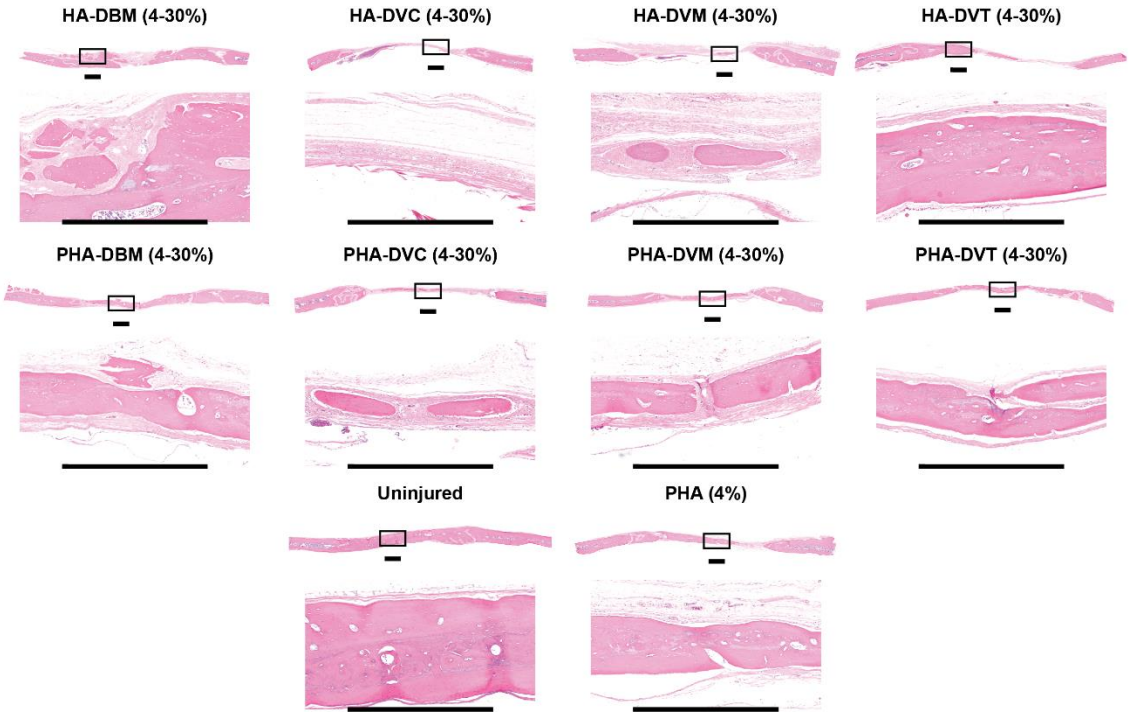


Figure 5.3: Aim 3 H&E Staining

Histological analysis of rat calvarial defects after 8 weeks post implantation (n = 5). Sections were taken from the sagittal plane in which the dural side of the calvaria is the bottom of each image. Sections were stained with hematoxylin and eosin (H&E) and magnified images shown below each overall section correlate to the box above. Note thicker bone formation in hydrogels containing PHA. Scale bar = 1 mm. HA = hyaluronic acid, PHA = pentanoate-functionalized hyaluronic acid, DBM = demineralized bone matrix, DVC = devitalized cartilage, DVM = devitalized meniscus, DVT = devitalized tendon.

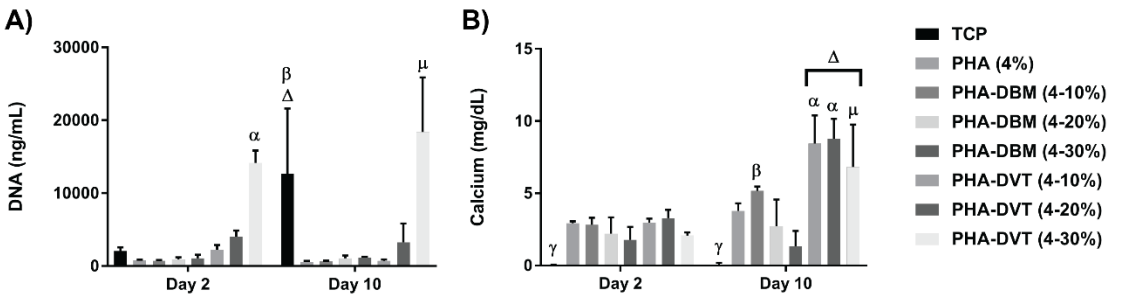


Figure 5.4: Aim 3 Biochemical Analysis

Biochemical analysis of hydrogels for 10 consecutive days of *in vitro* cell culture (n = 5). A) DNA content after 2 and 10 days of cell culture. Note high DNA content on PHA-DVT (4-30%) hydrogels after 2 days of culture. α = significantly greater DNA content compared to all other day 2 groups ($p < 0.0001$). Δ = significantly greater increase in DNA content between day 2 and day 10 ($p < 0.0001$). β = significantly larger value compared to all day 10 groups except PHA-DVT (4-30%) ($p < 0.01$). μ = significantly larger value compared to all other day 10 groups except the TCP group ($p < 0.0001$). B) Deposited calcium content after 2 and 10 days of cell culture. Note increased calcium deposition on DVT hydrogels after 10 days of cell culture. γ = indicates a near zero result. Δ = significantly greater increase in calcium content between day 2 and day 10 ($p < 0.0001$). α = significantly larger value compared to all day 10 groups excluding those containing DVT ($p < 0.0001$). μ = significantly larger value compared to all day 10 groups excluding those containing DVT and the PHA-DBM (4-10%) group ($p < 0.05$). β = significantly larger value compared to PHA-DBM (4-30%) ($p < 0.001$). PHA = pentanoate-functionalized hyaluronic acid, DBM = demineralized bone matrix, DVT = devitalized tendon, TCP = tissue culture plastic.

Appendix B: Tables

Chapter 1: No tables

Chapter 2: Table 2.1

Chapter 3: No tables

Chapter 4: No tables

Chapter 5: No tables

Chapter 6: No tables

Table 2.1: Summary of Hydrogel Rheological Properties

Summary of rheological properties of hydrogel precursor solutions. Dash marks (-) = data not provided.

Reference	Hydrogel Type	Materials	Methods	Shear Response	Recovery Time	Yield Stress
Avery *et al.*(159)	Physical Charge	Gelatin and silicate nanoplatelets	25 mm cone and plate (1°)	Thinning	<1 min	-
Beck *et al.*(51)	Chemical Photoinitiated	Methacrylated hyaluronic acid and hyaluronic acid nanoparticles	20 mm parallel plate	Thinning	-	~18 to 160 Pa
Beck *et al.*(35)	Chemical Photoinitiated	Methacrylated hyaluronic acid and hyaluronic acid nanoparticles	20 mm parallel plate, 500 μm gap	Thinning	<5 mins	~200 to 700 Pa
Beck *et al.*(2)	Chemical Photoinitiated	Methacrylated solubilized devitalized cartilage and devitalized cartilage microparticles	20 mm parallel plate, 500 μm gap	Thinning	-	~30 to 1500 Pa
Beck *et al.*(48)	Chemical Photoinitiated	Methacrylated hyaluronic acid and devitalized/decellularized cartilage microparticles	20 mm cross-hatched parallel plate, 500 μm gap	Thinning	-	~90 to 240 Pa

Dennis *et al.*(34)	Physical Colloidal Flocculation	Chondroitin sulfate or hyaluronic acid with hydroxyapatite nanoparticles	20 mm parallel plate, 500 μm gap	Thinning	<5 mins	~1 to 1400 Pa
Dennis *et al*.(57)	Physical Colloidal Flocculation	Hyaluronic acid, hydroxyapatite nanoparticles, and micronized tissue ECM	20 mm cross-hatched parallel plate, 500 μm gap	Thinning	<5 mins	~100 to 1000 Pa
Diba *et al*.(160)	Physical Colloidal Flocculation	Bisphosphonate-functionalized hyaluronan and bioactive glass particles	8 mm parallel plate	Thinning	Immediate	~160 to 260% (Yield Strain)
Dumas *et al*.(64)	Chemical Reaction	Lysine-derived polyurethane and bone particles	25 mm parallel plate, 1000 μm gap	Thinning	-	2.1 Pa
Fakhari *et al.*(49)	Physical Entanglement	Hyaluronic acid nanoparticles	20 mm cone and plate (2°)	Thinning	-	~500 to 2300 Pa
Gaharwar *et al.*(59)	Physical Charge	Gelatin and silicate nanoplatelets	Static Tests: 25 mm Parallel Plate, 500 μm gap	Thinning	<10 s	2 to 89 Pa

			Transient Tests: 25 mm Cone and Plate (1°)			
Geisler *et al*.(45)	Physical Peptide Interactions	Peptide (VKVKVKVKVKV-NH2)	25 mm parallel plate, 500 nm gap	Thinning	Immediate	-
Glassman *et al*.(46)	Physical Peptide Interactions	Protein-polymer triblock copolymer	25 mm sandblasted cone and plate (1°)	Thinning	-	~9 kPa
Gao *et al*.(62)	Physical Hydrophobic Interactions	Pyrene-tailored pyridinium and 2,4,7-trinitrofluorenone	25 mm parallel plate	-	<180 s	78% (Yield Strain)
Hao *et al*.(58)	Physical Entanglement	Hydrophobically modified polyacrylamide and sodium oleate micelles	40 mm cone and plate (1°)	-	<10 s	-
Li *et al*.(161)	Chemical Reaction	Glycol-chitosan and dibenzaldehyde-terminated polyethylene-glycol	20 mm parallel plate	-	40 to 84 min	-

Liu *et al*.(61)	Physical Hydrophobic Interactions	Dexamethosone phosphate, betamethasone phosphate, and hydrocortisone phosphate	20 mm cone and plate	Thinning	<10 s	9.8% (Yield Strain)
Lu *et al*.(47)	Physical Peptide Interactions	Peptide-PEG copolymer with dimerization and docking domain polypeptide	20 mm cone and plate, 27 μm gap	Thinning	~6 s	~100 to 400% (Yield Strain)
Olsen *et al*.(60)	Physical Peptide Interactions	Telechelic proteins with coiled-coil endblocks and flexible polyelectrolyte midblocks	25 mm cone and plate	Thinning	<10 s	~1400 Pa
Rodell *et al*.(162)	Physical Hydrophobic Interactions	Hyaluronic acid functionalized with guest (adamantine) and host (β-cyclodextrin)	20 mm cone and plate (1°)	Thinning	<10 s	~60% (Yield Strain)
Rodell *et al*.(163)	Combinational Hydrophobic Interactions and Chemical Reaction	Dual crosslinking hyaluronic acid functionalized with guest (adamantine) and	20 mm cone and plate	Thinning	<3 s	35% (Yield Strain)

		host (β-cyclodextrin), and thiol/methacrylate groups				
Rughani *et al*.(98)	Combinational Peptide Interactions and Photoinitiated	Self-assembling β-hairpin peptide incorporating non-natural sorbamide residues	25 mm parallel plate, 500 μm gap	Thinning	<2 h	-
Samaniuk *et al*.(67)	-	Mayonnaise	25.4 mm diameter, 150 mm long vane rheometer	-	-	~200 Pa
	-	Play-Doh		-	-	~3000 Pa
Townsend *et al*.(164)	Physical Colloidal Flocculation	Hyaluronic acid, hydroxyapatite nanoparticles, and micronized tissue ECM	20 mm cross-hatched parallel plate, 500 μm gap	Thinning	-	~100 to 550 Pa
Tsaryk *et al*.(50)	Physical Entanglement	Collagen and hyaluronic acid semi-interpenetrating network loaded with gelatin microspheres	15 mm cross-hatched parallel plate, 1000 μm gap	Thinning	-	-
Vulpe *et al*.(165)	Chemical Reaction	Collagen, hyaluronan, and sericin	Concentric cylinder geometry	Thinning	-	-

Wang *et al*.(26)	Physical Charge	Cationic and anionic gelatin nanospheres	20 mm parallel plate, 500 μm gap	Thinning	<1 min	-
Yu *et al*.(63)	Chemical Reaction	Chain-extended PEO-PPO-PEO multiblock copolymer	40 mm cone and plate (1°)	-	Immediate	130% (Yield Strain)